Communications Research Centre

MEASUREMENTS AT 11 AND 17 GHZ OF TERRESTRIAL MICROWAVE FADING AND DEPOLARIZATION

by

R.S. BUTLER

Department of Communications
Ministère des Communications

CRC REPORT NO. 1358

OTTAWA, SEPTEMBER 1982

COMMUNICATIONS RESEARCH CENTRE

DEPARTMENT OF COMMUNICATIONS
CANADA

MEASUREMENTS AT 11 AND 17 GHZ OF TERRESTRIAL MICROWAVE FADING AND DEPOLARIZATION

by

R.S. Butler

(Radar and Communications Technology Branch)

CRC REPORT NO. 1358

September 1982

OTTAWA

TABLE OF CONTENTS

MEASUREMENTS AT 11 AND 17 GHZ OF TERRESTRIAL MICROWAVE FADING AND DEPOLARIZATION

by

R.S. Butler

ABSTRACT

This report presents the results of a microwave propagation experiment which was conducted in the 11 GHz and 17 GHz frequency ranges on two adjacent 16 km paths near Ottawa, Canada. Direct and cross-polarized signal levels were measured for six months in mid-1979, and significant attenuation and depolarization were observed during periods of rainfall as well as at certain times when the atmosphere was clear.

The probabilities of occurrence of attenuation and depolarization, and the relations between them, comprise a major part of the report. Statistics of the durations and of the rates-of-change of attenuation are also presented. There is also a discussion of the relation of depolarization during rainfall to the canting angles of raindrops, and a procedure is developed by which the statistics of the canting angles are obtained.

Throughout the report, reference is made to relevant CCIR documents to test the appropriateness to Canadian conditions of presently recommended predictions of various propagation phenomena. Finally, the magnitudes of attenuation during rainfall and attenuation in clear air, and of depolarization in both circumstances, are compared and assessed for their effects on microwave communication system design.

1. INTRODUCTION

The initial decision to include propagation experiments at 11 and 17 GHz in the research program of the Department of Communications was made in 1974. At that time it had become clear that knowledge of propagation conditions in the frequency range above 10 GHz was inadequate considering the user demands for spectrum space that were expected in the 1980s. In partic-

ular, there was little information on the differences which might exist between vertical and horizontal linear polarization propagation effects or on cross-polarization phenomena. This lack was particularly critical because of the expectation that the use of dual polarizations might be a practicable technique for frequency conservation.

Consequently, it was decided to emphasize the collection of propagation data in dual linear polarizations. Because there were some indications that terrain effects might be important, two adjacent paths were chosen, over quite different types of landscape. This report presents an analysis of both the co-polar and cross-polar propagation effects observed on these two paths in 1979. The following section of the report provides necessary information on the properties of the experimental system.

Section 3 of the report contains the results of the experiment: these are subdivided into four categories. In subsection 3.2 the results obtained during periods of clear-air fading are presented, including duration of fade and rate-of-change statistics. Subsection 3.3 contains the cross-polarization results during clear-air periods, and relates them to the direct signal statistics. Rainfall fading results are presented in subsection 3.4, including data on fade durations and frequency scaling. Cross-polarization results obtained during periods of rainfall are contained in subsection 3.5, as well as a preliminary attempt to deduce the statistical properties of the rainfall which causes the observed signal depolarization. A summary of the results, with a comparison of the relative importance of clear-air and precipitation fading, is contained in section 4.

2. EXPERIMENT DESCRIPTION

2.1 PATH PARAMETERS

The geographical arrangement of the experimental links is shown in Figure 1. The receivers were situated at the Communications Research Centre, and the transmitters were located at Corkery 16.3 km distant at azimuth 241°, and at Kingsmere 15.7 km distant at azimuth 8°. The elevation angle from CRC to Corkery is +0.2°, and from CRC to Kingsmere is +0.6°.

Path profiles along both links are shown in Figures 2 and 3. The Corkery path is entirely over rolling farmland and lightly forested bushland, with path clearance in the range 20 to 40 metres above ground almost everywhere, which is reduced by 10 metre trees over about one-third of the path. The Kingsmere path crosses the Ottawa River which is 3 km wide at that point, and has a clearance exceeding 40 metres almost everywhere and ranging up to 150 metres. This significant difference in the paths is of great importance for the interpretation of the depolarization data later in this report.

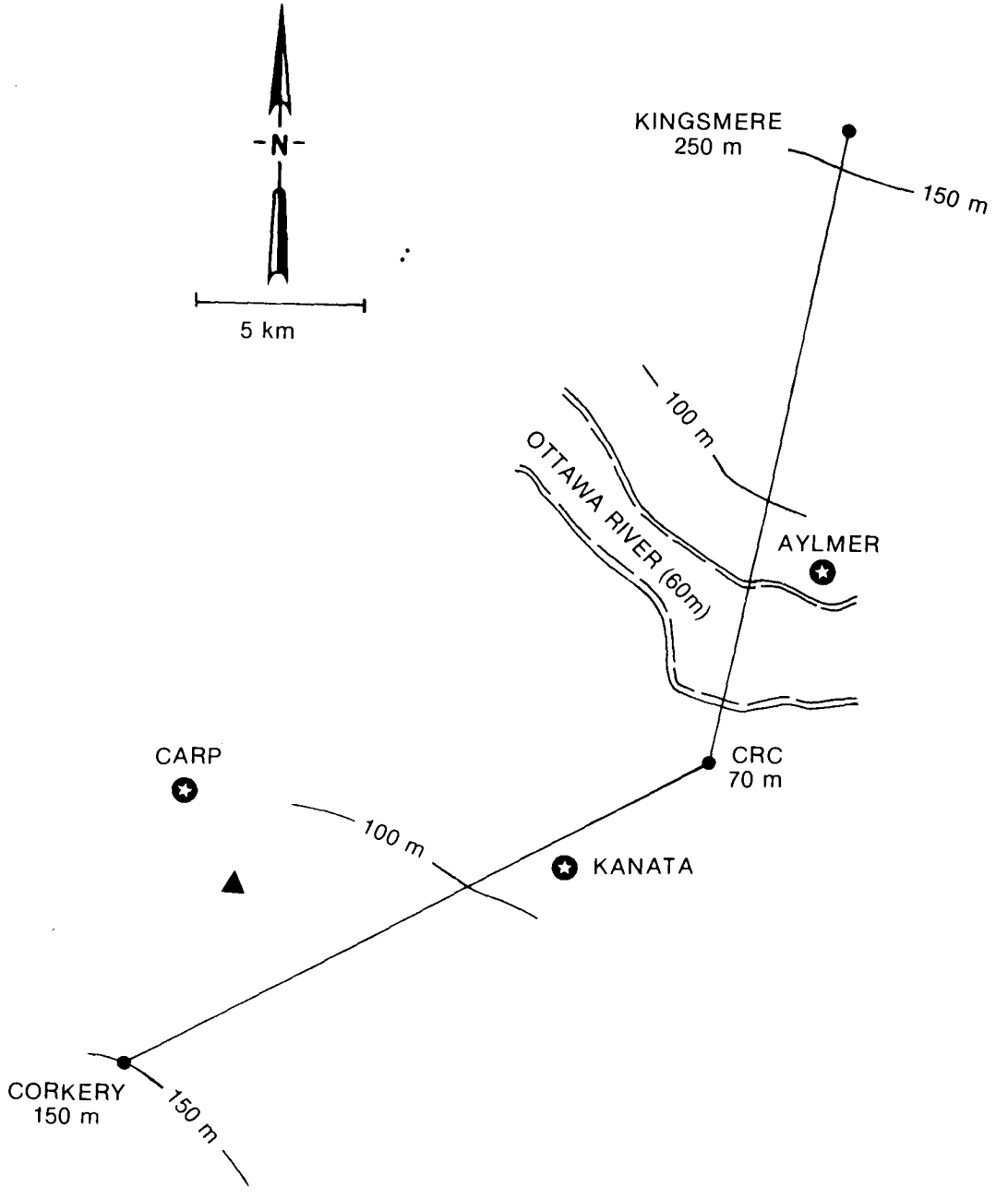

Figure 1. Geographical arrangement of experimental links

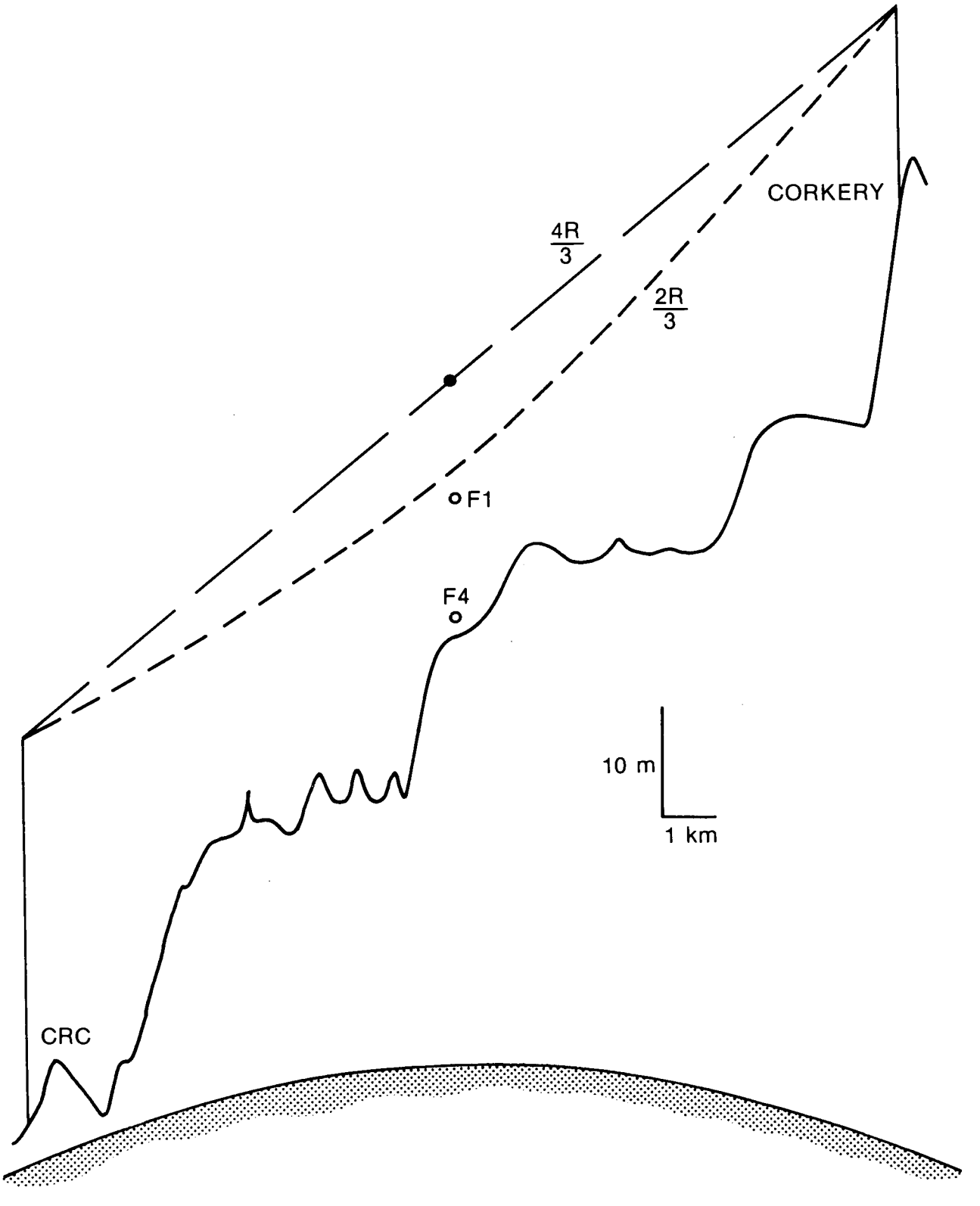

Figure 2. CRC – Corkery path profile

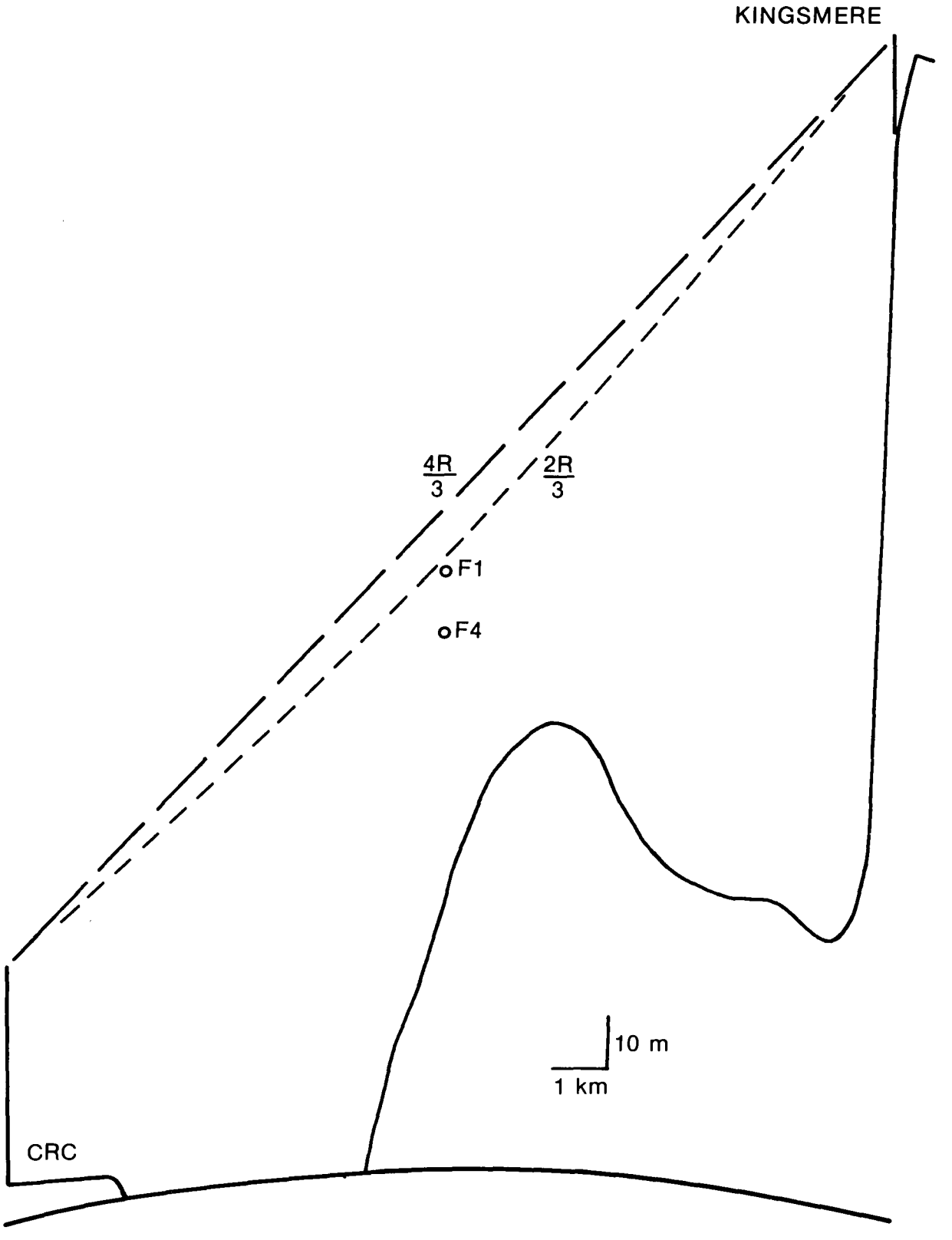

Figure 3. CRC — Kingsmere path profile. F1 and F4 are first and fourth Fresnel Zone Clearances at 11 GHz. Note that vertical scale is twice that of Figure 2.

2.2 LINK PARAMETERS

A block diagram of the experimental link arrangement is shown in Figure 4, with some basic data collected in Table 2.1. In this table the Margin is the difference between the normal received day-time signal level and the lowest usable signal level, approximately 7 dB above the theoretical receiver noise floor, while the static XPI is the median cross-polar isolation of the antennas under unfaded conditions.

TABLE 2.1

Basic Characteristics of Experimental Microwave Links

Site	Frequency (GHz)	Polarization	Margin (dB)	Static XPI (dB)
Corkery	10.80	Vertical	63	37.5
Corkery	11.08	Horizontal	60	33.0
Corkery	16.53	Vertical	48	33.0
Corkery	16.81	Horizontal	46	42.0
Kingsmere	11.35	Horizontal	65	38.0
Kingsmere	17.71	Horizontal	50	34.0

All the antennas were paraboloids with dual-linearly-polarized focal-point feeds. At 11 GHz the antenna diameters were 1.2 m, with beamwidths of 1.5°, while at 17 GHz the diameters were 0.6 m, with beamwidths of 2.0°. The transmitting antennas at both Kingsmere and Corkery were mounted 18 m above ground level, while the receiving antennas at CRC were located 40 m above the ground. Each antenna was protected from direct precipitation by an aluminum shelter which projected forward far enough to shield the entire feed structure as well as the reflector surface.

The cross-polarization patterns of the antennas in the vicinity of the main beams were measured on a test range, with two examples being given in Figures 5 and 6. There is a tendency for these patterns to have four peaks disposed symmetrically within a couple of beamwidths of an on-axis minimum, and diagonally oriented with respect to the polarization direction. However, this tendency is complicated in some cases by asymmetries which are presumably unique to the antenna structure and, in particular, the cross-polarized relative minimum is not observed precisely on the axis of direct-polarized maximum signal in all cases. In setting up the experiment, the antenna alignments were optimized to give the greatest cross-polarization isolations that could be attained simultaneously in both polarizations, and the resulting median values are given in Table 2.1.

All the transmitters were crystal controlled phase-locked oscillators with a power output of approximately +20 dBm. At Kingsmere the oscillators at both frequencies were contained in a single thermally controlled box

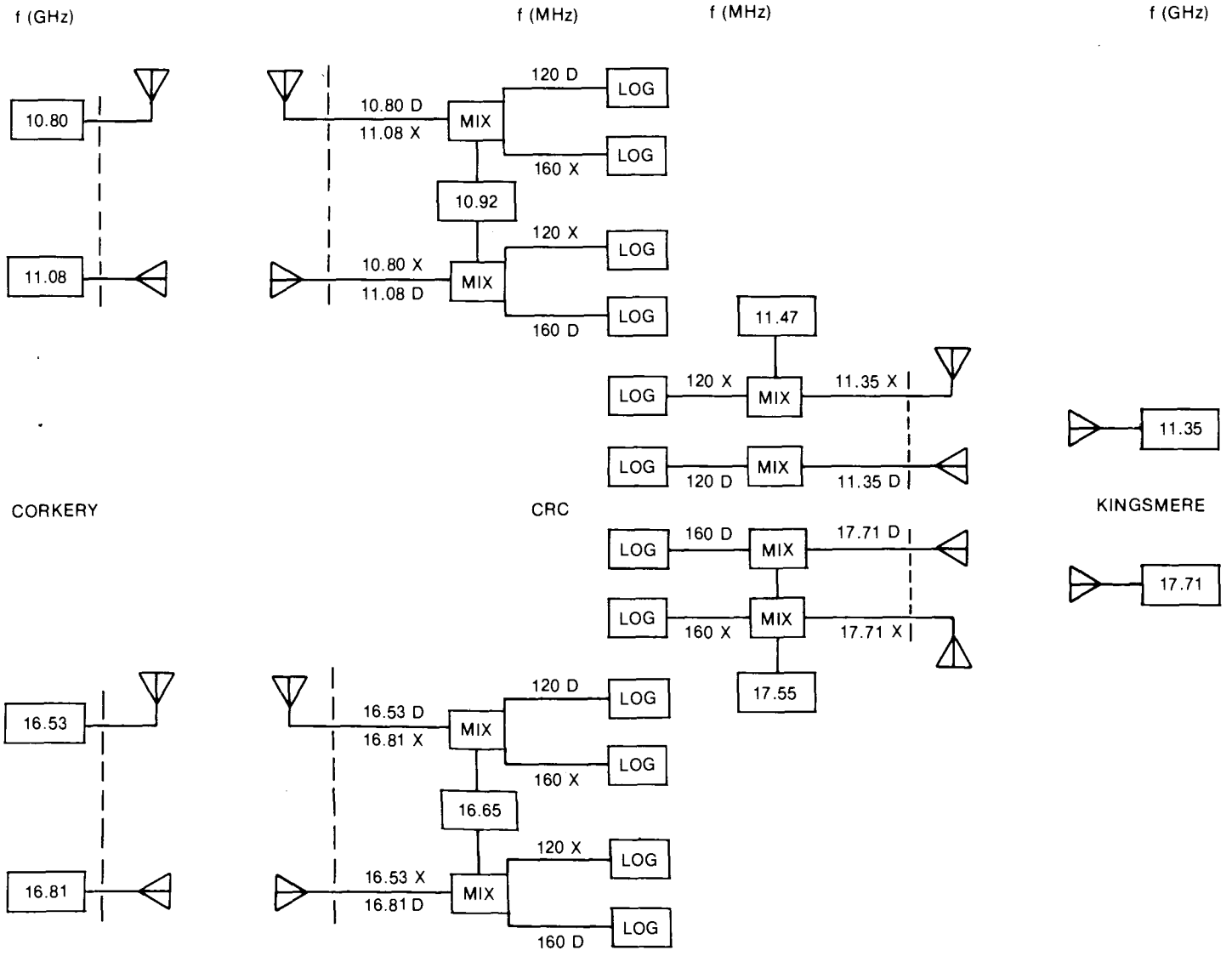

Figure 4. Block diagram of experimental links equipment

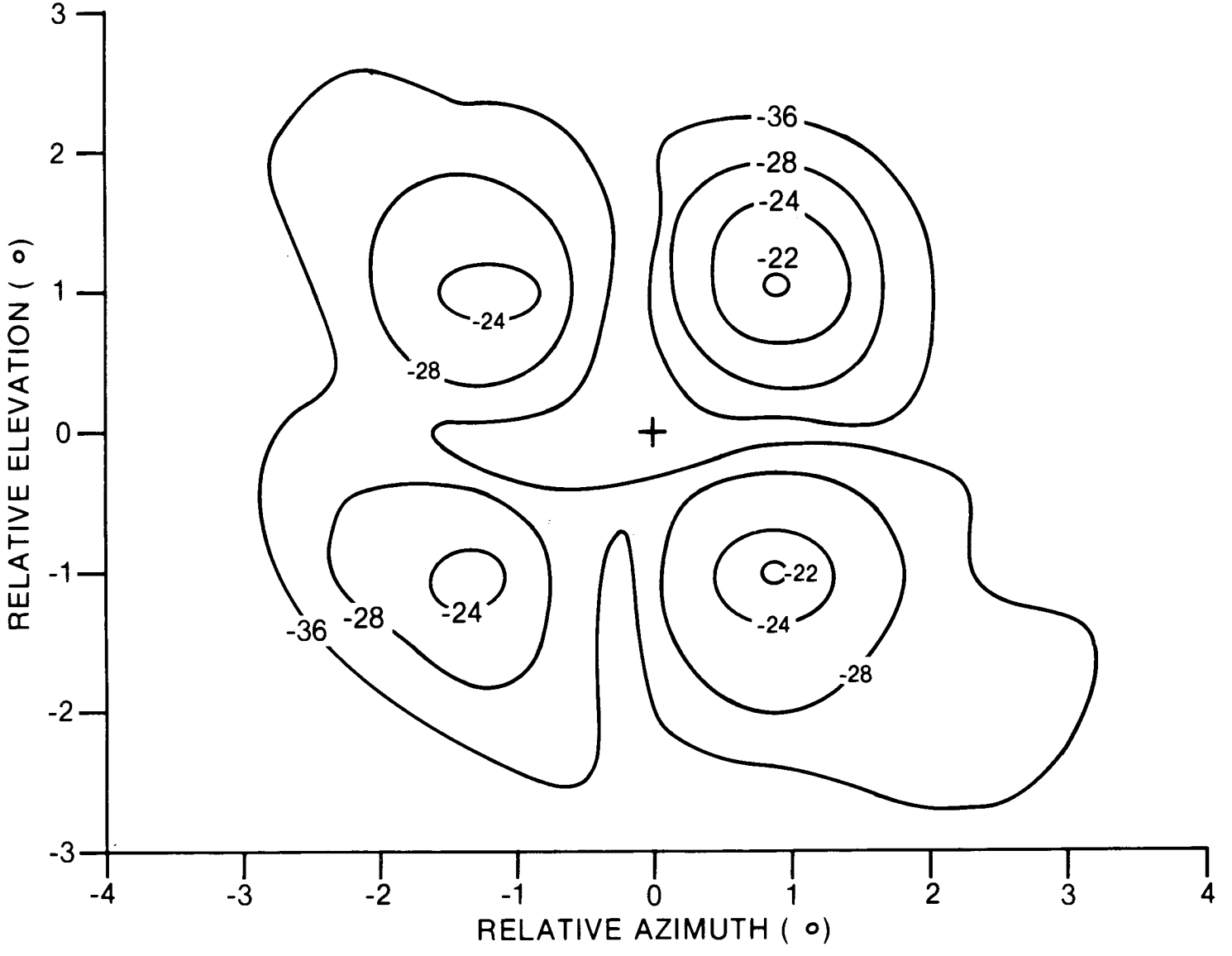

Figure 5. Cross-polarized power pattern of 10.80 GHz receiving antenna, Corkery path.

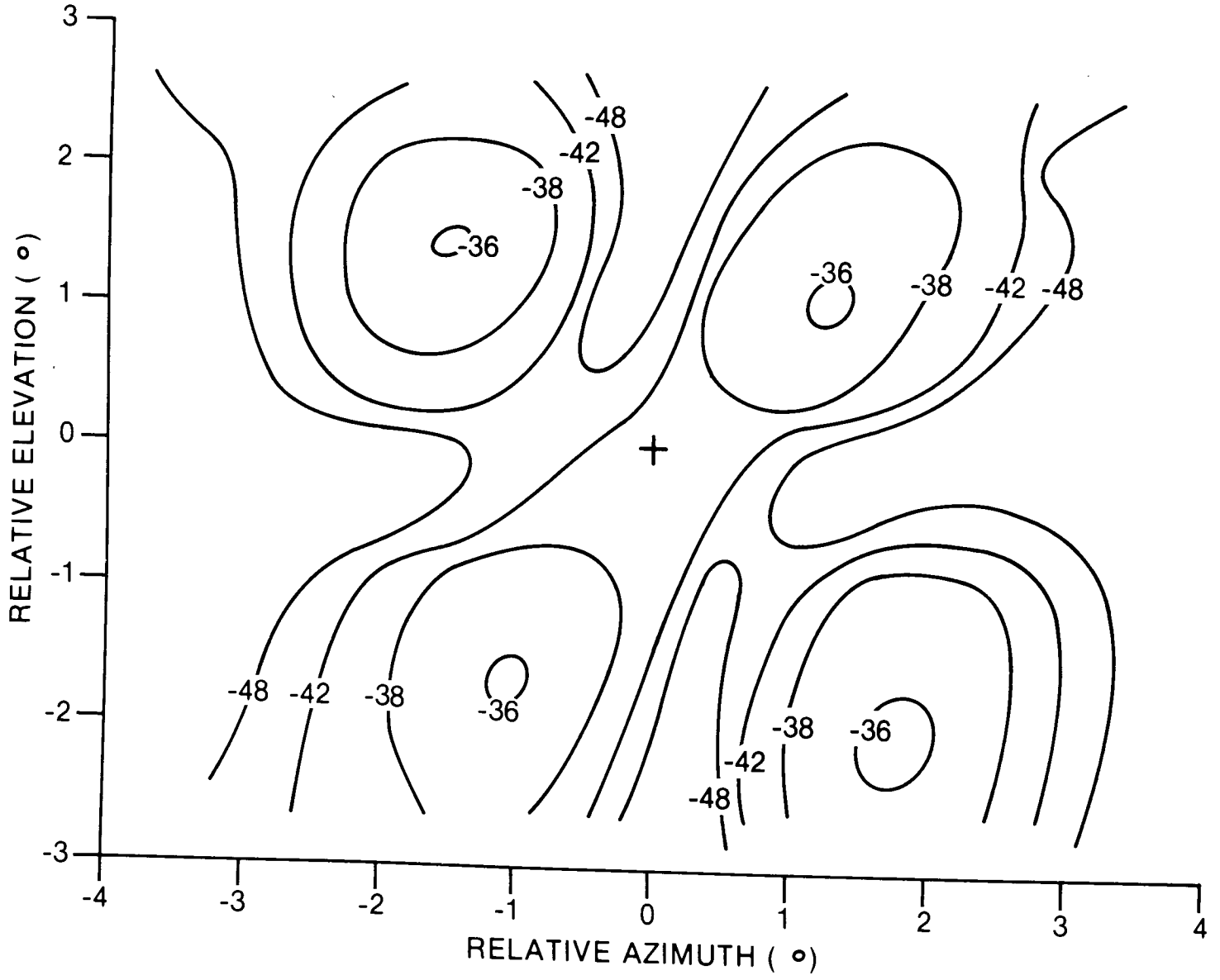

Figure 6. Cross-polarized power pattern of 16.53 GHz receiving antenna, Corkery path.

mounted at the antenna level. Power supplies and monitors were rack-mounted in a hut at the base of the tower. At Corkery the X-band oscillators were contained in one thermally controlled box, and the Ku-band oscillators in a second one. Both were mounted at the antenna level, with power supplies and monitors in a box at the tower base.

The receivers at CRC were contained in pairs in thermally controlled boxes, attached to the antennas with less than 50 cm of waveguide. The video output was detected and the level converted to a 12-bit binary number in a multiplexing sequence which repeated twice per second. The serial digital output was carried on an audio line approximately 300 meters to a computer which controlled the digital tape recorder on which the data were stored for later analysis.

Each receiver was calibrated at RF by direct insertion of a calibration signal through a directional coupler at the receiver input. Readings were made at 5 dB intervals over the dynamic range, typically 80 to 90 dB, from saturation to the noise limit. Examples of calibration curves are given in Figure 7, at both the Kingsmere frequencies. The approximate linearity over most of the operating range and the limiting behaviour at both extremes of the scale are typical. Over several sets of such measurements, the extreme scatter of the digital readings at a given frequency and calibration level are equivalent to less than 0.5 dB, which is of the order of the resettability of the calibration oscillator.

2.3 DATA HANDLING

For each of the twelve operating receivers blocks of 120 measurements of the signal level taken at 0.5 second intervals were recorded in digital form. In the first phase of the analysis these data were averaged to produce one-minute means and the means were plotted for each day on a graphics terminal. A fairly representative example of such a 24-hour record is shown in Figure 8. This processing was kept current throughout most of the year 1979 to facilitate comparison with recent weather, so that precipitation fading could be identified, and to check equipment operation.

Whenever the preliminary assessment located significant fading the data were reprocessed for that period, using five-second averaging (hence twelve times the time resolution), and two-hour segments of these data were plotted. Figure 9 shows an example of such a record from a period of active clear-air fading. Finally, in all cases in which the five-second records indicated rapid activity the raw data themselves were plotted for examination. Thus it appeared that no loss of detail occurred during precipitation fading if five-second averages were used, but for clear-air fading even the 0.5 second time resolution may not be adequate to resolve all the time-varying details. Figure 10 shows a twelve-minute segment of raw data during an active period.

After termination of the experiment all the data were critically reviewed and baseline levels were established on an objective basis for the entire data set. This was done by eliminating all periods of instability and fading, and averaging the one-minute average data in each continuous segment which was stable and reliable. These averages, which turned out to be restricted to the daytime hours 0900 to 1600 EST, were then plotted to enable

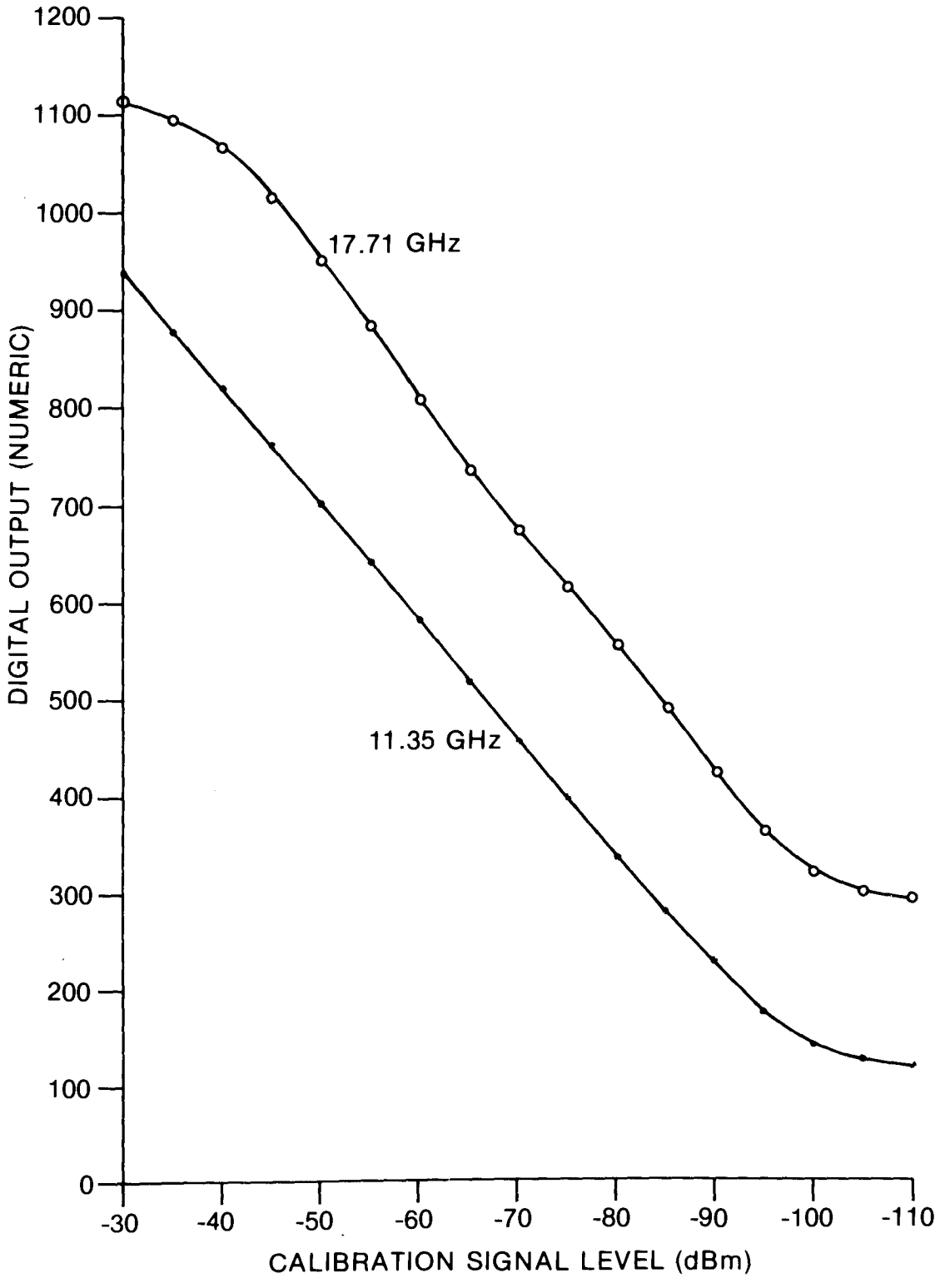

Figure 7. Typical receiver calibration curves at 11.35 and 17.71 GHz, on the Kingsmere path.

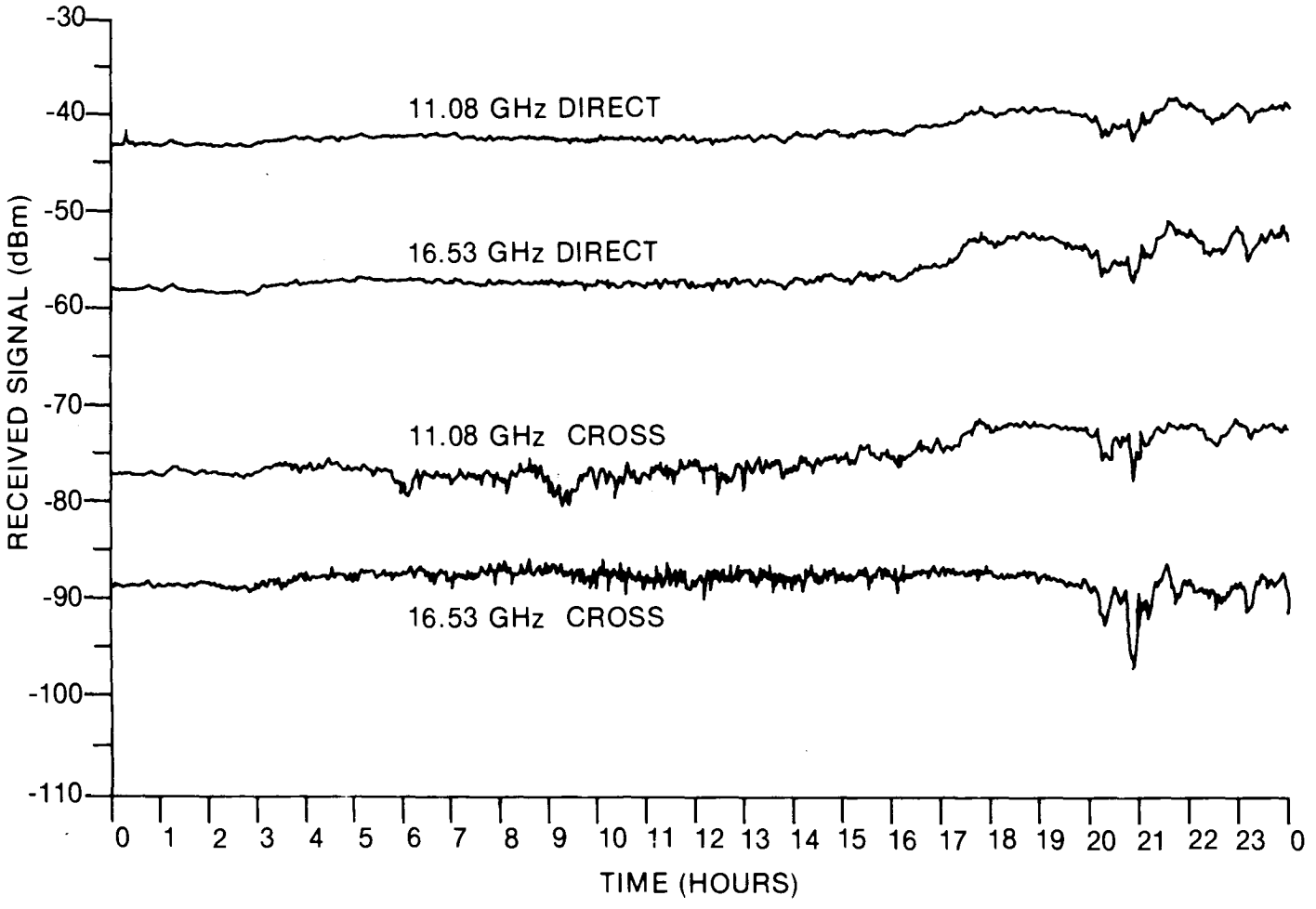

Figure 8. Typical 24-hour record of received signals averaged over one minute. Direct and cross-polarized signals at both 11.08 GHz and 16.53 GHz as shown.

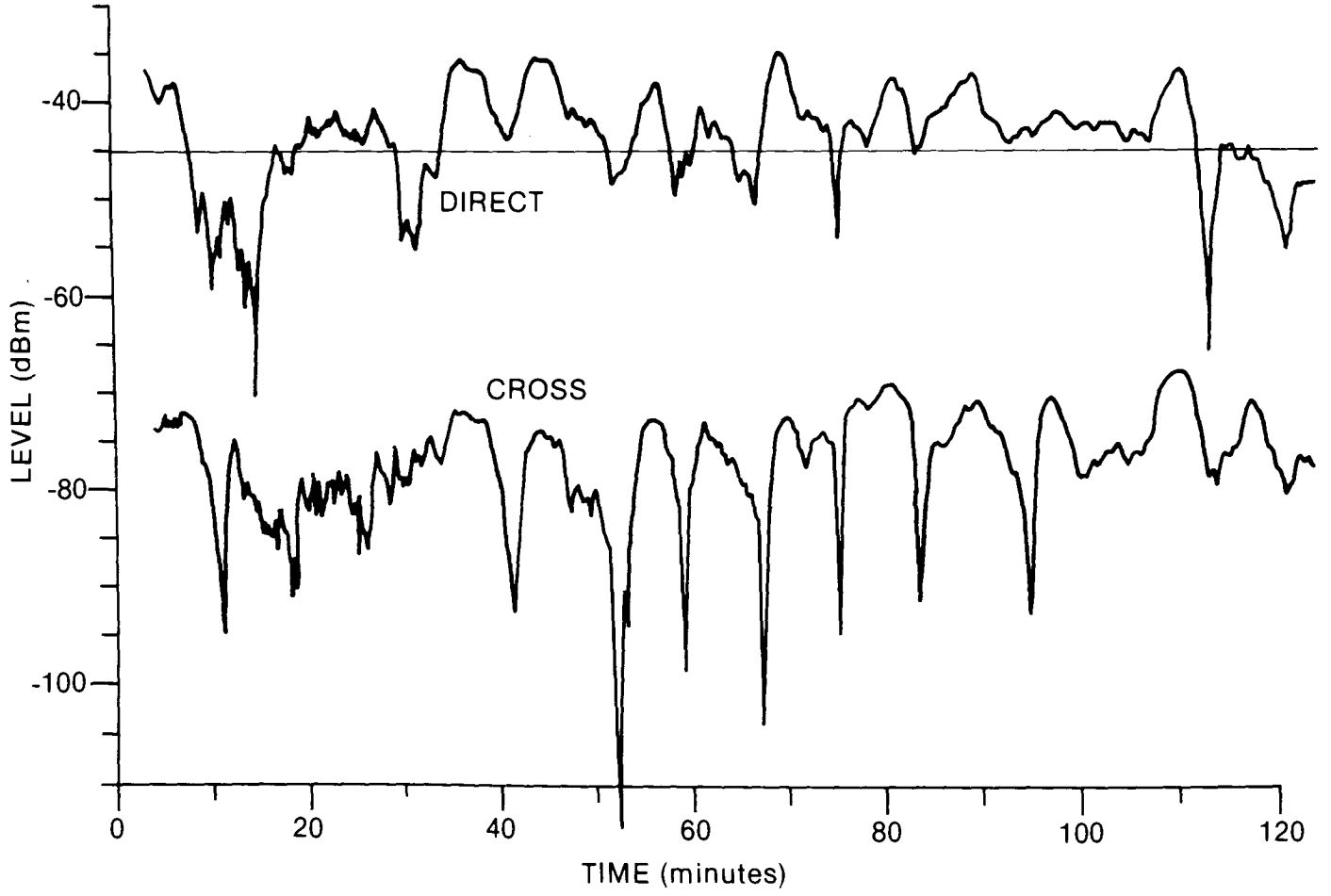

Figure 9. Example of 2-hour record of received signals during clear-air fading, averaged over five seconds for both direct and cross-polarized signals at 10.80 GHz.

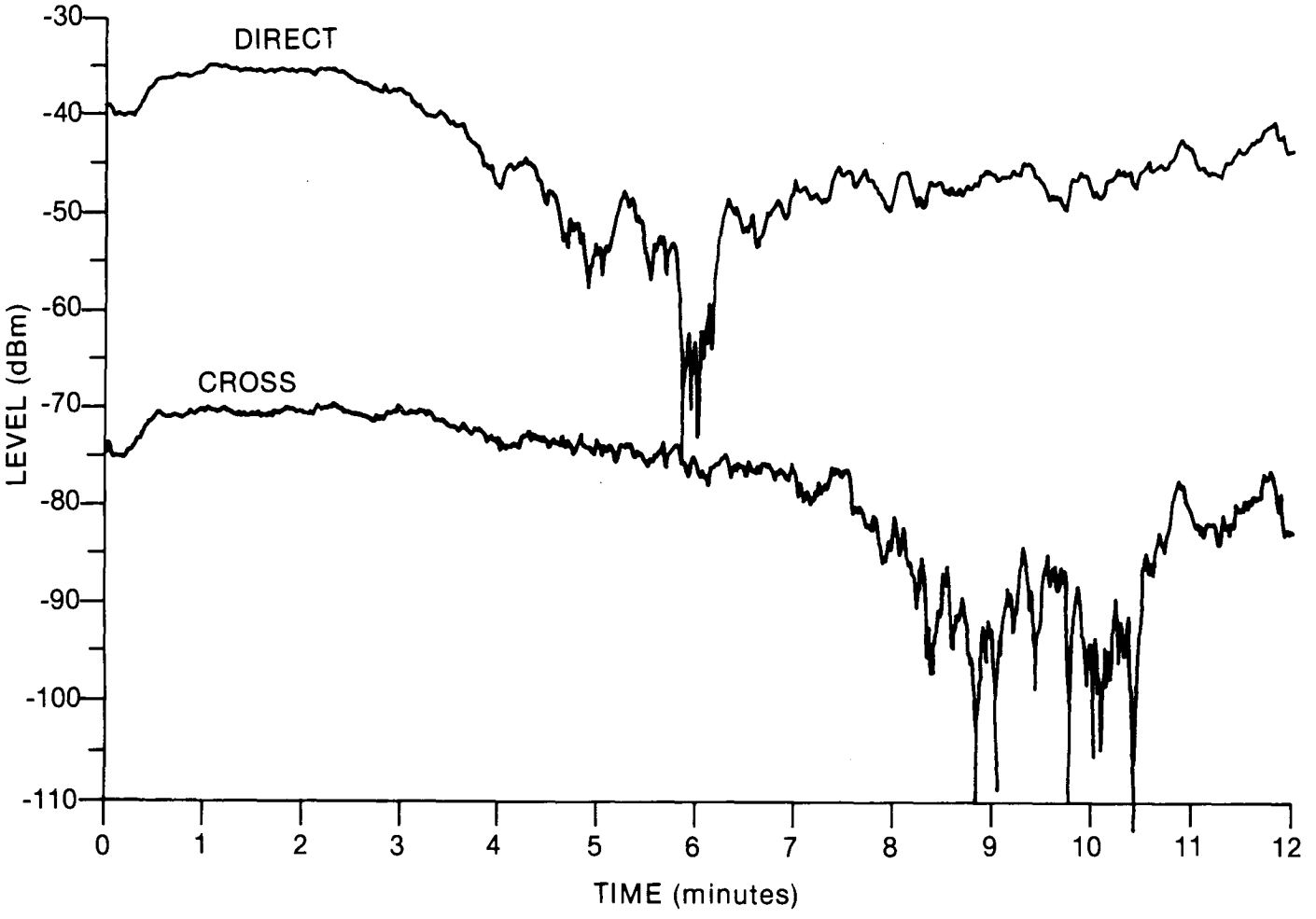

Figure 10. Example of 12-minute record of raw received signals during clear-air fading for both direct and cross-polarized signals at 10.80 GHz.

trends to be discovered, and for each time period established in this way for which the averages were statistically stable, a weighted overall average was calculated. It was found that between two and five such grand averages sufficed for each receiver channel, and that the dates of discontinuity agreed with times when some adjustment was made in the system. The resulting standard deviation of each baseline segment was typically 0.2 dB, and no significant improvement occurred for more elaborate baseline processing. Thus all fade depths are referred to these baseline levels, which represent the mean daytime undisturbed signal levels for each receiver channel.

3. RESULTS

3.1 DATA SET CHARACTERISTICS

The set of digitally recorded data obtained in 1979 was well-calibrated, reliable, and continuous enough for statistical analysis. A set of analogue records covering part of the year 1977 and most of the year 1978 also exists, although not in a form suitable of reduction with a precision comparable to the 1979 data. However, these earlier records confirm that severe clear-air fading and almost all intense thunderstorm activity are confined to the five months May to September. There does not appear to be a concentration of either clear-air or precipitation fading in any month, so that worst-month statistics do not emerge naturally from the present set of data.

The measurements to be described covered a period of 176 days, from 5 April to 27 September, during which the Kingsmere-CRC equipment operated with only one short outage, so that this data sub-set is virtually complete for both precipitation and clear-air fading statistics. There were a number of outages of longer duration on the Corkery path, but the combination of operating frequencies was such that the data are known to be complete during times of clear-air fading. However, only the measurements from Corkery at 10.80 GHz include almost all the precipitation data. At 11.08 GHz several major rainfall events were missed, while at the frequencies near 17 GHz a small number of events are also known to have been missed.

In the analysis below, percentage time statistics are referred to a six-month period, approximately 1.58×10^7 seconds. Because of the concentration of fading into five months, as mentioned above, this probably distorts the true picture by about 20%, but the correction is easy to apply if needed, and it seems more natural to deal with a half-year, or two consecutive seasons, than with the more unusual period.

3.2 CLEAR-AIR PROPAGATION

The behaviour of the received signals at night-time, when all clear-air fading occurred, was strikingly different on the two paths. On the Kingsmere path the night-time levels were typically within one or two dB of the stable day-time levels. On the Corkery path, however, signal levels increased during the early evening, typically by 8 to 10 dB at maximum, and remained enhanced until after sunrise on about one-half of the nights. Periods with fading

deeper than 18 dB below day-time signal levels were observed on only two occasions on the Kingsmere path, and no periods were observed with only moderate fading, between 6 and 18 dB. On the Corkery path deep fading occurred on eleven nights, always during times of strong enhancement, with fading activity lasting typically for two to four hours. Moderate fading was observed on this path on eight other nights, always during periods of enhancement.

3.2.1 Clear-air Fading Statistics

The cumulative distributions of fade depth for the frequencies on the Corkery path are shown in Figures 11 and 12, for vertical and horizontal polarizations, respectively. There does not appear to be any significant difference between the data sets in orthogonal linear polarizations. At both frequencies near 17 GHz the data can be reasonably represented by a straight line with a slope of three decades of time per 20 dB of fade depth. The 11 GHz data are more complex, showing evidence of possibly two components, one of which dominates the statistics at fade depths smaller than about 18 dB, the other at greater fade depths, in agreement with the phenomenological remarks in the previous section.

The predicted curves for Rayleigh-distributed multipath fading for the "average-month" for continental temperate regions of the United States (CCIR, 1982a) which might be expected to apply as well to this part of Canada, are also indicated. These values, for fade depths greater than 15 dB, are derived from the equation for the fading probability,

$$P(W) = \frac{2.1 \times 10^{-5}}{S^{1.3}} \cdot \frac{W}{W_o} \cdot f \cdot d^3$$

where: d is path length in kilometres,

f is frequency in GHz,

W and W_o are faded and unfaded reference power levels, respectively,

S is the terrain roughness in metres, derived as the standard deviation of terrain elevations at 1 kilometre intervals. For the Corkery path S has the value 5.38 m while for the Kingsmere path the value of S is 34.56 m.

The agreement between the observed and predicted probabilities for a given fade depth is not very good at 11 GHz. The predicted probabilities are about a factor of five to ten times greater than observed, when the difference between "average worst-month" and our time base is taken into accout. At 17 GHz the agreement is very poor indeed, and, in particular, the observations show less fading at 17 GHz than at 11 GHz, while the prediction is for more fading at the higher frequency.

The equivalent cumulative distributions of fade depth for the frequencies on the Kingsmere path are shown in Figure 13. The statistical reliability of these data is rather lower than for those from the Corkery path, because here only two events were observed to give fade depths greater than

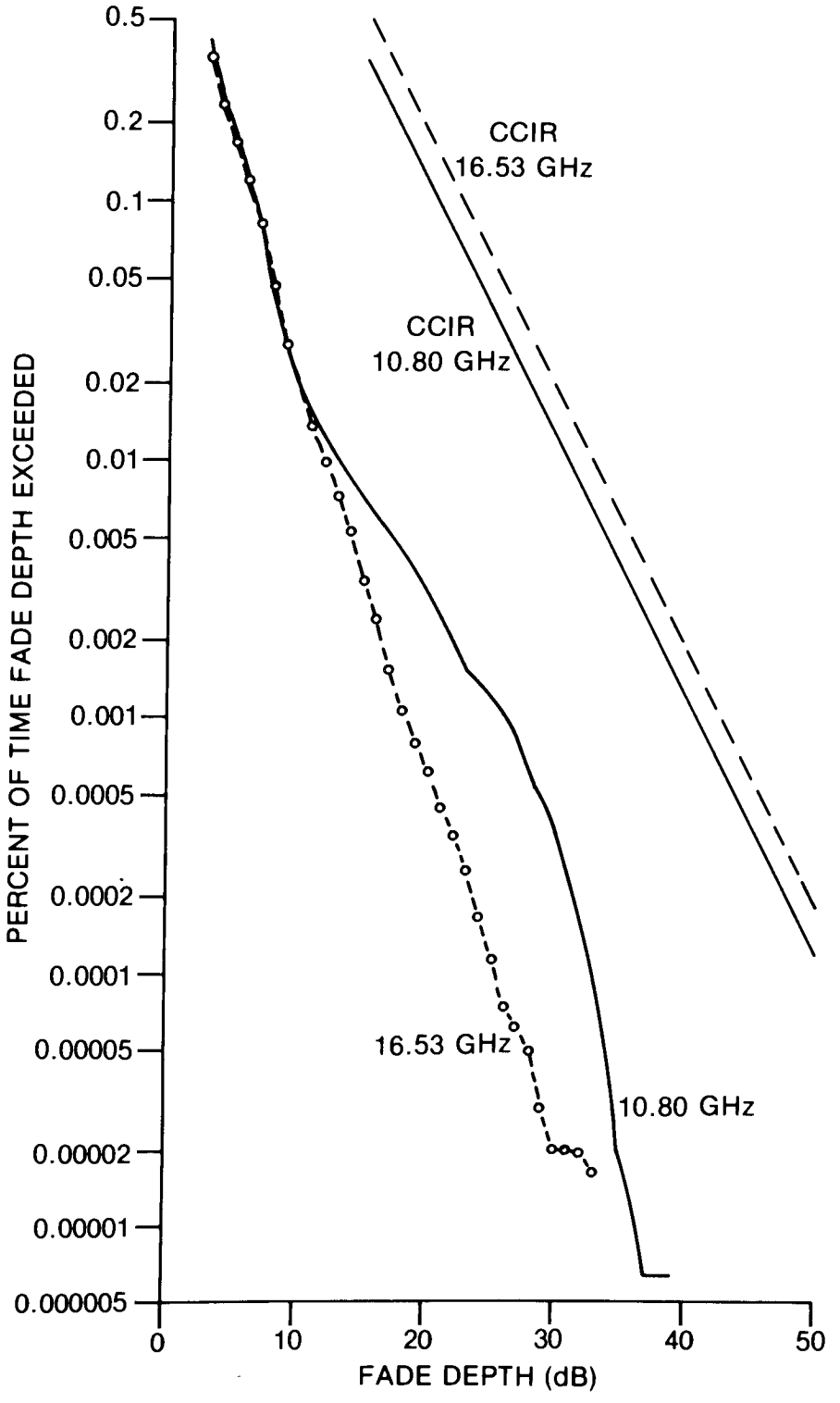

Figure 11. Cumulative distribution of clear-air fade depths at 10.80 and 16.53 GHz, Corkery path, vertical polarization. The straight lines are discussed in the text.

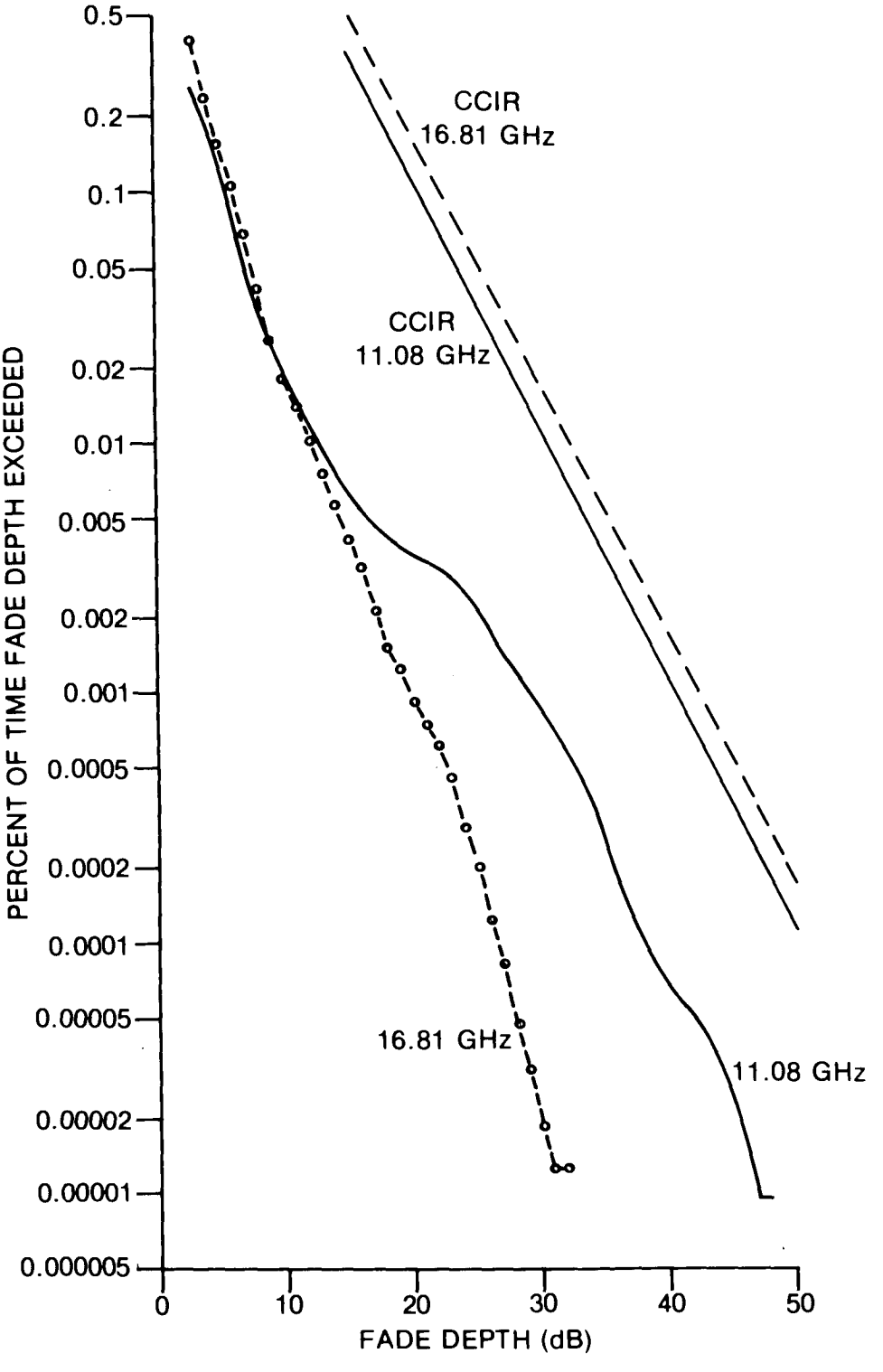

Figure 12. Cumulative distribution of clear-air fade depths at 11.08 and 16.81 GHz, Corkery path, horizontal polarization. The straight lines are discussed in the text.

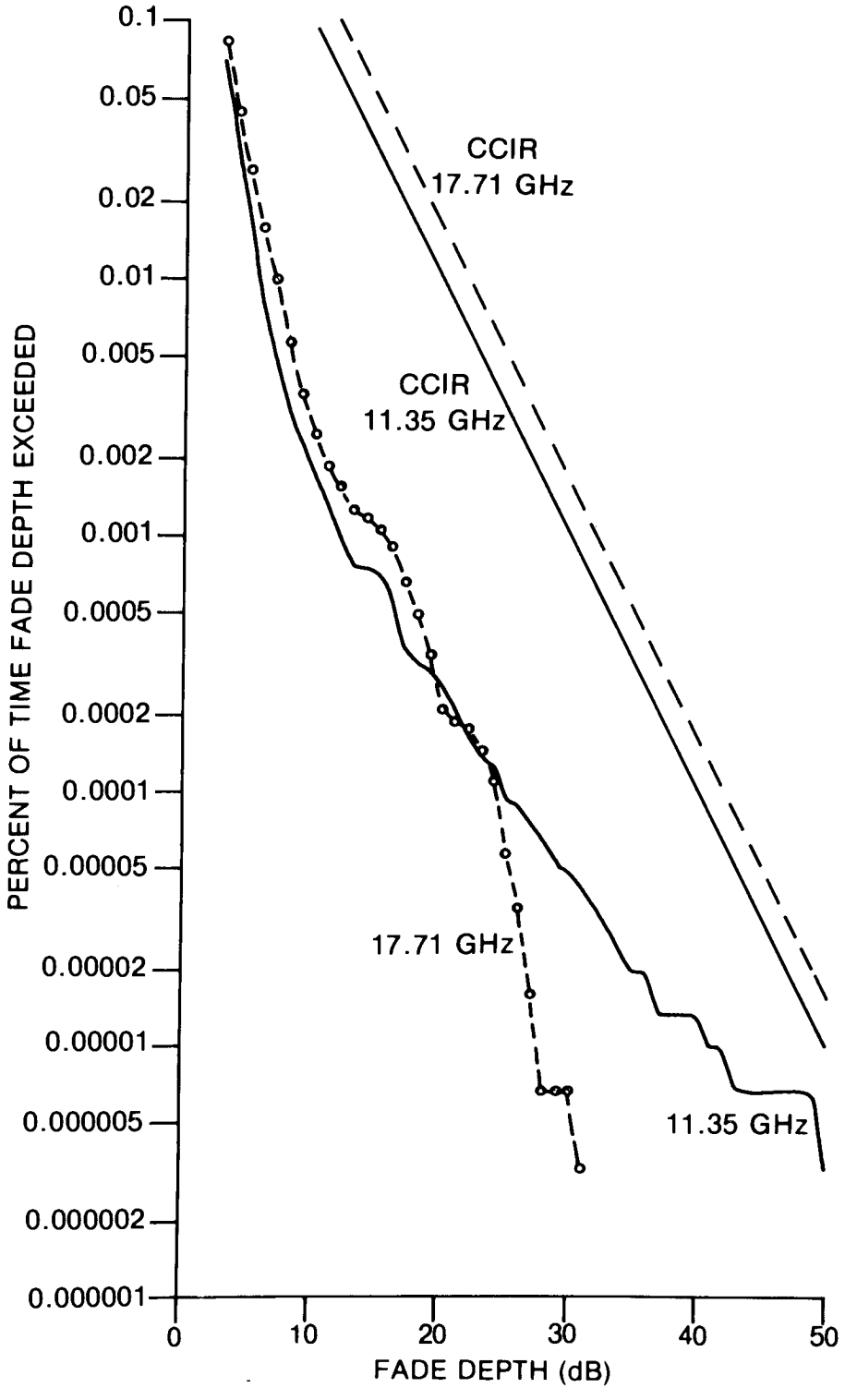

Figure 13. Cumulative Distributions of clear-air fade depths at 11.35 and 17.71 GHz, Kingsmere path, horizontal polarization. The straight lines are discussed in the text. Note that the vertical scale is different than in the preceding figures.

6 dB. At 11 GHz the observed ratios of percentages of time that a given fade depth is exceeded on the two paths are about 10 or 12, which agrees very well with the prediction of 11.2 based on terrain roughness differences. However, at 17 GHz the observed ratios are about 3 to 4, which suggests that other factors have to be taken into account. Of these, the difference in the slopes of the paths and the large difference in their clearances are likely to be very important, but neither can be assessed quantitatively at present. In spite of these differences between the paths, the agreement with predictions is about equally poor, and worse at 17 GHz, on both paths.

The explanation of the discrepancy between the observations and predictions is not obvious. Neither of the paths is "short" in the sense defined by Ruthroff (1971), as is evidenced by the occurrence of deep multipath fading. Nor is either path exceptional - with relatively little multipath fading, in the sense discussed by Lin (1971) - notably because the 11 GHz data agree fairly well with the Rayleigh slope of one decade of probability per 10 dB of fade depth, and the slopes of 17 GHz data discussed above do not agree with the "exceptional" slope of one decade of probability per 5 dB of fade depth. Both paths have adequate clearance - indeed, the Kingsmere path clearance is excellent - and neither shows evidence of ground or water reflections which generally cause additional ray interference and so greater incidence of fading. In the absence of additional information, perhaps it is legitimate to speculate that the prediction formula is inadequate at these frequencies simply because little work has yet been done, the equation having been established primarily using data gathered at frequencies below 11 GHz.

3.2.2 Number and Duration of Clear-air Fades

Since a fade is a reduction of the received signal level, the number of fades which occur depends on the fade depth. As Figure 10 shows, during a complex fading event this dependence need not be monotonic. For example, at -55 dBm there are five distinct fades, at -60 dBm there is only one, and at -65 dBm there are three. The duration of each individual fade to a given fade level is simply the period during which the signal continuously remains below that level. Thus in Figure 10, at the -60 dBm level the duration of the single fade is about 25 seconds, while at -65 dBm each of the fades lasts for only two or three seconds. All clear-air fading events were analysed at 1 dB intervals of fade depth, starting at 3 dB, to find the number of fades at each level and their durations, which have a quantization increment of 0.5 seconds.

The distributions of number of fades observed as a function of fade depth are shown in Figures 14, 15, and 16. For the Kingsmere path at 11.35 GHz only a single fade occurred with a depth greater than 14 dB, but it extended all the way to 49 dB. For the Corkery path the trends of the 11 GHz number data are not simply linear. This may reflect the division referred to earlier of the fading events into two classes with a dividing line around 18 dB. A similar behaviour is noted for the 17 GHz Kingsmere data, with a division near 9 dB. At 17 GHz on the Corkery path the data trends are more nearly linear, with slopes of about one decade per 10 dB of fade depth. This disagrees with the slope of one decade per 20 dB of fade depth expected from the work of Lin (1971), (see also CCIR (1982a)).

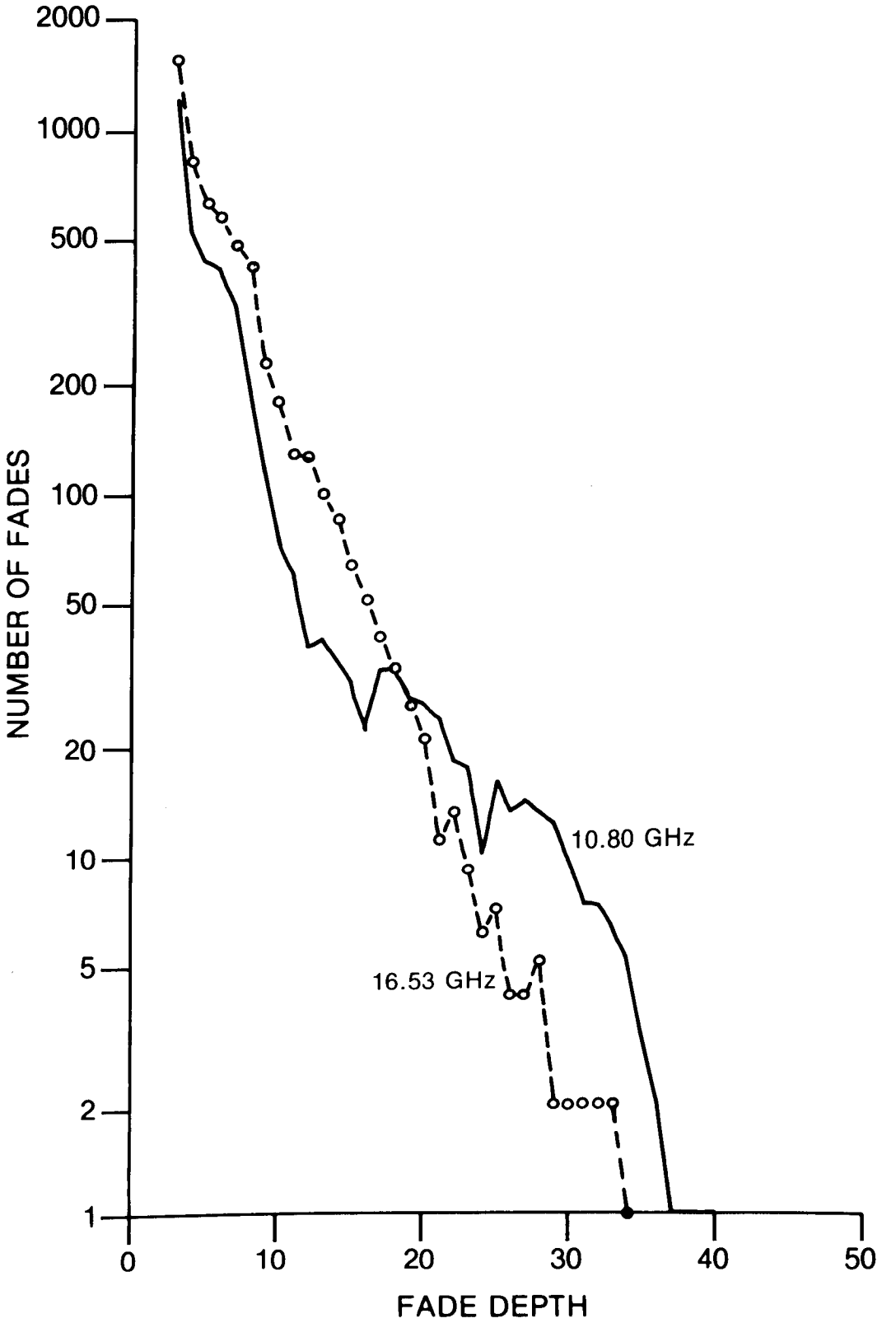

Figure 14. Numbers of clear-air fades at 10.80 and 16.53 GHz, Corkery path, vertical polarization.

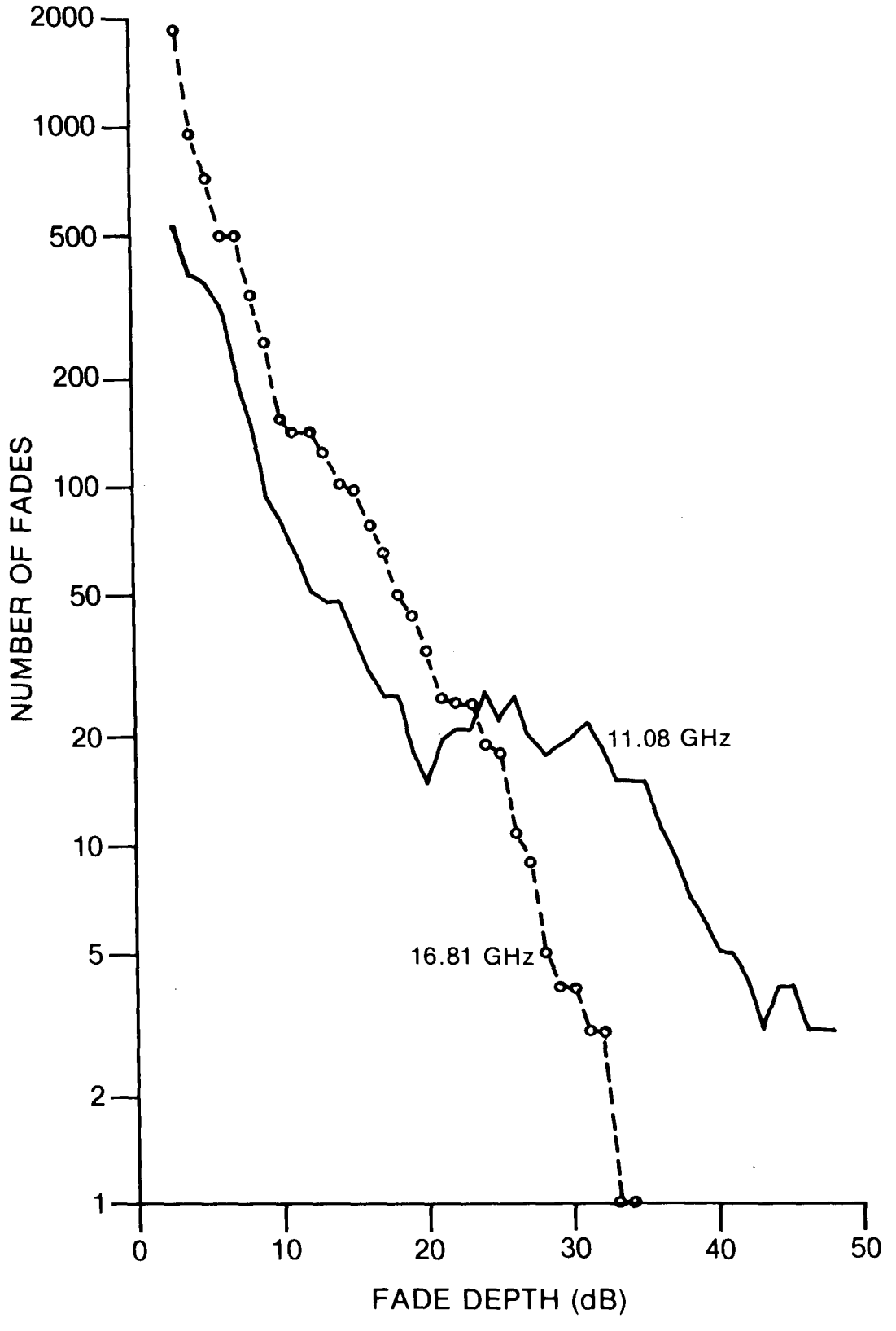

Figure 15. Numbers of clear-air fades at 11.08 and 16.81 GHz, Corkery path, horizontal polarization.

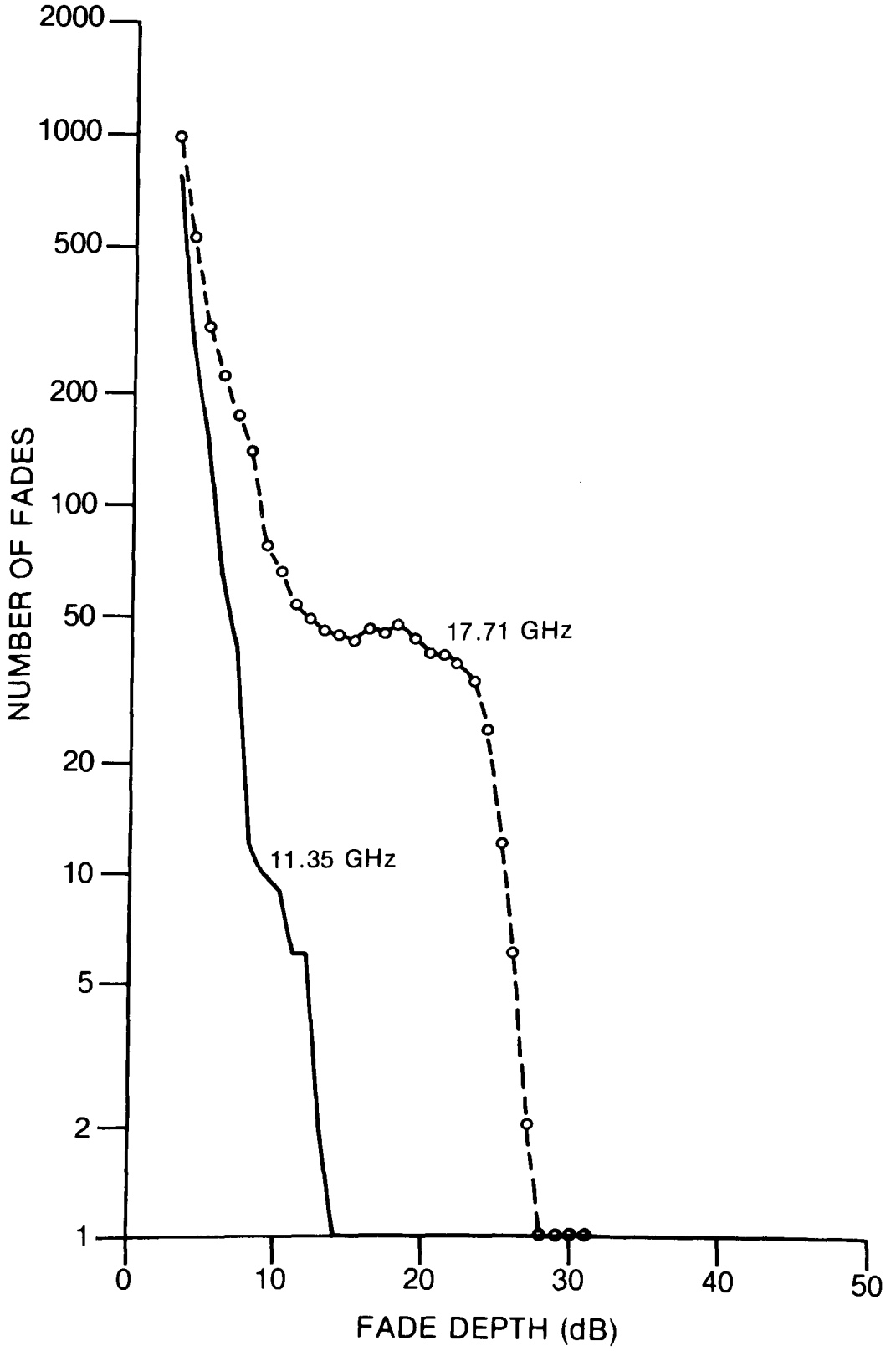

Figure 16. Numbers of clear-air fades at 11.35 and 17.71 GHz, Kingsmere path, horizontal polarization.

In Figures 17, 18, and 19 the average durations of clear-air fades as a function of fade depth are presented, together with a line having a slope of one decade per 20 dB fade depth. It can be seen that this slope agrees reasonably well on average with all the data, and considering the magnitude of the fluctuations this confirms reasonably well the suggestion of Lin (1971) that this slope is universally applicable to such data. The average fade duration at the higher frequencies is considerably smaller than at the lower: on the Corkery path, for which the data are statistically more reliable, over the fade depth range 15 to 30 dB the average of the duration ratios for both polarizations is about 0.21. This is much smaller than the ratio of 0.81 predicted for United States conditions by CCIR (1982a), and implies that average fade duration varies nearly as $(\text{frequency})^{-4}$, if indeed the difference is a frequency effect.

The form of the distribution of the fade duration at a given fade depth was found to be log-normal in every case for which adequate statistics were available. An example of the quality of the fit is shown in Figure 20, for three fade depths on the 16.53 GHz Corkery path. At fade depths much greater than 15 dB, the data become too sparse to permit the form of the distribution to be firmly established. Note that the average fade duration occurs at about the 10% probability level as the distribution is very skewed. Because of this skewness, the mean is not the most useful statistic for system designers who need information on the extreme durations to be expected. Because of the rarity of deep fades, reliable statistical information at some prescribed low level of probability could not be obtained. As an alternative, Figures 21 and 22 show the longest event durations observed in 1 dB increments of fade depth. For shallow fades this corresponds to about 0.1% conditional probability, and at the 25-30 dB level to about 10% conditional probability. The trend of the data in every case is reasonably linear in the given presentation.

3.2.3 Rate of Change of Fade Depth

For all periods when clear-air fading occurred, the rate of change of signal level, in dB/sec, was calculated for all consecutive pairs of measurements separated by one-half second of time. Rates were calculated separately for three intervals of fade depth: less than 3 dB, including all enhancements; 3 dB and greater; and 20 dB and greater. In all cases, positive and negative rates of change were computed independently: no significant differences were found between these two sets of results, so that they have been combined regardless of sign in the analysis which follows.

All the rate-of-change data for times of shallow fading and enhancement (fade depth less than 3 dB) are shown in Figure 23. The "percentages of active period" refer to the aggregate time of about 300 hours (nineteen samples of 16 hours each, approximately) for which the analysis was done. There were many evenings of moderate enhancement but no significant fading, which were not included in the present sample. The qualitative effect of their omission is to under-present the fraction of time for which small rates of change occur. However, for the faster rates of change, say greater than 1 dB/sec, the present data are probably representative. Therefore, if it is desired to convert these "percentages of active period" to percentages of the six-month sample period, they may be multiplied by the factor 0.0617 for the 11.08 GHz data, and 0.0690 for all others. Note that in none of these cases did the rate of change exceed 6 dB/sec, and that in every case at a given percentage of time the rates of change at 17 GHz are about 50% greater than at 11 GHz.

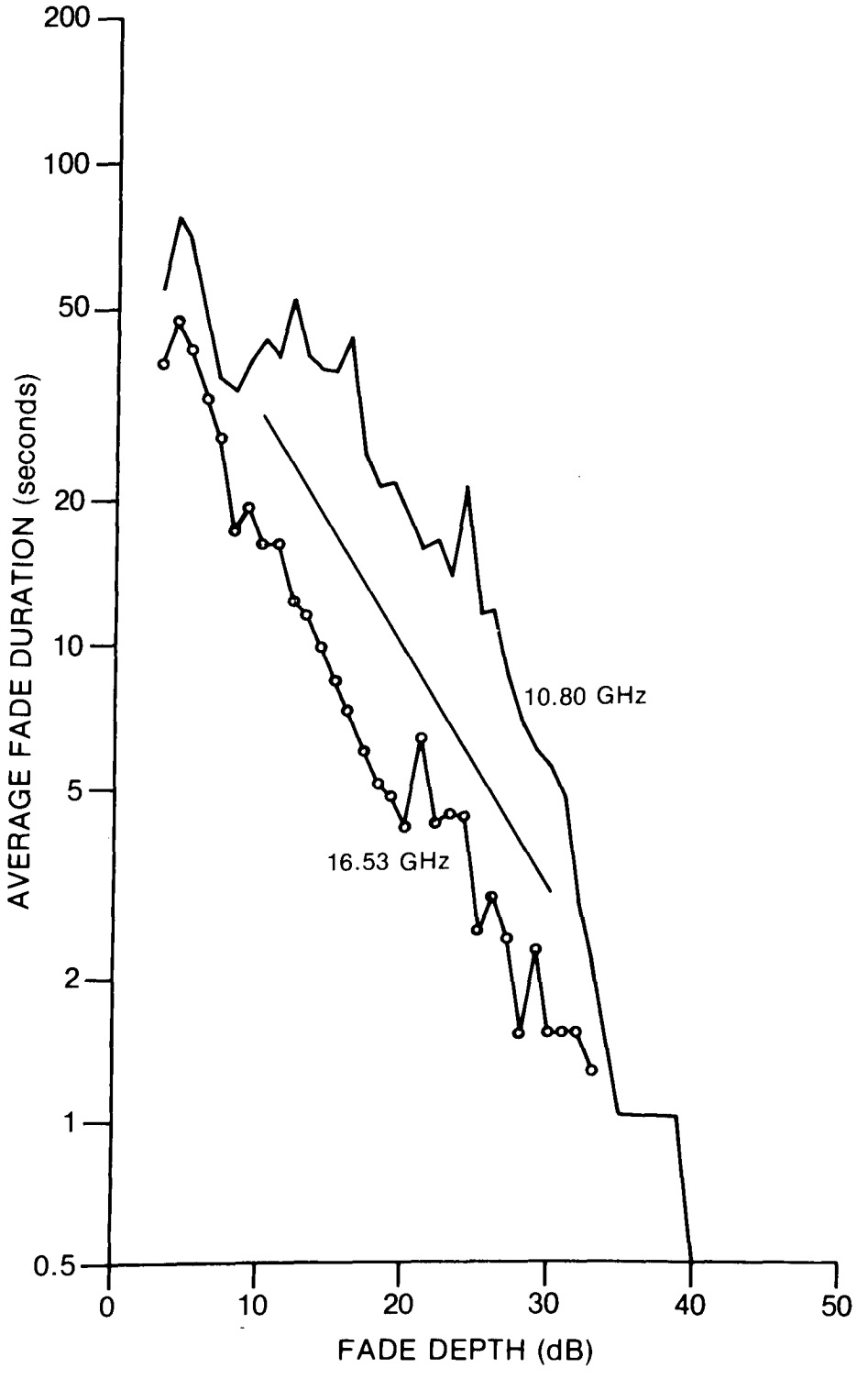

Figure 17. Clear-air fade average durations at 10.80 and 16.53 GHz, Corkery path, vertical polarization. The straight line has a slope of one decade of time per 20 dB fade depth.

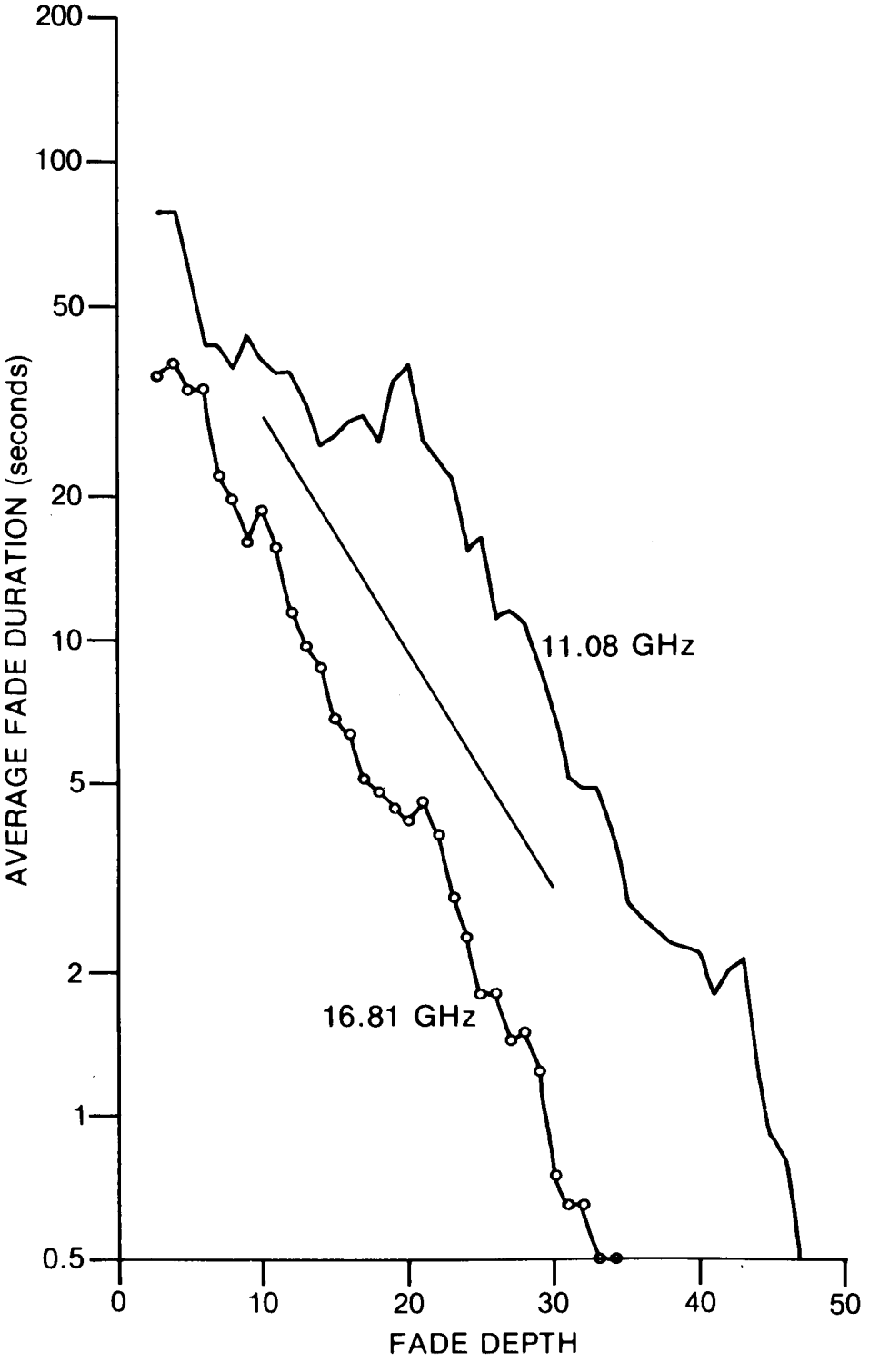

Figure 18. Clear-air fade average durations at 11.08 and 16.81 GHz, Corkery path, horizontal polarization. The straight line has a slope of one decade of time per 20 dB fade depth.

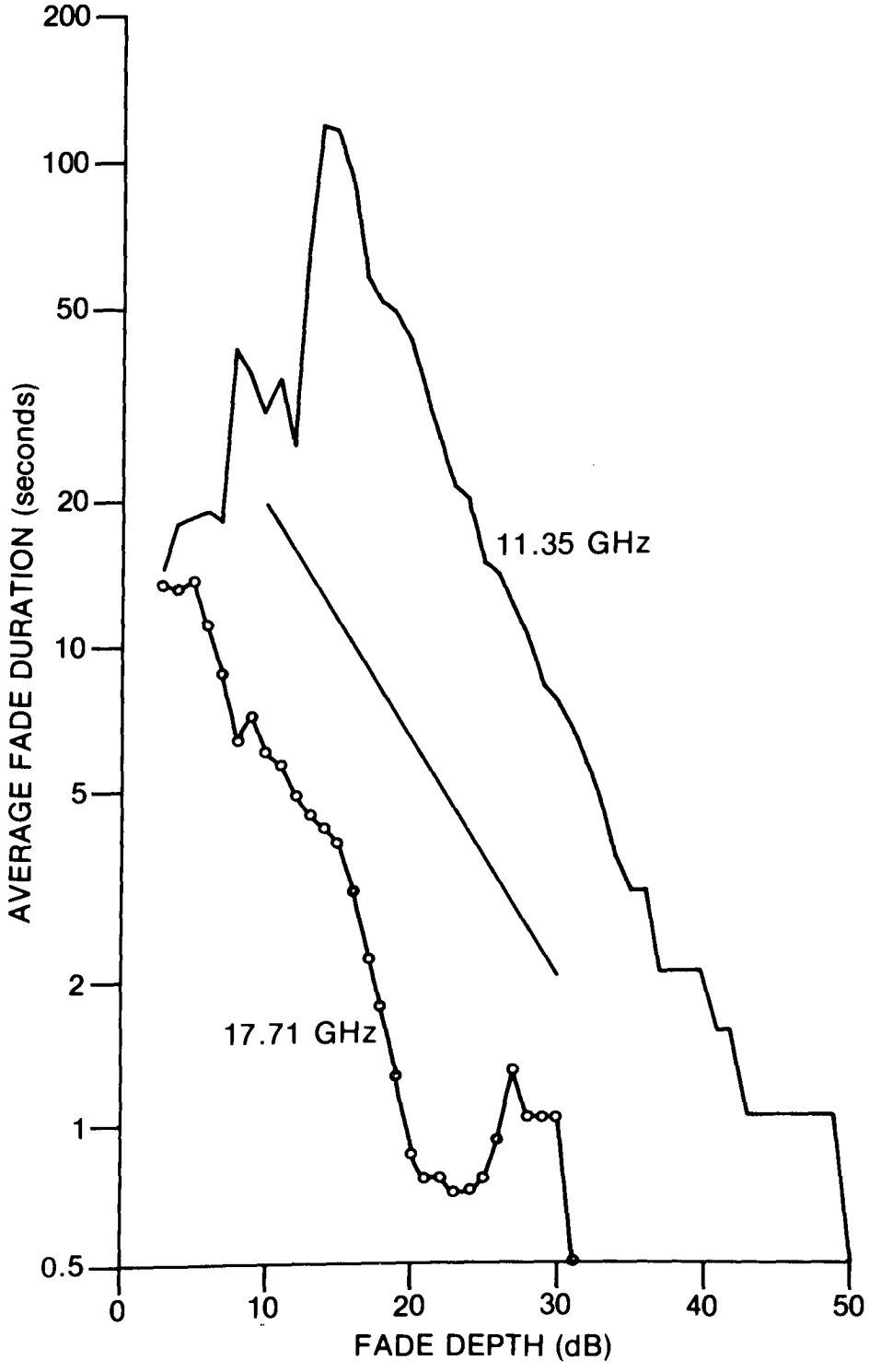

Figure 19. Clear-air fade average durations at 11.35 and 17.71 GHz, Kingsmere Path, horizontal polarization. The straight line has a slope of one decade of time per 20 dB fade depth.

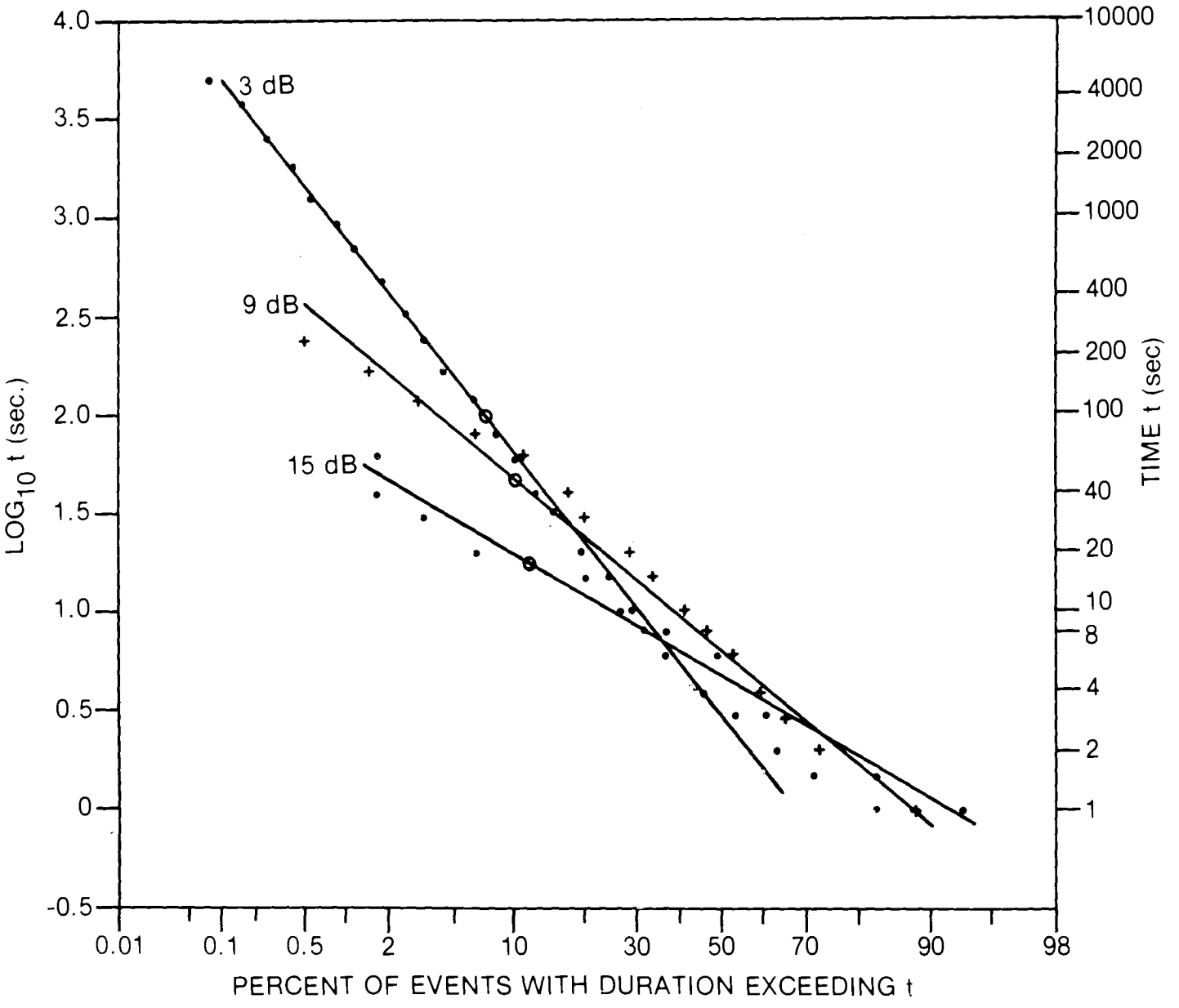

Figure 20. Conditional Distributions of fade durations at fade depths of 3, 9, and 15 dB, Corkery path, 16.53 GHz.

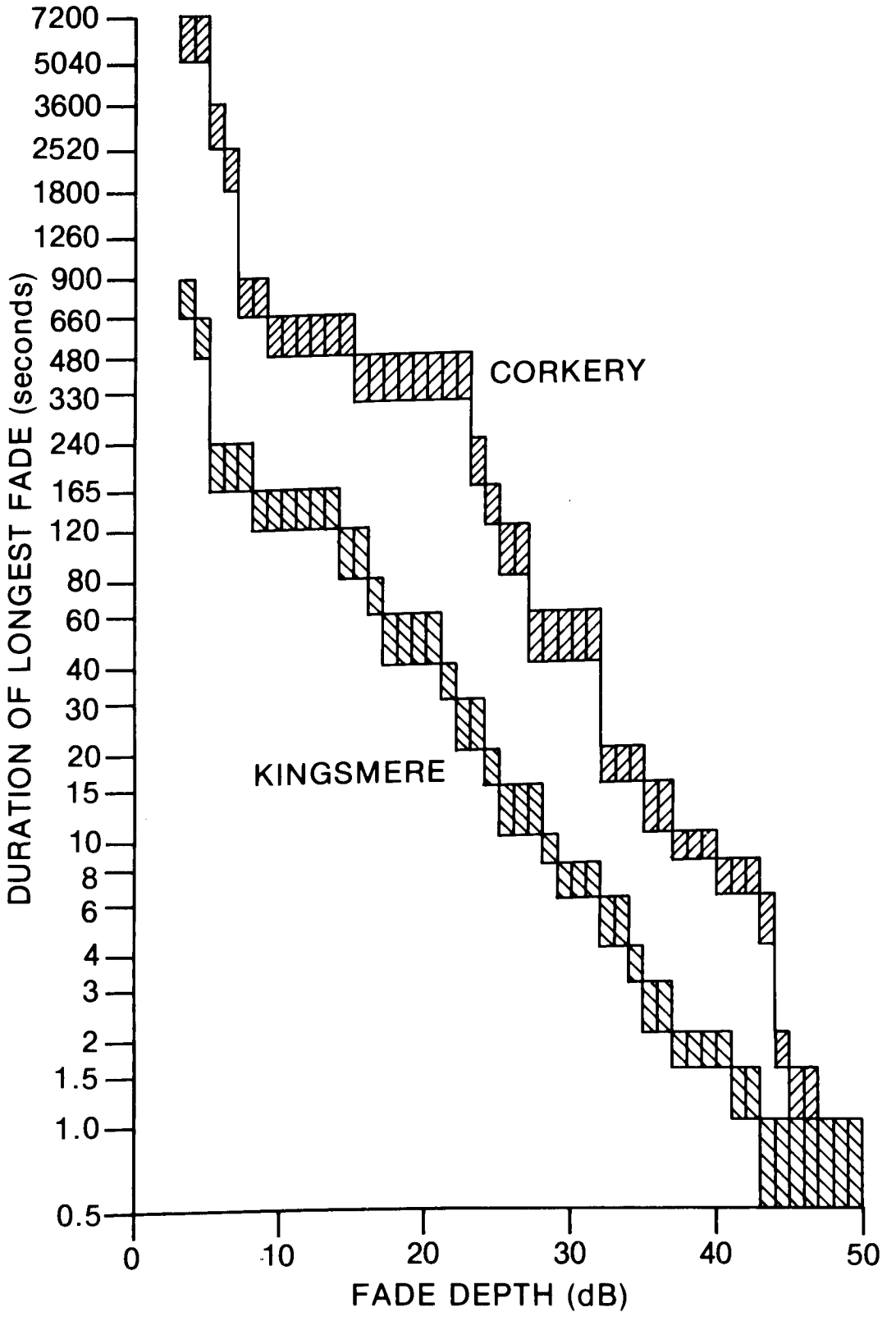

Figure 21. Durations of longest clear-air fades at 11 GHz on both paths. The abscissa scale is logarithmic.

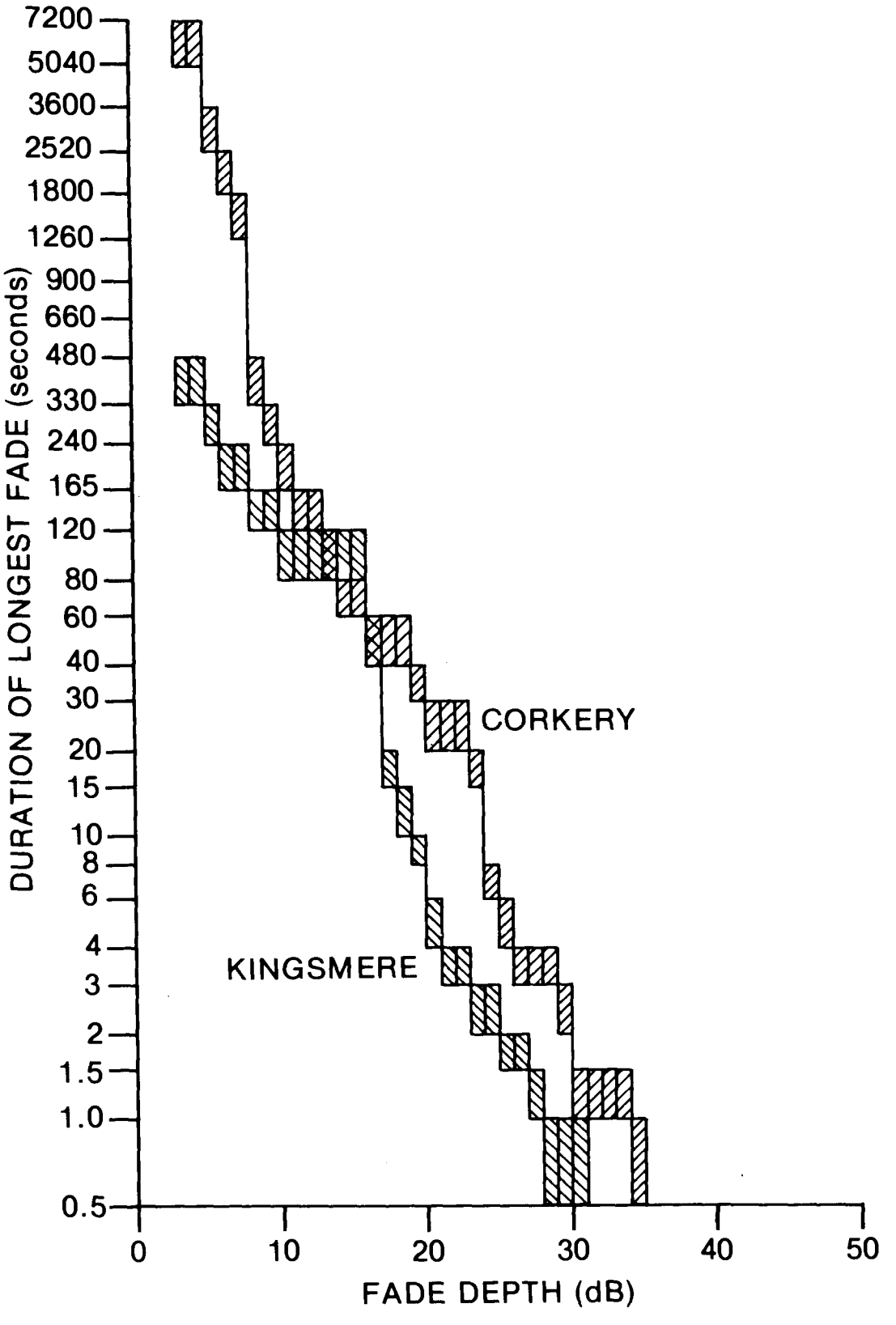

Figure 22. Durations of longest clear-air fades at 17 GHz on both paths. The abscissa scale is logarithmic.

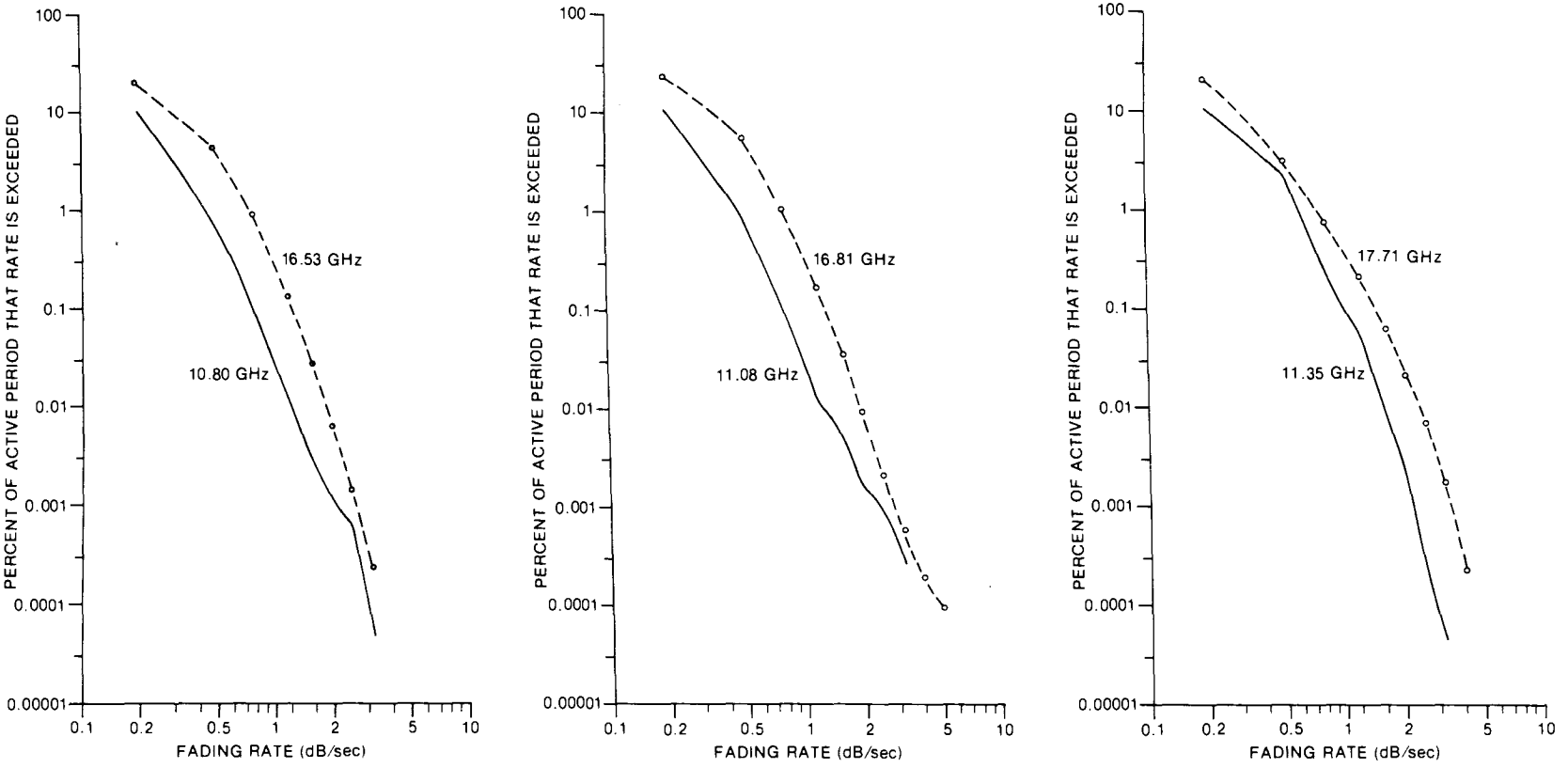

Figure 23. Cumulative distributions of rate of change of fade depth, for fade depths smaller than 3 dB. Left: Corkery path, vertical polarization; Centre: Corkery path, horizontal polarization; Right: Kingsmere path, horizontal polarization.

All periods for which clear-air fading of 3 dB or greater occured have been included in the present analysis, so that the percentages of time in the cumulative distributions of rates of change in Figures 24, 25, and 26, are properly referred to the whole sample period. Except at the extremes, the cumulative distributions on the Corkery path are well represented by a power law, so that the percentage of time for which a given fading rate is exceeded is proportional to (fading rate $)^{-2}$. In addition, at a given percentage of time the fading rate exceeded at 17 GHz is approximately 50% to 60% greater than at 11 GHz, which is consistent with the fading rate being directly proportional to frequency. This agrees with the result noted above for the case of enhancements and shallow fading. The greatest rate of change observed is about 30 dB/sec. The data from the Kingsmere path in Figure 26 are generally of the same form as the Corkery data, but at a given fading rate the percentages of time are about a factor of four or five smaller, which probably results from the smaller data sample available on the Kingsmere path.

The cumulative distributions of fading rate at fade depths of 20 dB and greater, averaged for the pairs of frequencies near 11 GHz and 17 GHz on the Corkery path, are shown in Figure 27, and are seen to be log-normal with the same variance. Since there is a tendency for greater fading rates to occur at greater depths, this allows estimates to be made of the (very small) probability of occurrence of very great fading rates. On the Kingsmere path the sample sizes are too small to be statistically reliable. This is also true on the Corkery path for data samples restricted to even greater fade depths than 20 dB. The existence of two fading components, as discussed earlier, probably accounts for the difference in the forms of distributions at greater and shallower fading depths: this will be treated in more detail later.

3.3 CLEAR-AIR CROSS-POLARIZATION PHENOMENA

3.3.1 Cross-polarization Statistics

The cross-polarized signal level received at each frequency remained relatively constant during day-time, and varied only moderately during most night-time periods. For example, as shown in Figure 8, the onset of the evening enhancement at about 1600 results in a slowly decreasing cross-polarization discrimination (XPD) at 11.08 GHz (the separation between the curves decreases), and in a slowly increasing XPD at 16.53 GHz (the separation between the curves increases). However, during active periods of clear-air direct-signal fading, the cross-polarized signal also becomes highly variable. For example, in Figure 9, the interval from about 40 to 100 minutes has seven minima in the cross-polarized signal level which are not matched by strong direct signal fading: at these times the XPD becomes very large. Conversely, in Figure 9, at about 16 minutes and 113 minutes deep fades of the direct signal occur which are not matched by strong cross-polarized signal minima: at these times the XPD becomes quite small. As shown in Figure 10, the XPD can become zero (or negative, in some cases) when the cross-polarized signal level is essentially invariant at times of very strong fading of the direct signal. Such changes in the cross-polarized signal level were found to be almost totally uncorrelated at different frequencies on the same path. The Kingsmere path differed from the Corkery one by about an order of magnitude in the frequency of occurrence of these cross-polar variations, as it does in the case of direct signal fading.

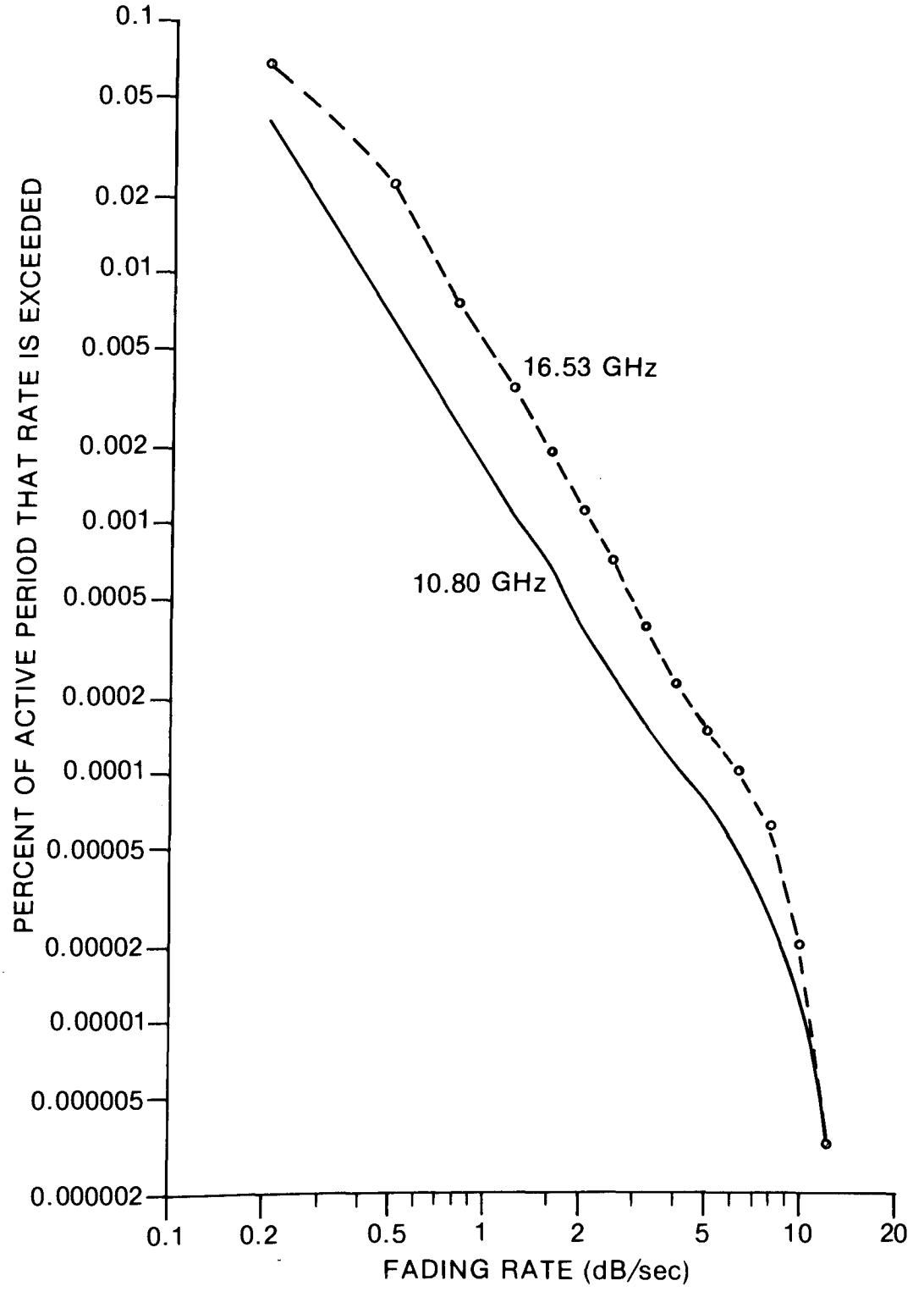

Figure 24. Cumulative distributions of rate of change of fade depth, for fade depths of 3 dB and greater, Corkery path, vertical polarization.

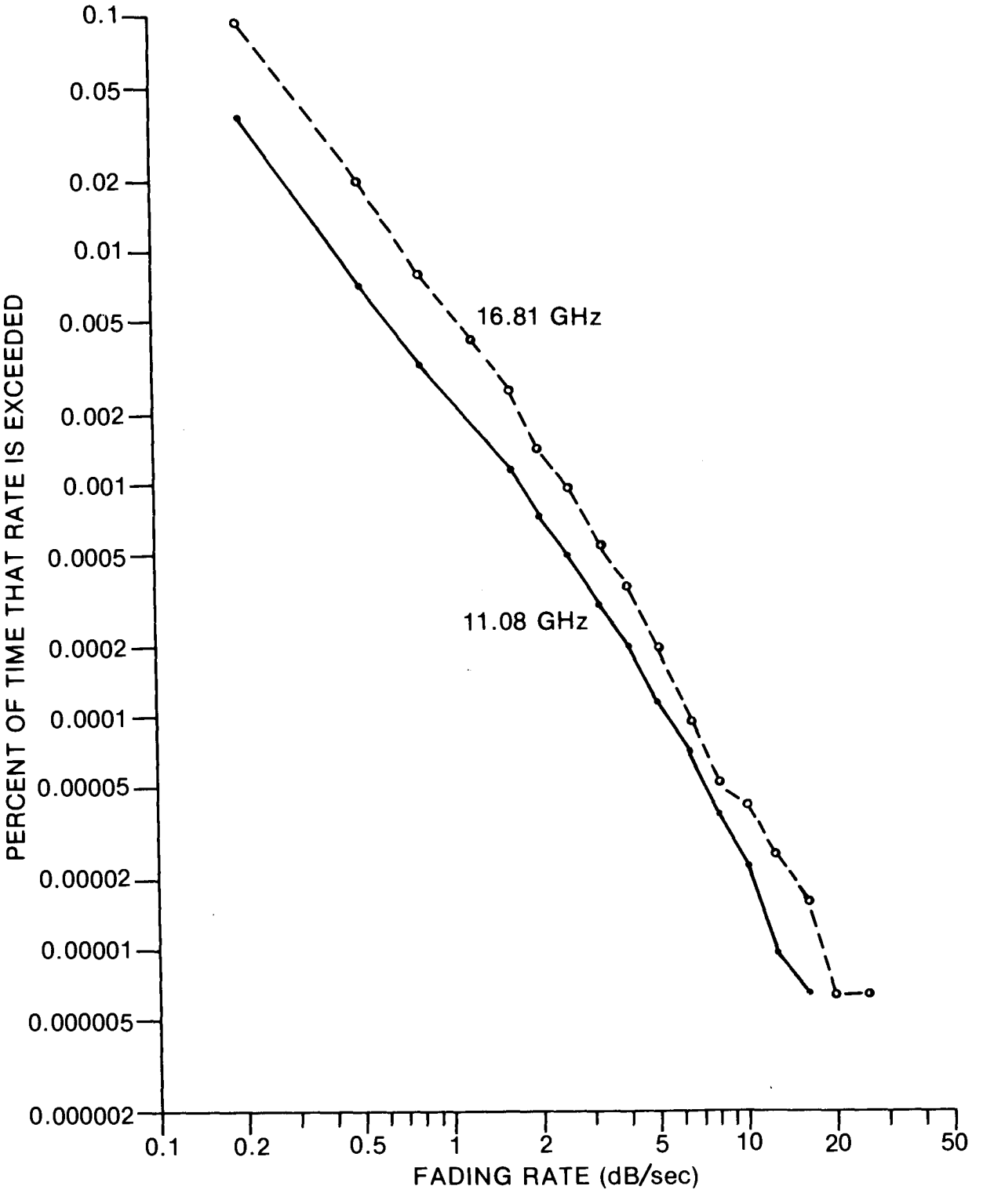

Figure 25. Cumulative distributions of rate of change of fade depth, for fade depth of 3 dB and greater, Corkery path, horizontal polarization.

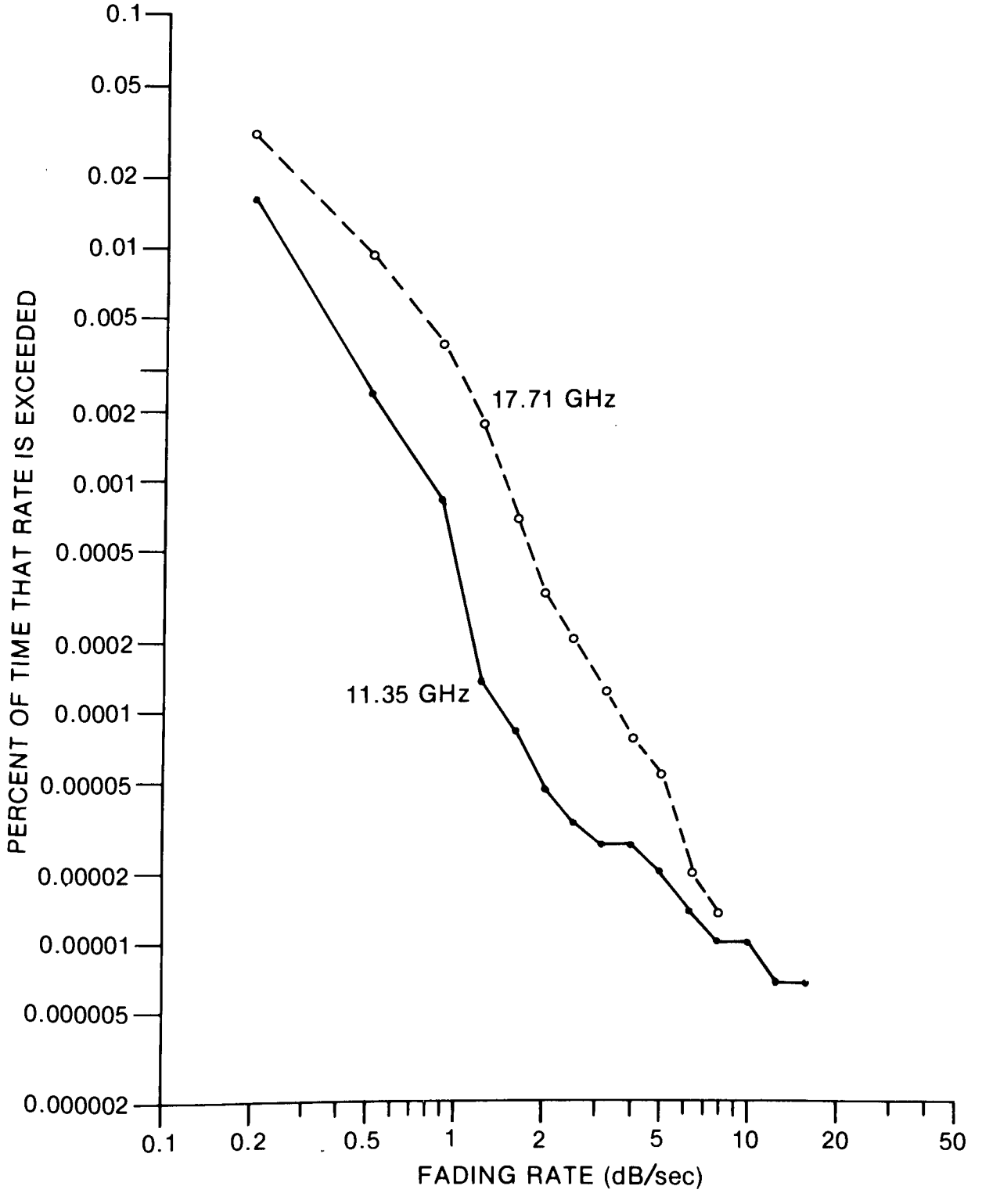

Figure 26. Cumulative distributions of rate of change of fade depth, for fade depths of 3 dB and greater, Kingsmere path, horizontal polarization.

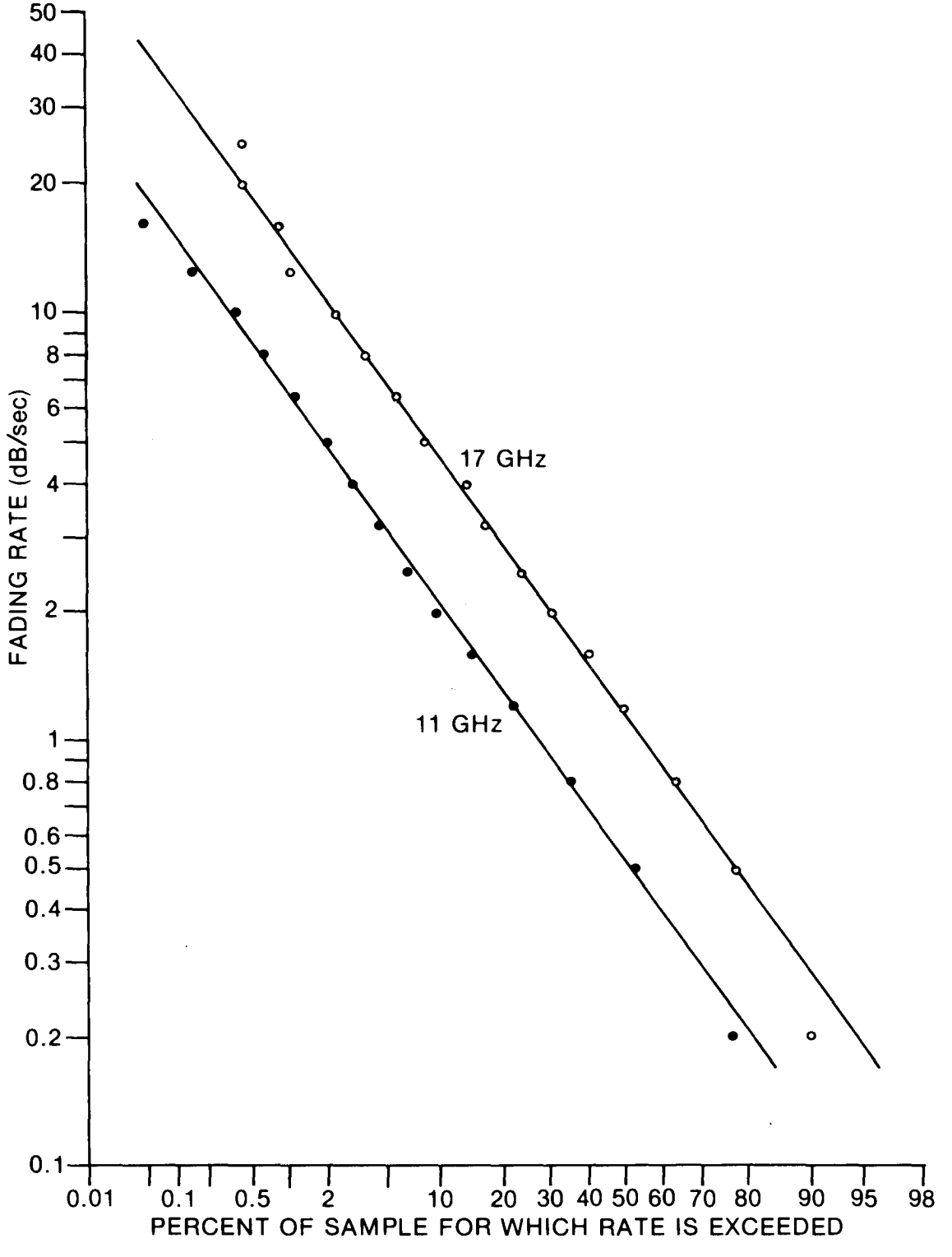

Figure 27. Cumulative distributions of rate of change of fade depth, for fade depths of 20 dB and greater, Corkery path, both polarizations.

The cumulative distributions of cross-polarization discrimination (XPD) during clear air conditions are given in Figures 28, 29, and 30. The distributions are approximately normal over the 5% to 95% range, but differ significantly from normality at both extremes: the median values have been given in Table 2.1. It is obvious in every case that the distributions are composite, with a transition at about 0.01% of the time on the Corkery path, and at about 0.001% of the time on the Kingsmere path, from a steeply declining curve to a much more slowly falling one. This transition corresponds to the onset of very active fading of the direct signal (as in Figure 10) which is attributed to multipath interference.

3.3.2 Relations Between Direct and Cross-polarized Signal Fading

Equiprobable values of fade depth and cross-polarization discrimination have been plotted in Figure 31 for the frequencies on the Corkery path. A reasonable fit in each case can be made using two straight line segments. One of these, extending to large fade depths and small XPD, has a slope of -1 in each case. It corresponds to the regime in which the cross-polar signal level is constant during deep fading of the direct signal. The other line segment has a much smaller slope and corresponds to the regime of shallower, longer-lasting fading. The intersection of the lines thus corresponds roughly to a change in the type of fading, both in depth and duration. It seems certain that the very deep fading is caused by multipath interference, while the shallower type may result from variations in the angle of arrival of the signal. On this assumption an estimate of the maximum value of the angle of arrival can be made. The mean fading depth at the transition point for the two 11 GHz frequencies is about 19.5 dB, which corresponds approximately to alignment of the -10 dB points on the 11 GHz antenna beams. At the 17 GHz frequencies the mean fading depth is about 12.5 dB, corresponding to alignment of the -6 dB points of the 17 GHz antenna beams. These alignments agree, and are consistent with an extreme angle of arrival of about 1.2° from the receiving antenna axis, or about 1.4° from the horizontal. This agrees very well with the direct measurements of angle of arrival made by Webster and Lam (1980) in south-western Ontario in the 9 GHz frequency band.

When a similar plot is made from the data from the Kingsmere link the results are not consistent with the argument given above. The XPD data at large fade depths have a steeper slope than -1, the complete data set cannot be well represented by only two straight line segments, and attempts to perform such a fit lead to disagreement between the 11 GHz and 17 GHz results. The poorer statistics of the small Kingsmere data set may be partly responsible for this, but an absence of moderate, long-lasting fading is qualitatively obvious, as mentioned earlier. Thus it appears reasonable to conclude that significant beam deflections resulting in large angle-of-arrival variations did not occur on this path.

Figure 31 allows a convenient comparison of the relative importance of clear-air fading and depolarization on the availability of dual-polarized frequency re-use communications systems for moderate path lengths. Thus, for example, at 10.80 GHz when the fade depth is 30 dB, the XPD has deteriorated to 12 dB, and the results are similar at the other frequencies. It appears that clear-air depolarization will be an important limiting factor, therefore, in system design.

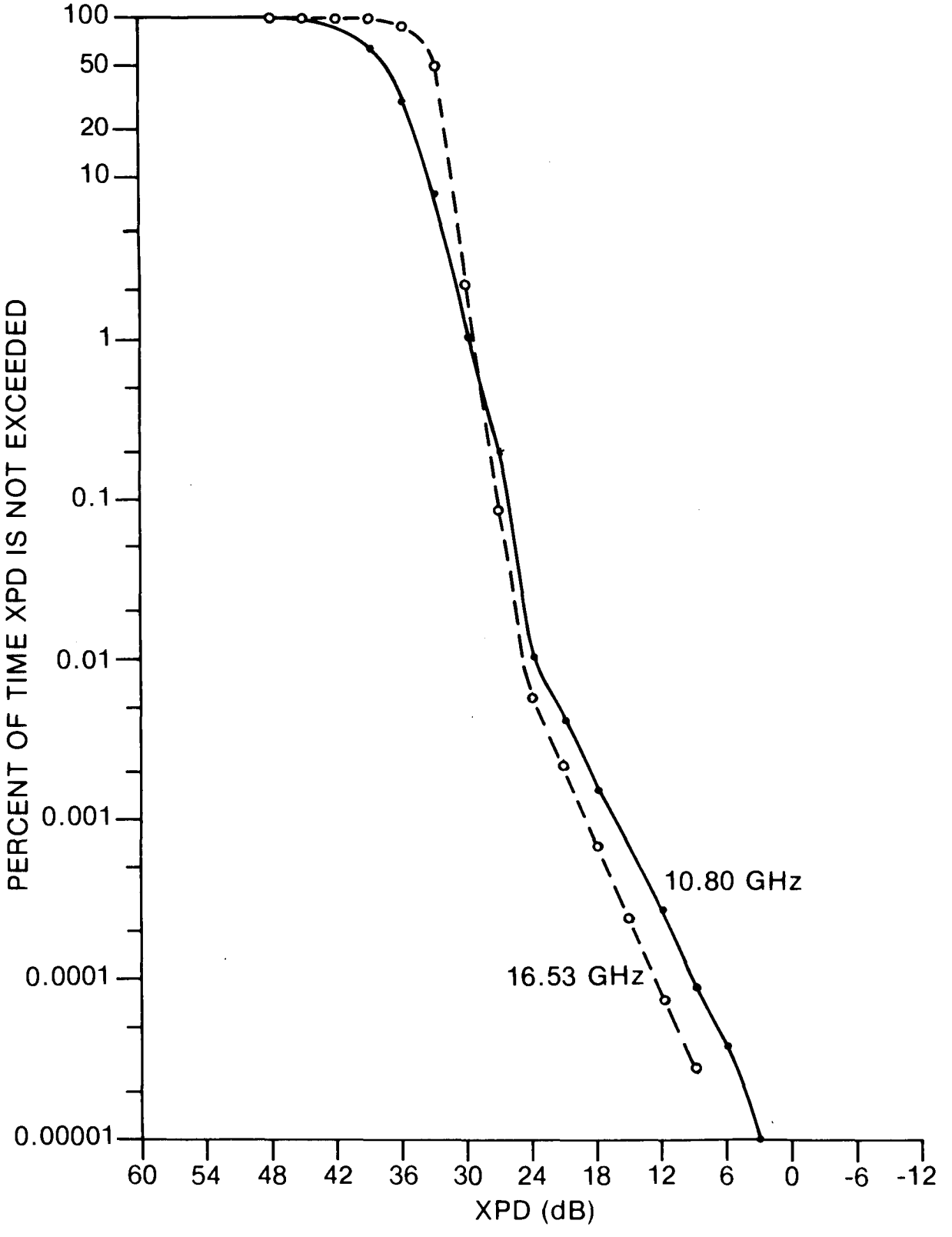

Figure 28. Cumulative distributions of clear-air cross-polarization discrimination; Corkery path, vertical polarization.

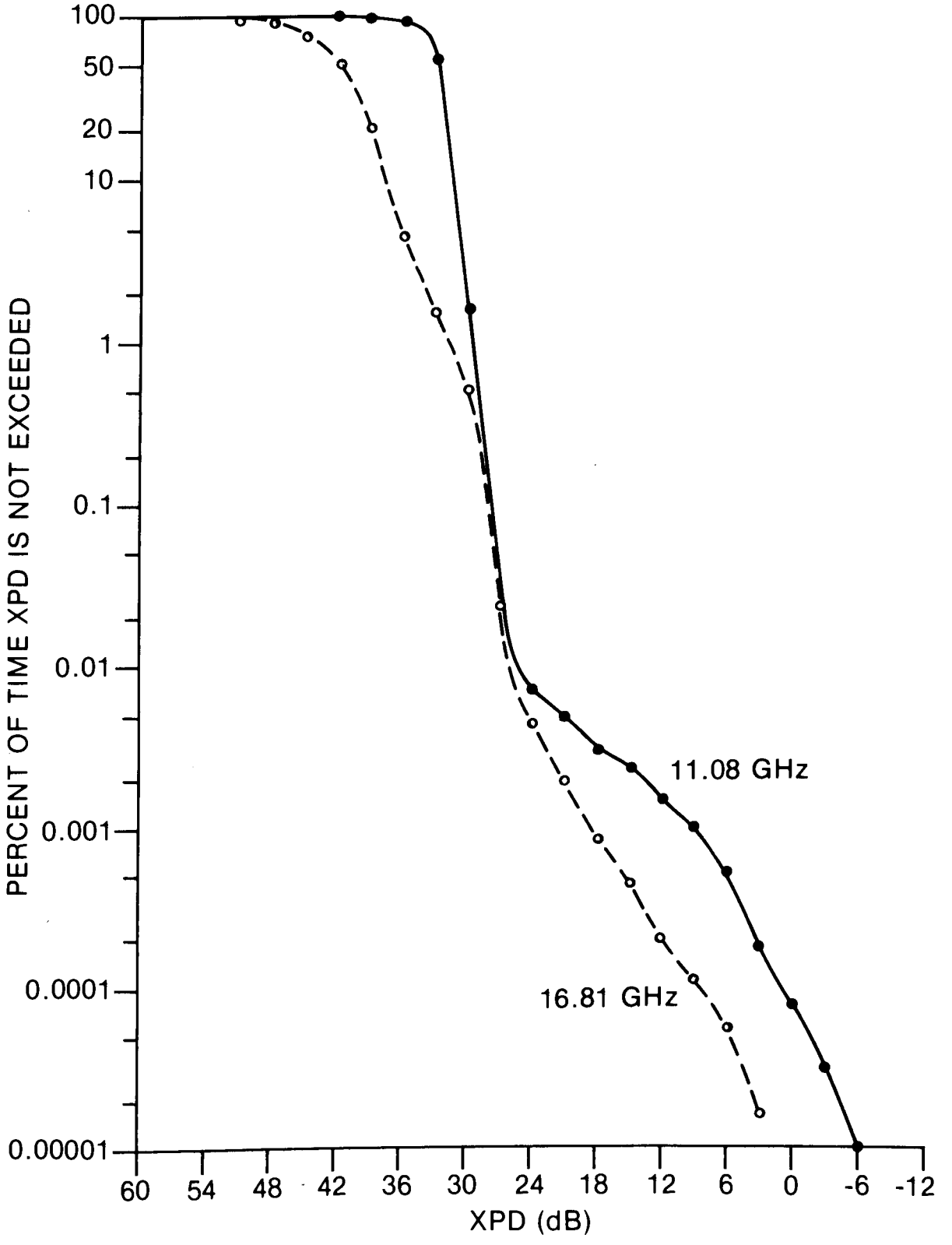

Figure 29. Cumulative distributions of clear-air cross-polarization discrimination; Corkery path, horizontal polarization.

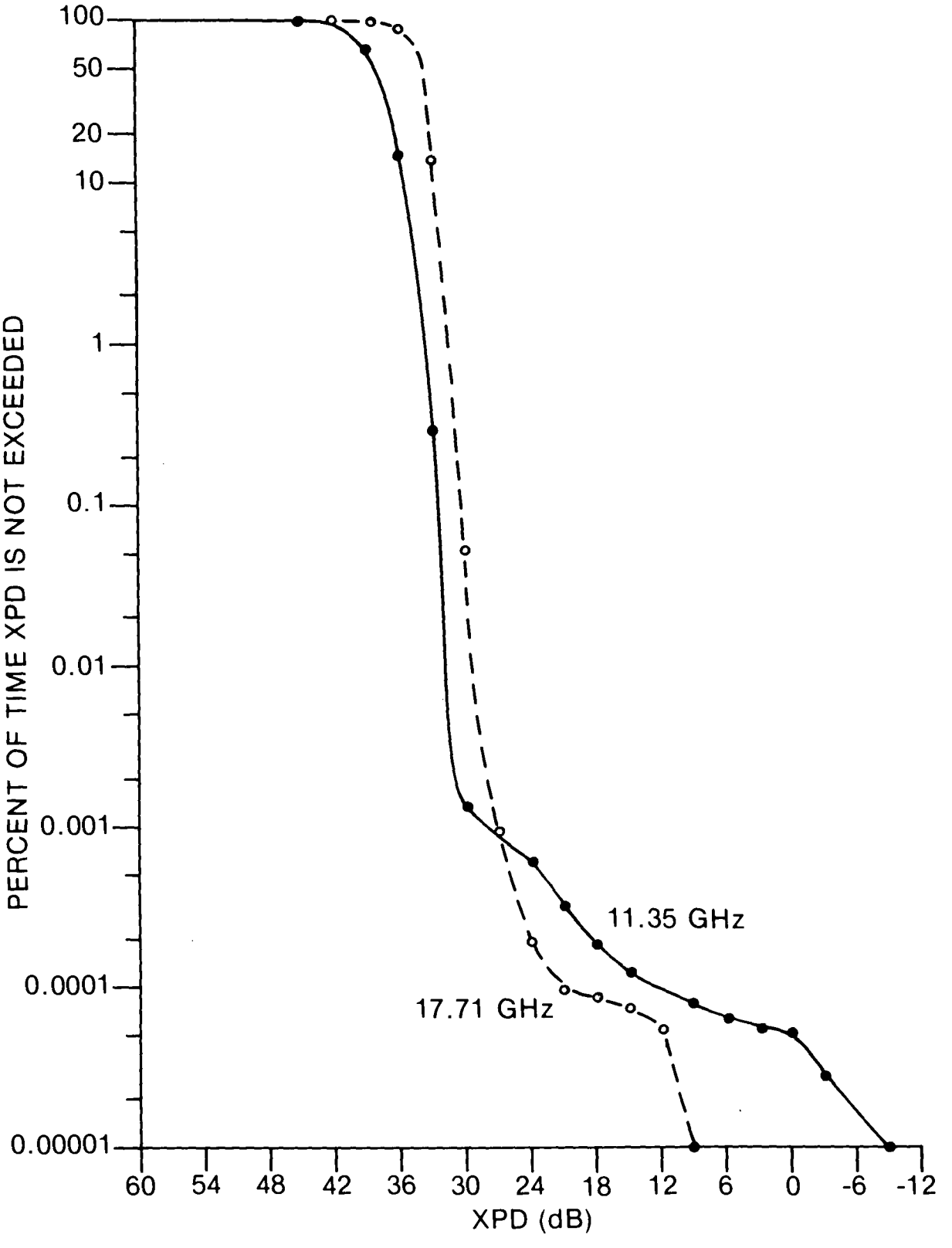

Figure 30. Cumulative distributions of clear-air cross-polarization discrimination; Kingsmere path, horizontal polarization.

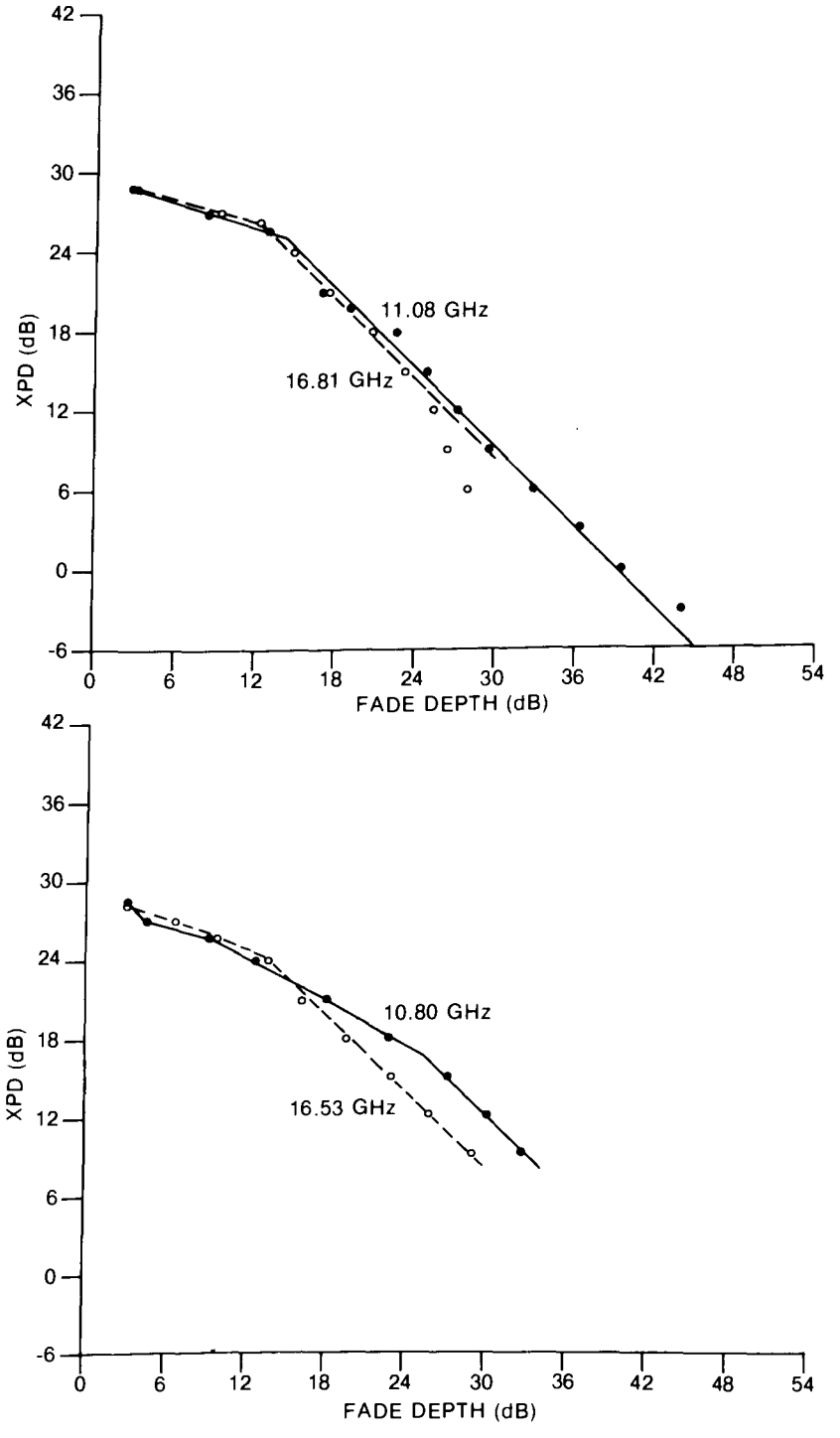

Figure 31. Equiprobable fade depth and cross-polarization discrimination in clear air; Corkery path. Upper: horizontal polarization; Lower: vertical polarization.

In Figures 32, 33, 34 the equiprobability XPD data have been plotted against fade depth, together with the root-mean-square (rms) and the median XPD, each calculated at 5 dB increments of fade depth for intervals 5 dB wide, except at 0 dB where the intervals were 1 dB wide in fade depth. The mean XPD has been plotted as well in Figure 33a, at 11.08 GHz: at the other frequencies it has been omitted to reduce crowding but its relation to the other central measures is similar. The consistency in the trends of all these measures for the Corkery data is striking, and confirms that for fade depths (or co-polar attenuation, CPA) greater than about 15 dB the relation XPD = -CPA + Constant, holds regardless of whether the mean, median, rms, or equiprobable XPD is used. For the Kingsmere links it appears that the equiprobable data do not agree well with the other measures, but this conclusion may not be statistically significant.

The theory developed by Mottl (1977) was used to derive the curves fitted to the rms data in Figures 32, 33, and 34. In this theory the cross-polarization interference is assumed to be the sum of two components, one proportional to the co-polar signal and the other having a random phase and amplitude distribution, so that the cross-polar (XP) and "in-line" (IL) signal amplitudes are related by:

$$V_{XP} = \left| k\, V_{IL} + \varepsilon\, e^{j\phi} \right|$$

If the conditional distributions of V_{XP} are Rayleigh distributed, then V_{XP} is Rice-Nakagami distributed and

$$V_{XP\ (rms)} = \left(k^2\, V^2_{IL} + \varepsilon^2 \right)^{\frac{1}{2}}$$

This equation can be used to deduce that

$$XPD_{rms} = -10 \log \left[k^2 + \varepsilon^2_{rms}\ 10^{CPA/10} \right]$$

which for large values of CPA (or sufficiently small k values) reduces to the earlier form

$$XPD = -CPA + Constant$$

as shown by Olsen (1981a), where

$$Constant = -20 \log \varepsilon_{rms}$$

However, while the fit of the curves to the data is excellent, the conditional distributions of the data are not Rayleigh in form, unlike the Bell Laboratories data (Lin, 1977) to which the model was first applied. In Figure 35 the conditional distributions of cross-polar signal level at a fade depth of 10 dB are seen to be normal at the 11 GHz Corkery frequencies, so that the signal amplitude distribution is log-normal: this behaviour is also observed at the other fade depths for which the statistics are adequate. However, in Figure 36, the conditional distributions at the 17 GHz Corkery frequencies are not log-normal. This is probably a result of loss of data because of the limited dynamic range of the cross-polarized receiver, which

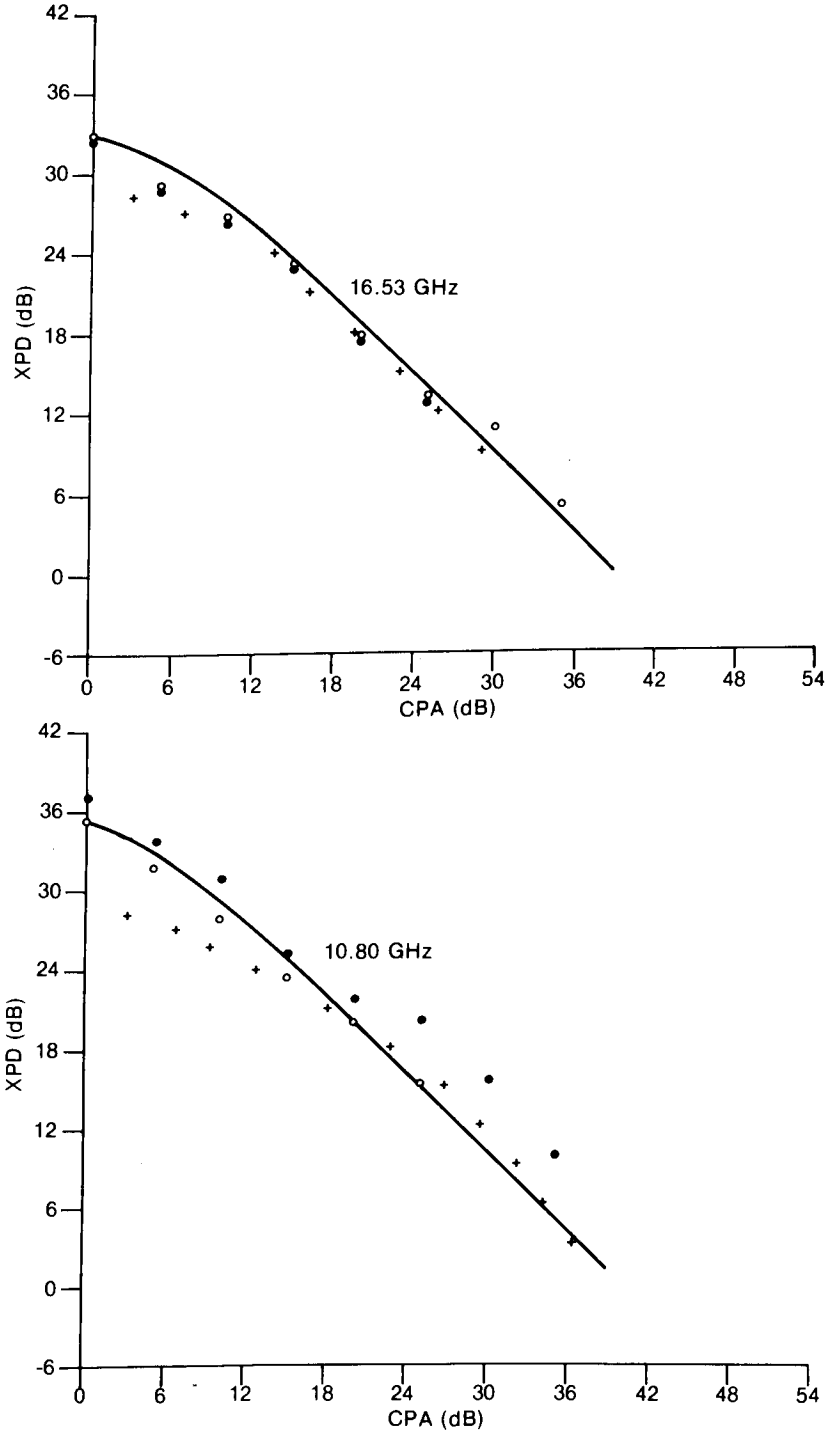

Figure 32. Median (dots), root-mean-square (circles), and equiprobable (crosses) cross-polarization discrimination as functions of fade depth (CPA) in clear air; Corkery path, vertical polarization.

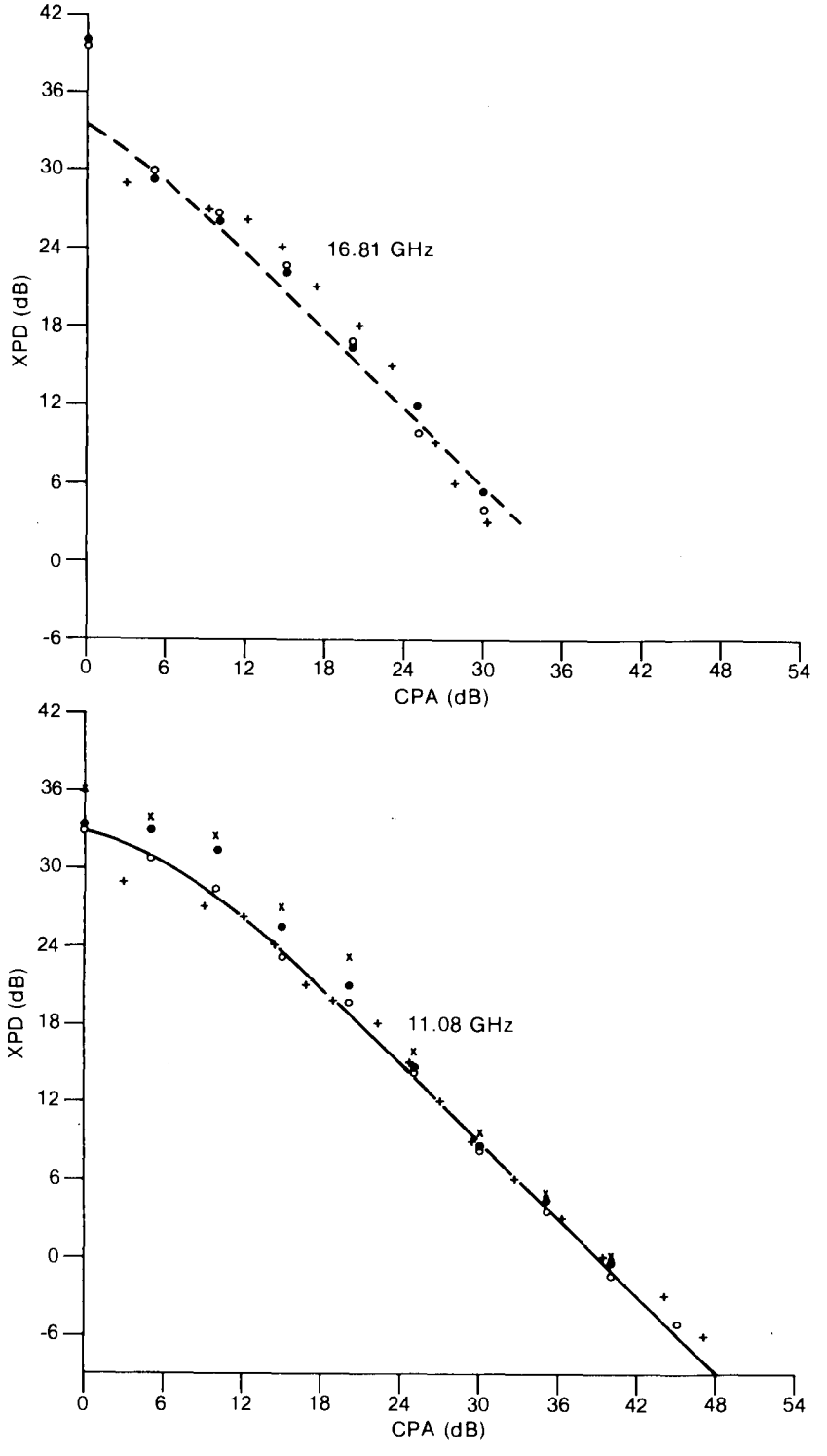

Figure 33. Mean (exes), median (dots), root-mean-square (circles), and equiprobable (crosses) cross-polarization discrimination as functions of fade depth (CPA) in clear air; Corkery path, horizontal polarization.

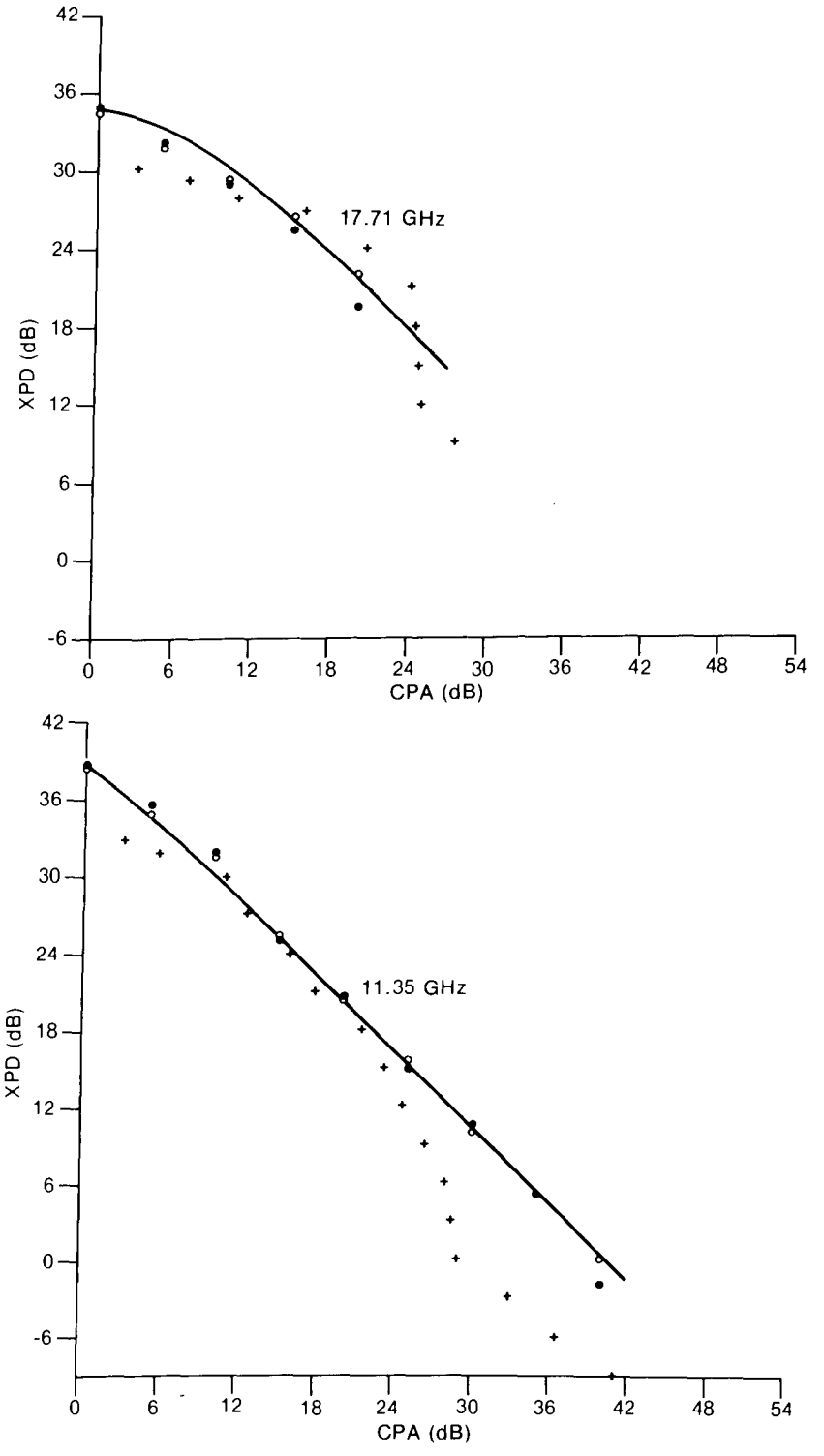

Figure 34. Median (dots), root-mean-square (circles), and equiprobable (crosses) cross-polarization discrimination as functions of fade depth (CPA) in clear air; Kingsmere path, horizontal polarization.

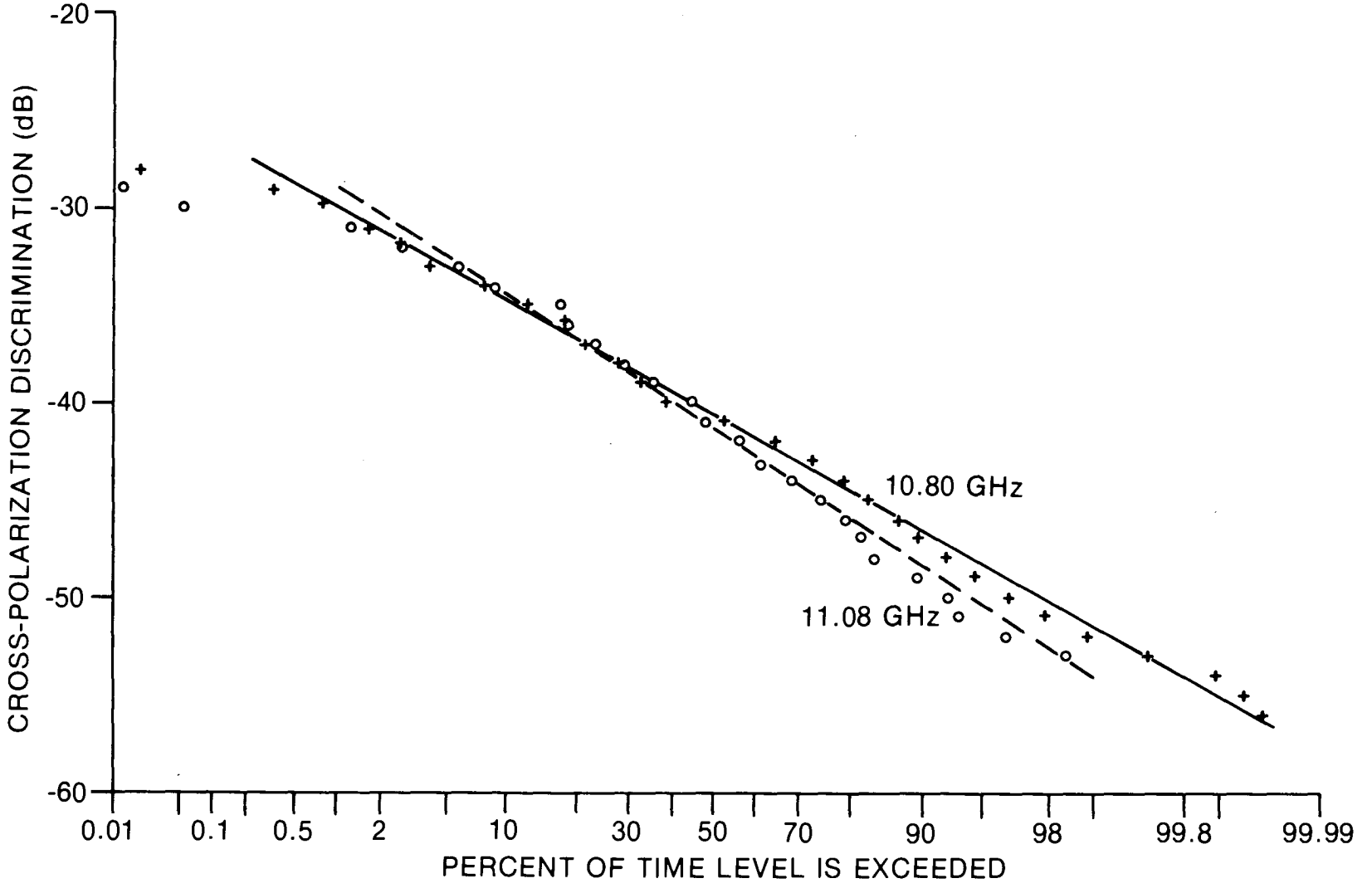

Figure 35. Conditional distributions of cross-polarization discrimination at 10 dB fade depth in clear air, Corkery path, 11 GHz.

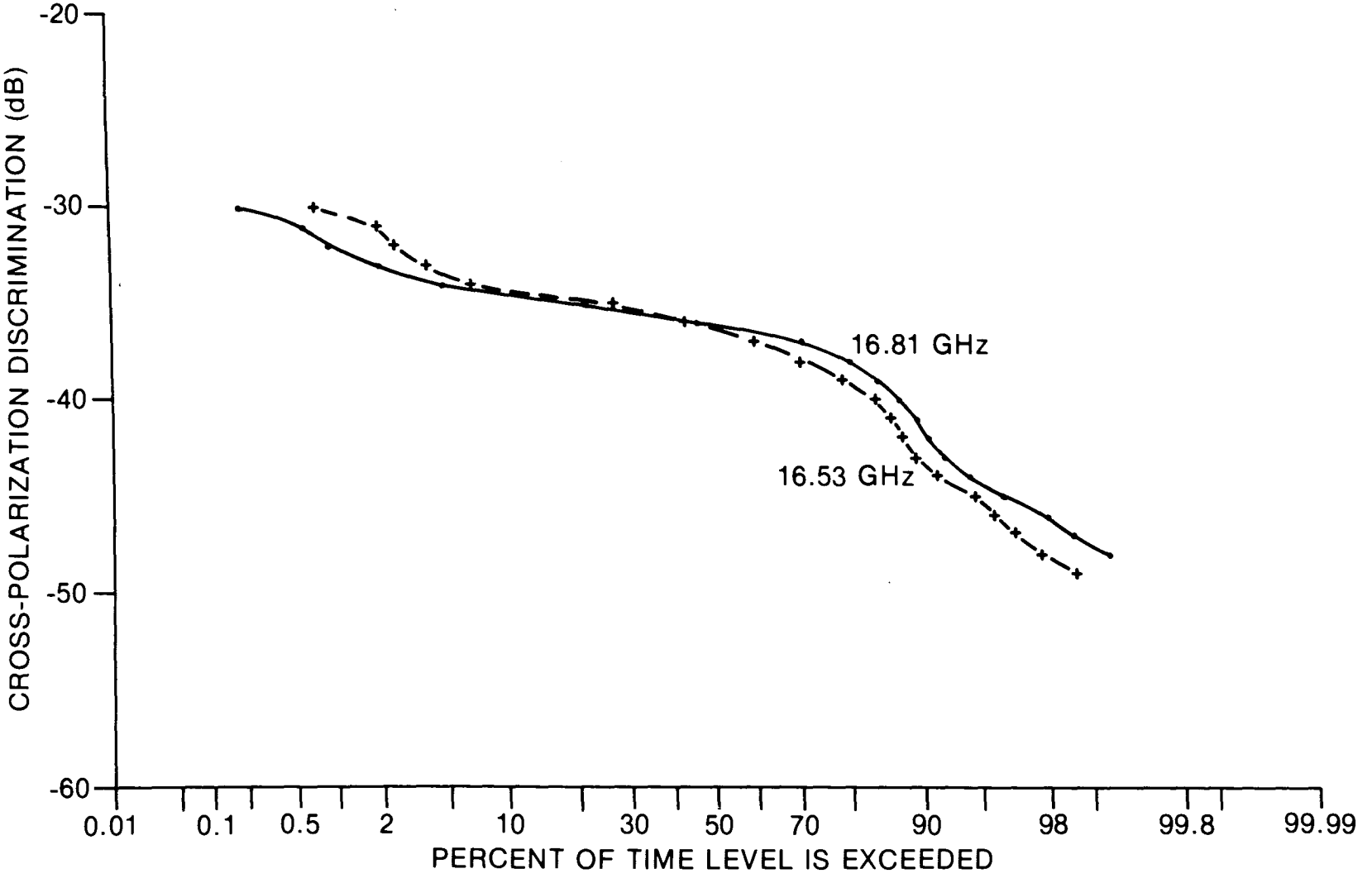

Figure 36. Conditional distributions of cross-polarization discrimination at 10 dB fade depth in clear air; Corkery path, 17 GHz.

skews the distribution to higher signal levels, so that no firm conclusion about the form of the distribution can be drawn at 17 GHz. The behaviour at 11 GHz, however, agrees with similar observations performed in France (Martin, 1977). Olsen (1981a) has discussed this topic in detail, making use of the results given here.

3.4 PROPAGATION THROUGH PRECIPITATION

Light to moderate rainfall is usually widespread, that is, typical dimensions exceed the 16 km lengths of the present paths, so that both paths tend to experience approximately the same propagation conditions at such times. However, intense rainfall, particularly during thunderstorms, occurs over areas with dimensions of only a few kilometers, so that in general large attenuations are not experienced simultaneously on the two paths. In addition there appear to be topographic influences in the Ottawa area which produce differences in the precipitation patterns immediately over the river valley and in the adjacent areas. Thus one does not expect to find identical results during propagation through precipitation on the two paths, and this expectation is confirmed by the observations.

3.4.1 Rainfall Attenuation Statistics

The cumulative distributions of rainfall attenuation are presented in Figure 37 for the frequencies on the Corkery path and in Figure 38 for those on the Kingsmere path. As discussed earlier, the Kingsmere statistics are essentially complete and those from Corkery at 10.80 GHz are almost complete: they therefore give a reliable picture of the distribution. The effective path length calculated by the formula given in CCIR (1982a) is about 9.3 km, and the rainfall intensity exceeded for 0.01% of the time is about 37 mm/hr (Segal, 1979). Using the specific attenuations recommended by CCIR (1982b), the predicted attenuations exceeded for 0.01% of the time are thus 11.9 dB at 11.35 GHz and 29.4 dB at 17.71 GHz. These results are only about 15% smaller than the observed values of 13.0 dB and 34.2 dB, respectively, at the 0.02% level, which for our six month time base corresponds approximately to 0.01% of the year.

All the 17.71 GHz data and the 11.35 GHz data at fade depths less than about 30 dB are well fitted by a power law with the same exponent:

$$P(\%) = 0.340\ [A(dB)]^{-1.375} \qquad (11.35\ GHz)$$

$$P(\%) = 1.273\ [A(dB)]^{-1.375} \qquad (17.71\ GHz)$$

These functions are so close to the data points as to be hardly distinguishable on the scale of Figure 38, hence they have not been plotted. This power law is equivalent to the functional form of equation (10) of CCIR (1982a),

$$A_p = A_{0.01}(P/0.01)^{-a}$$

where P is percentage of time and A is attenuation. For the present data a = 0.727, which is significantly larger than the values suggested by CCIR (1982a), namely:

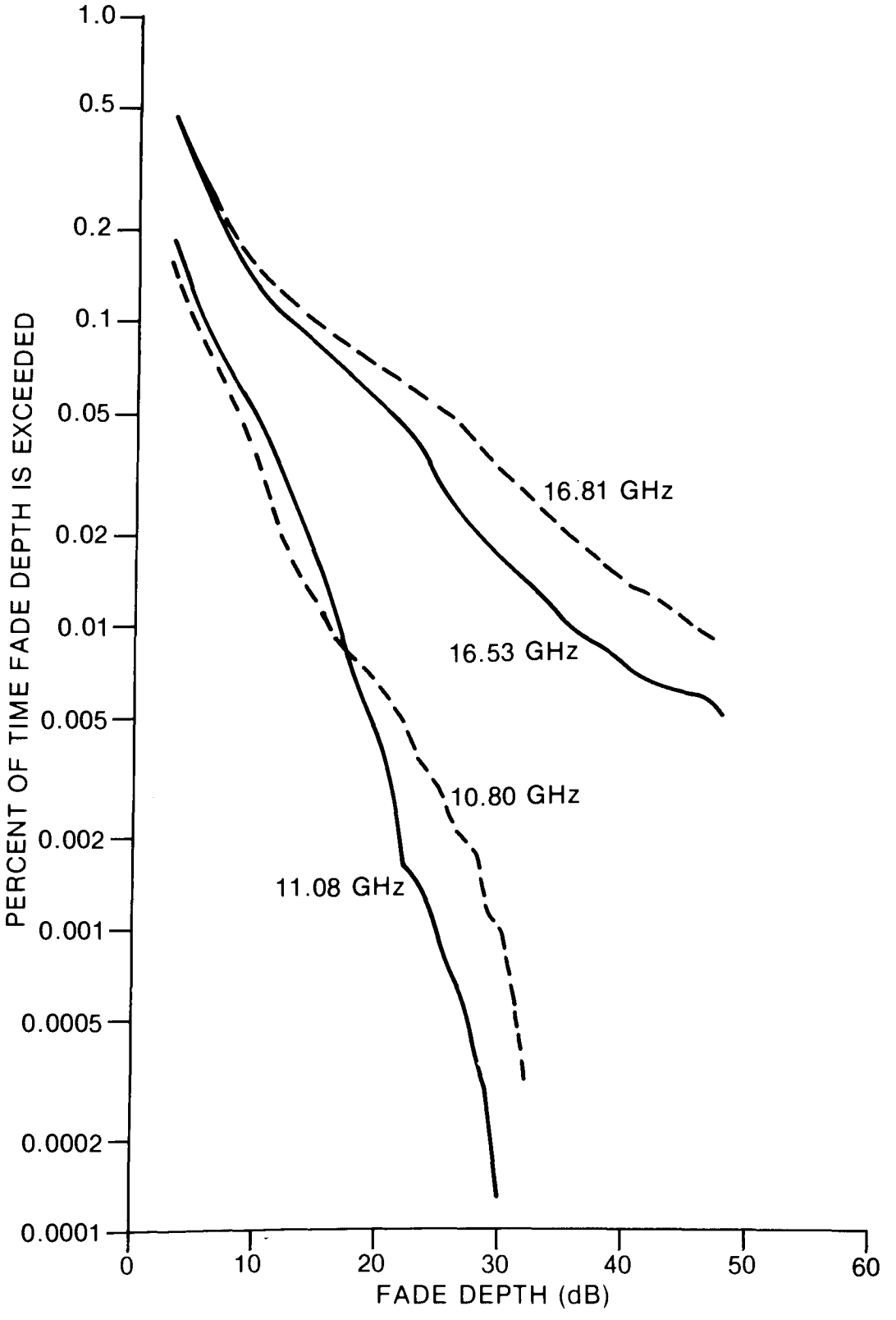

Figure 37. Cumulative distributions of fade depth during rainfall; Corkery path.

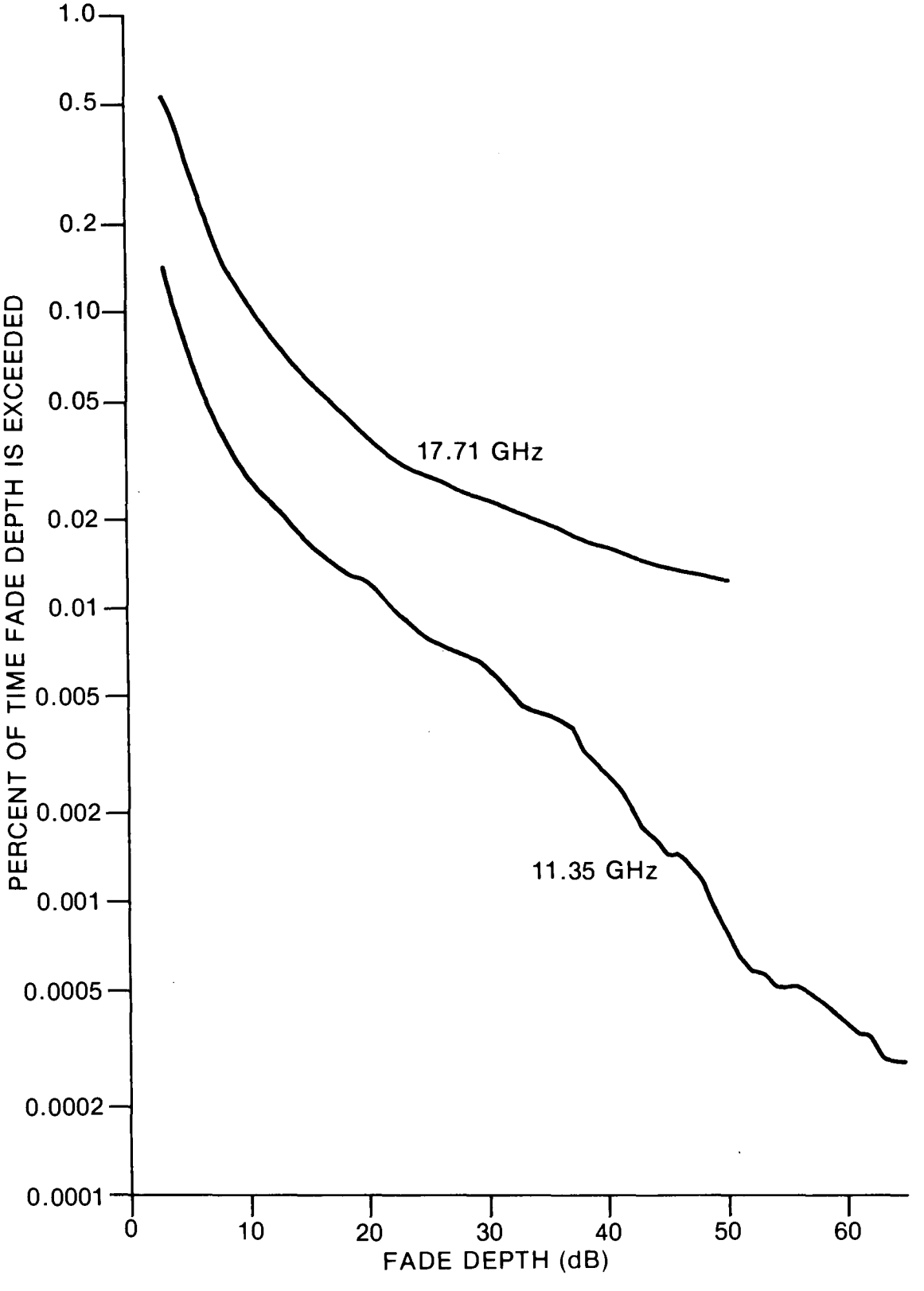

Figure 38. Cumulative distributions of fade depth during rainfall; Kingsmere path.

$$a = 0.33 \text{ for } 0.001 \leq P \leq 0.01\%$$

$$a = 0.41 \text{ for } 0.01 < P \leq 0.1\%$$

There is no clear suggestion in the present data that a changes for different ranges of P. The discrepancy at 11.35 GHz for A>30 dB largely results from a loss of data part way through a single severe attenuation event, which has proportionately reduced the cumulative time at large fade depths more than at smaller ones. Similar, but much more extensive, losses of data may explain why the Corkery observations are not well fitted by this power law.

3.4.2 Frequency and Polarization Scaling

For each separate precipitation event scatter plots were made of the attenuations observed for various pairs of signals, differing either in frequency or in polarization, and straight lines were fitted to these data. In almost every case the quality of the linear fit was excellent, with scatter commonly of the order of 1 dB over a 40 dB or greater dynamic range. A typical example of such a plot is shown in Figure 39 for the pair of frequencies 10.80/16.53 GHz. In every case the slope is equal to the average ratio of the attenuations for those sets of data.

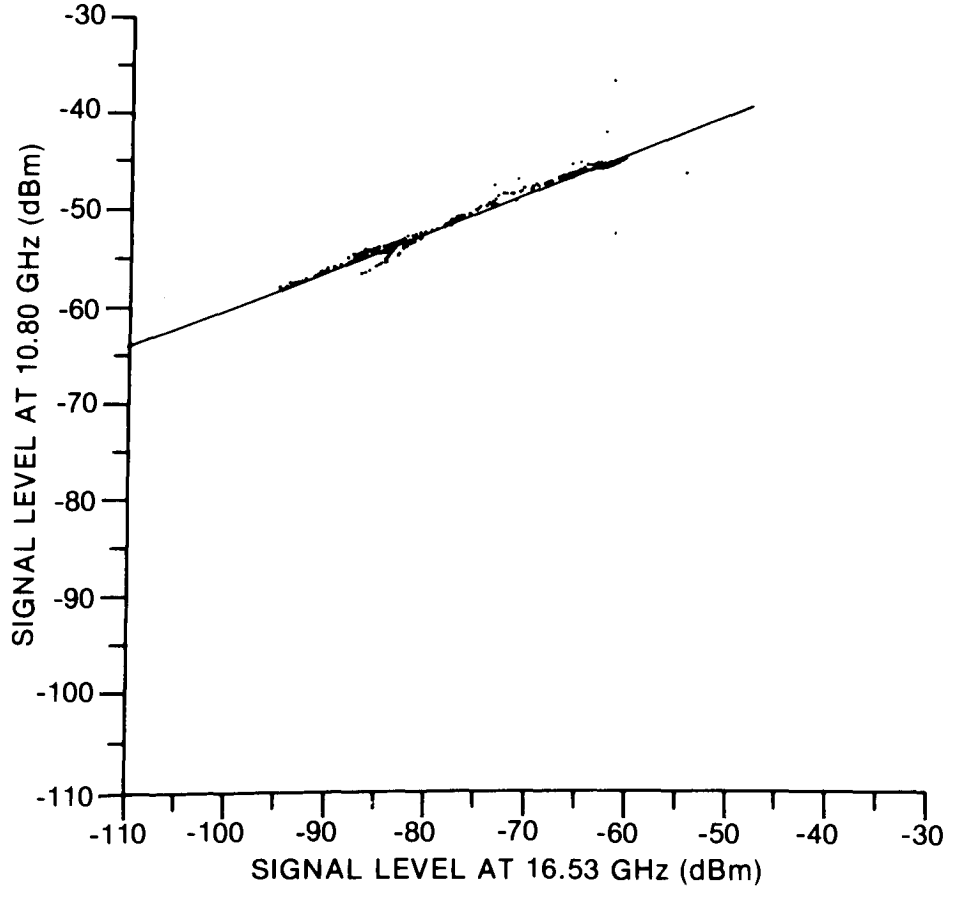

Figure 39. Scatter plot of signal levels at 10.80 and 16.53 GHz, vertical polarization, Corkery path, during the rain event of 26 July 1979.

The pairs of frequencies 10.80/11.08 GHz and 16.53/16.81 GHz each have orthogonal linear polarizations. The observed differential distributions of the linear slopes, k_p, for both pairs were found to be statistically indistinguishable so that they have been combined: the result provides information on the polarization dependence of rainfall attenuation in the 11 GHz to 17 GHz frequency range. Similarly, the parallel-polarized frequency pairs 10.80/16.53 GHz and 11.08/16.81 GHz have statistically indistinguishable differential distributions of linear slopes k_F, and these have been combined. Together with the distribution for the parallel-polarized frequency pair 11.35/17.71 GHz on the Kingsmere path, this provides information on the frequency dependence of rainfall attenuation. Histograms of those distributions are presented in Figure 40 for each data set and for the subsets of events which produced at least 18 dB of attenuation at one of the frequencies. This represents a simple attempt to isolate the thunderstorm-related attenuations from those of the complete sample. The statistics are summarized in Table 3.1.

TABLE 3.1

Attenuation Ratios and Standard Deviations for Various Signal Pairs Derived from Slope Statistics of Scatter Plots

Frequency Pair	Attenuation Ratio ± s.d.		No. of Cases
	All Data	Data A > 18 dB	A > 18 dB
11.35/17.71 k_F	0.430 ±0.048	0.425 ±0.039	13
10.80/16.53, 11.08/16.81 k_F	0.453 ±0.047	0.442 ±0.039	19
10.80/11.08, 16.53/16.81 k_P	0.781 ±0.057	0.787 ±0.038	19

It appears that during precipitation, attenuation in vertical polarization is only about 79% of that experienced in horizontal polarization, and that this depends very little on the attenuation or the frequency in the range 11 to 17 GHz. This result may be compared with the prediction derived from the regression coefficients for specific attenuation calculations provided by the CCIR (1982b). At 11 GHz these give a ratio

$$\frac{Av}{Ah} = 0.871\ R^{-0.020}$$

where R is the rainfall rate in mm/hr. At 17 GHz the ratio is

$$\frac{Av}{Ah} = 0.906\ R^{-0.025}$$

Thus the frequency dependence and attenuation (and therefore rain rate) dependence are indeed small. For example at R = 50 mm/hr the ratios at

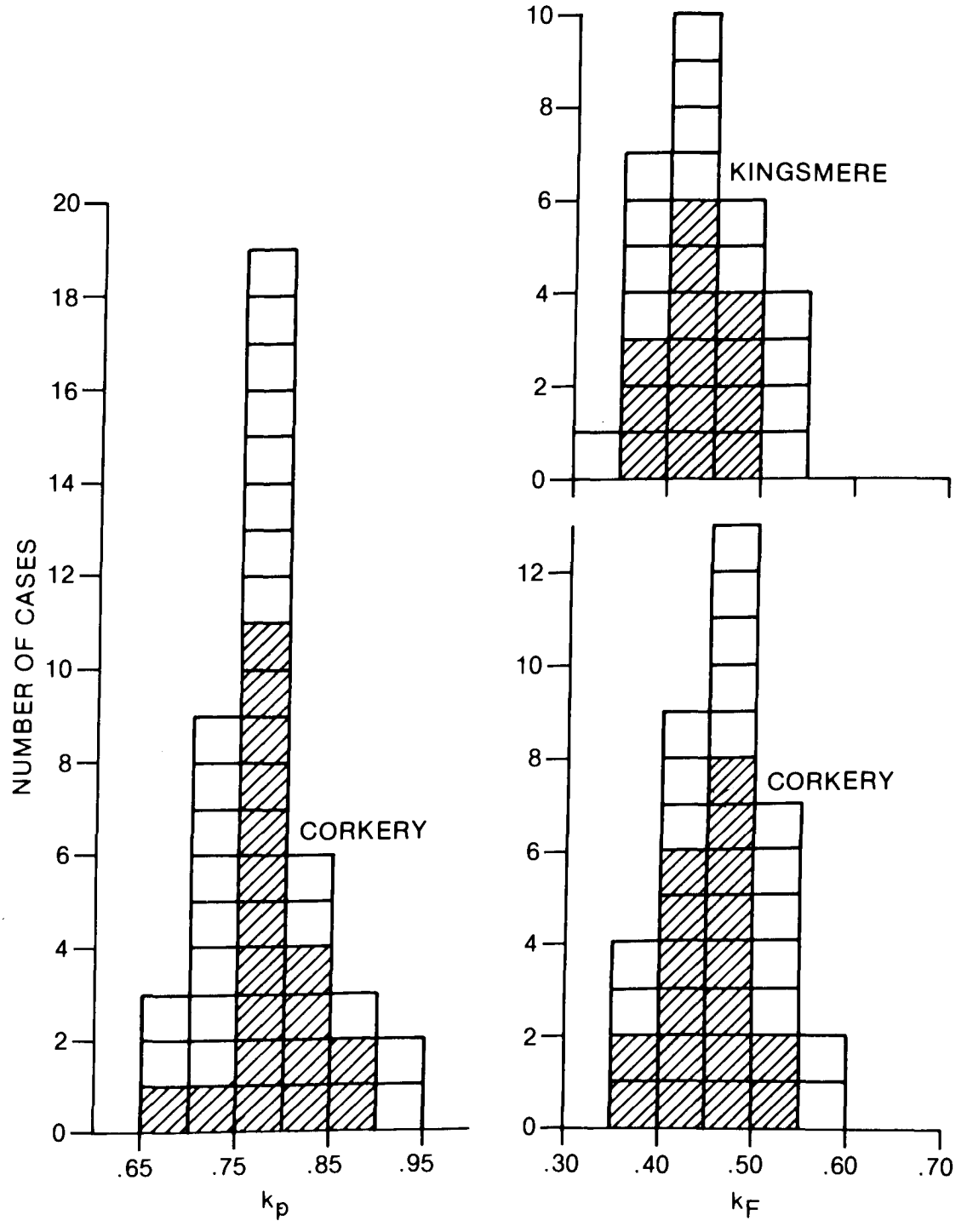

Figure 40. Histograms of slopes fitted to scatter plots for frequency and polarization scaling. Left: polarization data; Right: frequency data. The cross-hatched data are for rainfall events with attenuation exceeding 18 dB.

11 GHz and 17 GHz are 0.805 and 0.822 respectively. This rainfall rate occurs about 0.005% of the time (Segal, 1979), and although the weighting of the linear fit is biased to larger attenuations it seems likely that this is very much an upper limit to the overall average rainfall rate. Thus the CCIR predictions may provide a slight overestimate of the ratio. The same is true of the ratio derived from long-term observations in France [CCIR (1982a)], which for this percentage of the time (equivalent to an attenuation of 30 dB) predict a ratio of 0.822, with no mention of frequency dependence.

The frequency dependent ratios, k_F, may be used to allow an estimate to be made of the exponent C in the expression commonly used for frequency scaling

$$\frac{A(f1)}{A(f2)} = \left(\frac{f_1}{f_2}\right)^C = k_F$$

Combining the Kingsmere and Corkery data, the result is C = 1.93 ± 0.15, which is comparable to, but of greater statistical reliability than, the value C = 1.72 over approximately the same frequency range determined by Drufuca (1973) for a region near Montreal, about 150 km distant from the present experiment site. The present value agrees remarkably with the rain attenuation analysis by Segal (1982), based on the synthetic-storm model applied to rainfall statistics at Ottawa, in which a mean value C = 1.92 is applicable on a 40 km path for probabilities of occurrence between 0.01% and 0.1% over the frequency range 8 GHz to 25 GHz.

The exponent C = 1.93 derived from the scatter plots may be compared with the value C = 2.16 derived from the cumulative distributions of Figure 38, for percentages of time ranging from 0.006 to 0.07. The discrepancy has at least two sources. One is that the fitting of lines to individual events averages the two-dimensional scatter of the measurements, while the cumulative distribution method assigns all data to bins on the implicit assumption that they have no scatter, thus handling the measurements at the two frequencies differently. The other is that the cumulative distribution method is only strictly applicable if the time series are identical at both frequencies, while the event fitting method has no such limitation. Even with the excellent time coverage at the Kingsmere frequencies this ideal of identical time coverage is not quite met, and of course at the other frequencies it is far from being met. The event fitting method should therefore be more reliable in its estimate of frequency scaling parameters, and one should be wary of results from the cumulative distribution method if they do not come from data sets strictly matched in time.

3.4.3 Duration of Precipitation Fading

In Figure 41 the number of fades caused by precipitation is plotted as a function of fade depth for each frequency of observation. It will be remembered that the Kingsmere data sets are the most complete, so it is slightly surprising to find more fades at each frequency on the Corkery path for attenuations less than about 25 dB at 11 GHz and for almost the whole attenuation range at 17 GHz. Scaling from one frequency to another should probably be done at attenuations corresponding to equal percentages of time as deduced from the cumulative distributions, and when this is done the agreement in numbers is quite good. A small polarization-dependent variation is

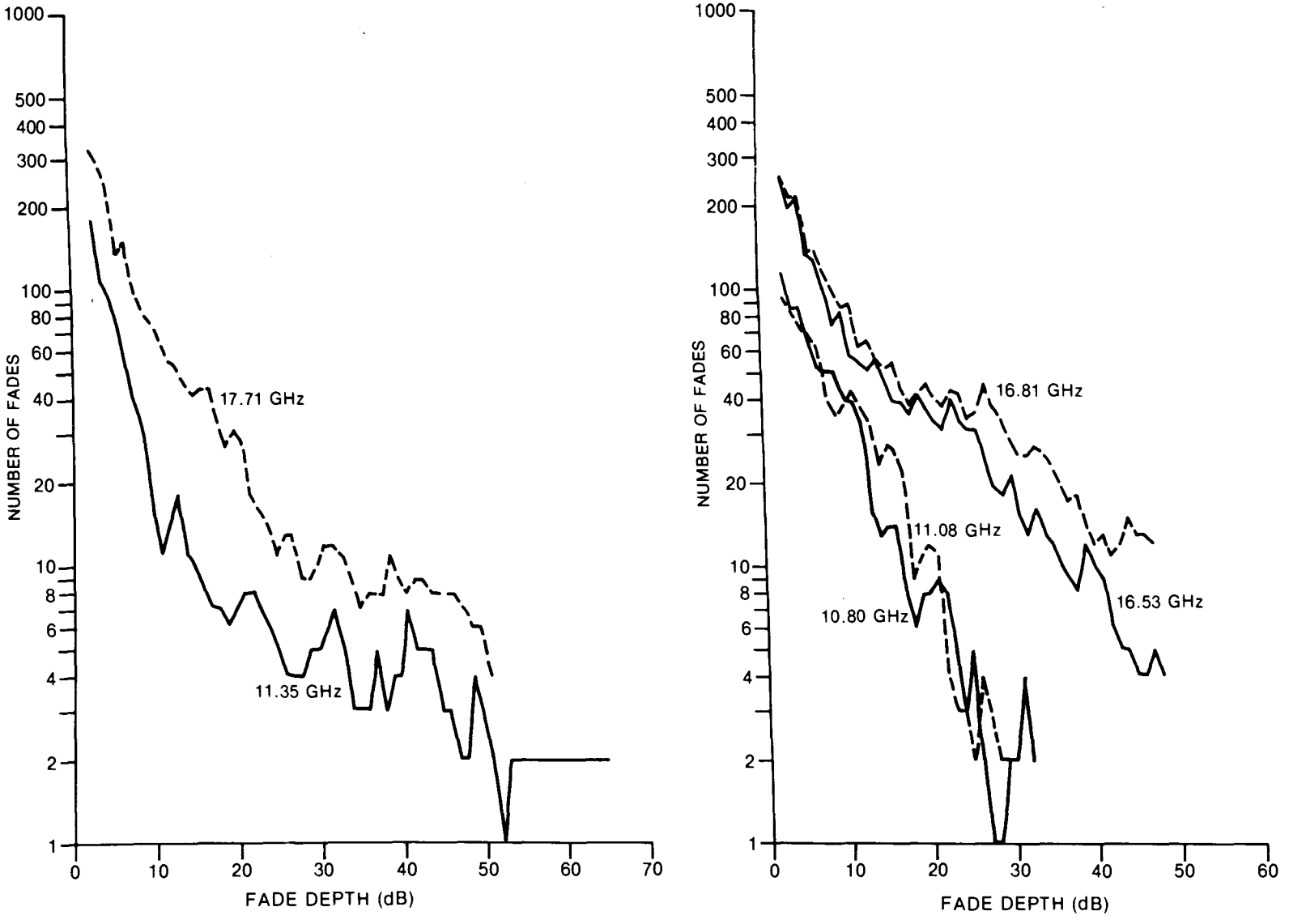

Figure 41. Numbers of rainfall fades. Left: Kingsmere path; Right: Corkery path.

apparent, with rather larger attenuation for the same number of fades at horizontal polarization as compared with vertical: this is expected from the discussion in the previous section.

The mean rainfall fade durations at each frequency on the Corkery path are shown in Figure 42 and for the Kingsmere path in Figure 43. Even if allowance is made for statistical fluctuations (for example the large value at about 27 dB for the 10.80 GHz data) there seems to be little coherence in the data sets or among them. There is a general tendency at 11 GHz for the mean durations to be shorter at larger fade depths, declining to a few seconds from a few tens of seconds. Even this is not certainly seen in the 17 GHz data, although one must remember the scaling factor in attenuation, with 50 dB at 17 GHz corresponding to only about 20 dB at 11 GHz: thus the data sets are rather difficult to compare. Perhaps the strongest conclusion is that mean fade durations are consistently less than 100 seconds.

The sparseness of the data rendered it impossible to establish the form of the conditional distribution of fade duration at a given fade depth. However, as for the multipath case the extreme values observed have been plotted as a function of fade depth and are shown in Figure 44, in which each small cross-hatched rectangle represents a two-dimensional bin containing the extreme duration observed in each 1 dB range of fade depth. Comparison with the mean values emphasizes that the distribution must be very skew in form. It is also striking that the extreme durations are quite long, especially at 17 GHz, and do not decrease very much with increasing fade depth. Once again scaling between frequencies based on equiprobable attenuations from the cumulative distributions seems approximately correct.

3.5 RAINFALL DEPOLARIZATION

In Figure 45.the cumulative distributions of cross-polarization discrimination (XPD) during rainfall fading are shown for the frequencies on Kingsmere path. Results at the other frequencies are similar but of much poorer quality because of the smaller sample sizes. The 11.35 GHz data are very well represented by a straight line having a slope of two decades of time for a 10 dB interval of XPD, and the 17.71 GHz data are consistent with this although a rather smaller slope would be a better fit. During rain events the cross-polar signals are attenuated at the same time as the co-polar signals, so that the dynamic ranges of the systems limit the XPD for which reliable statistics can be obtained to about 24 dB. The CCIR (1982a) formula for scaling XPD between frequencies at the same percentage of time predicts that the 17.71 GHz data lie 6.4 dB lower than those at 11.35 GHz, as compared to the mean observed value of about 6 dB which is in good agreement over the reliable data range.

Because a statistical relationship between rain depolarization and attenuation was known from the work of Nowland, et al. (1977) and Olsen and Nowland (1978), values of XPD were plotted against the equally probable values of co-polar attenuation (CPA) on a logarithmic scale. The results for the frequencies on the Kingsmere path are shown in Figure 46. The system limit for each frequency is the envelope of XPD + CPA at which the cross-polar signal decreases below the system noise limit, so that XPD becomes undefined. It is apparent that sufficiently far from these limits

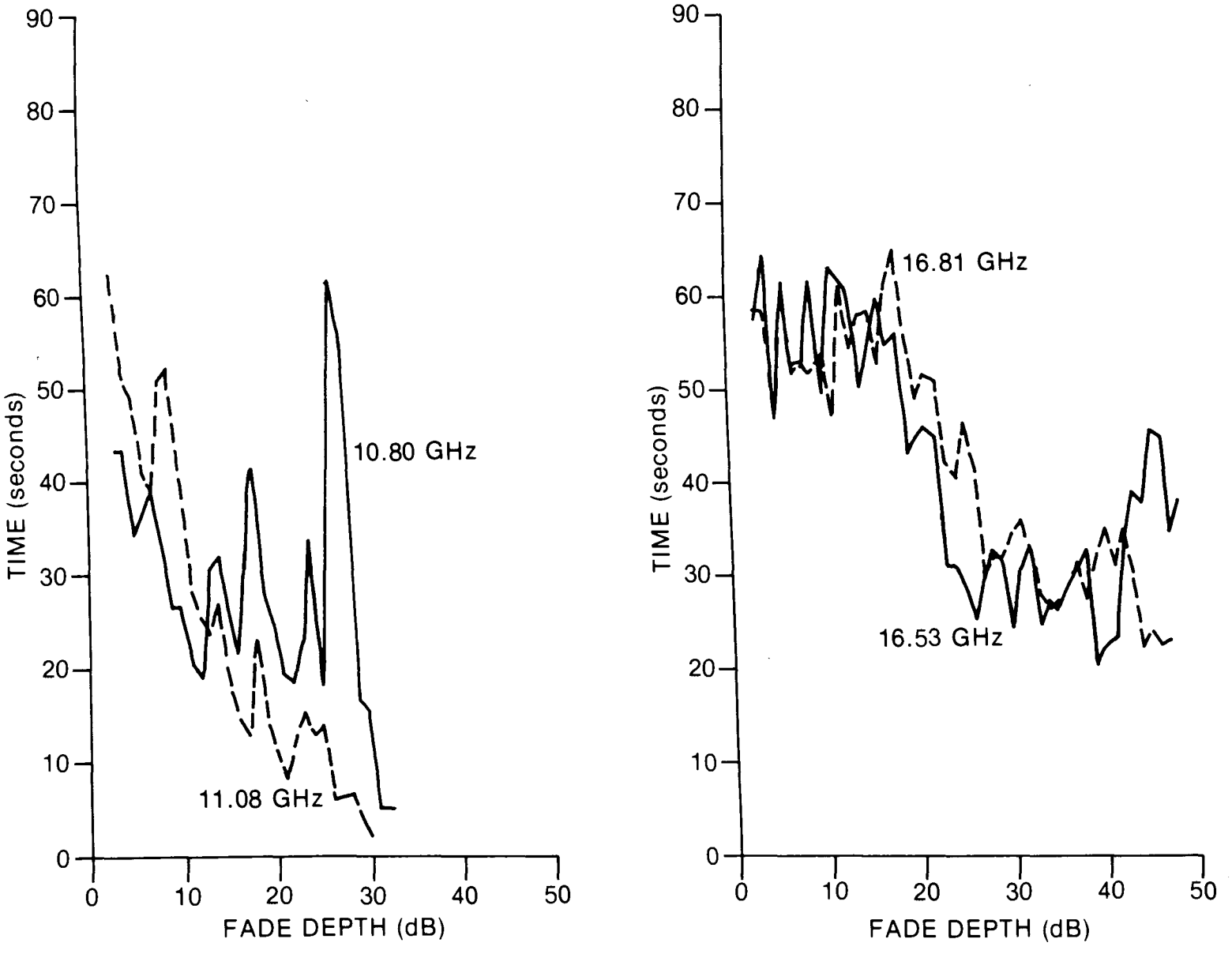

Figure 42. Average rainfall fade durations, Corkery path.

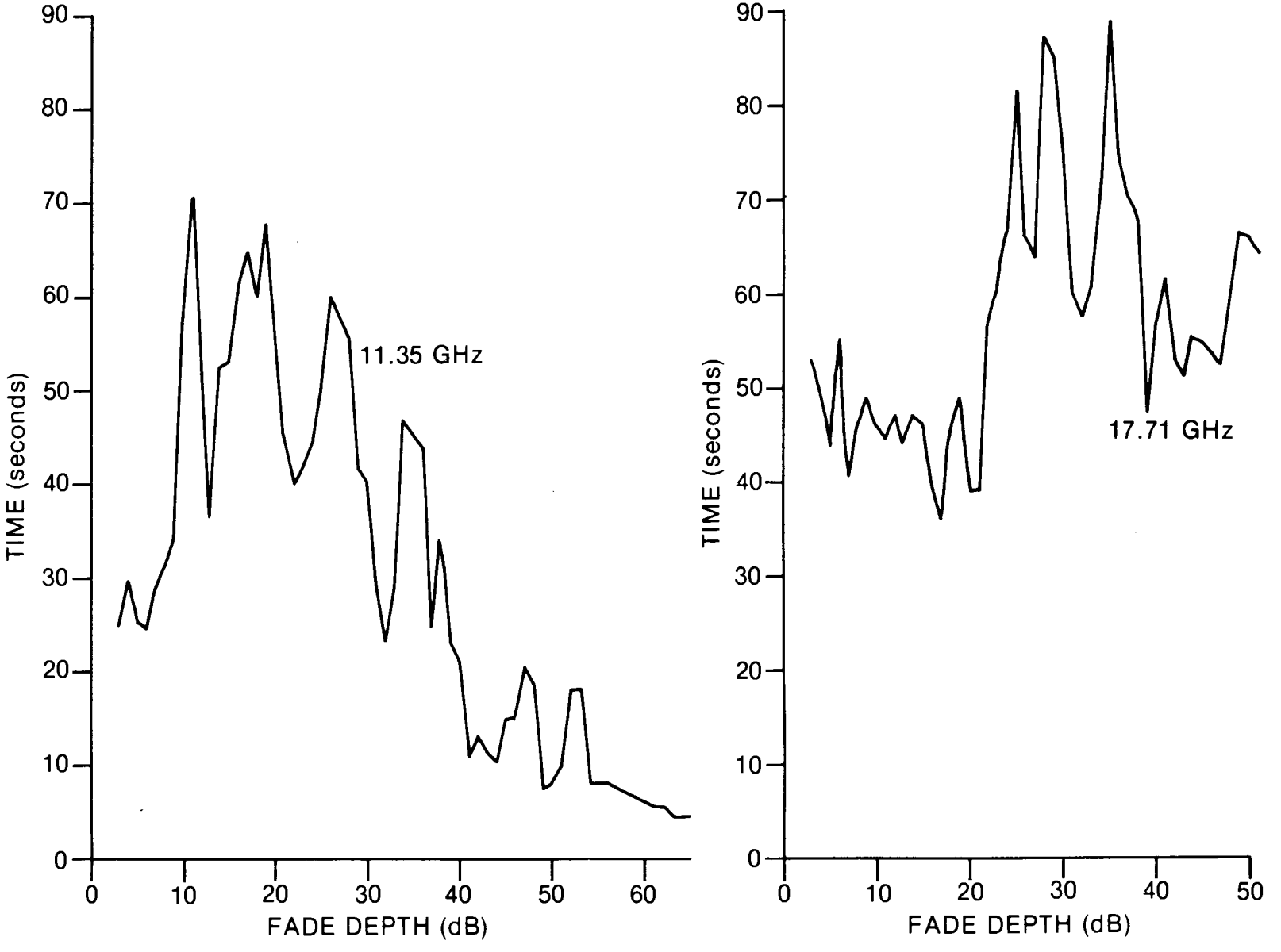

Figure 43. Average rainfall fade durations, Kingsmere path.

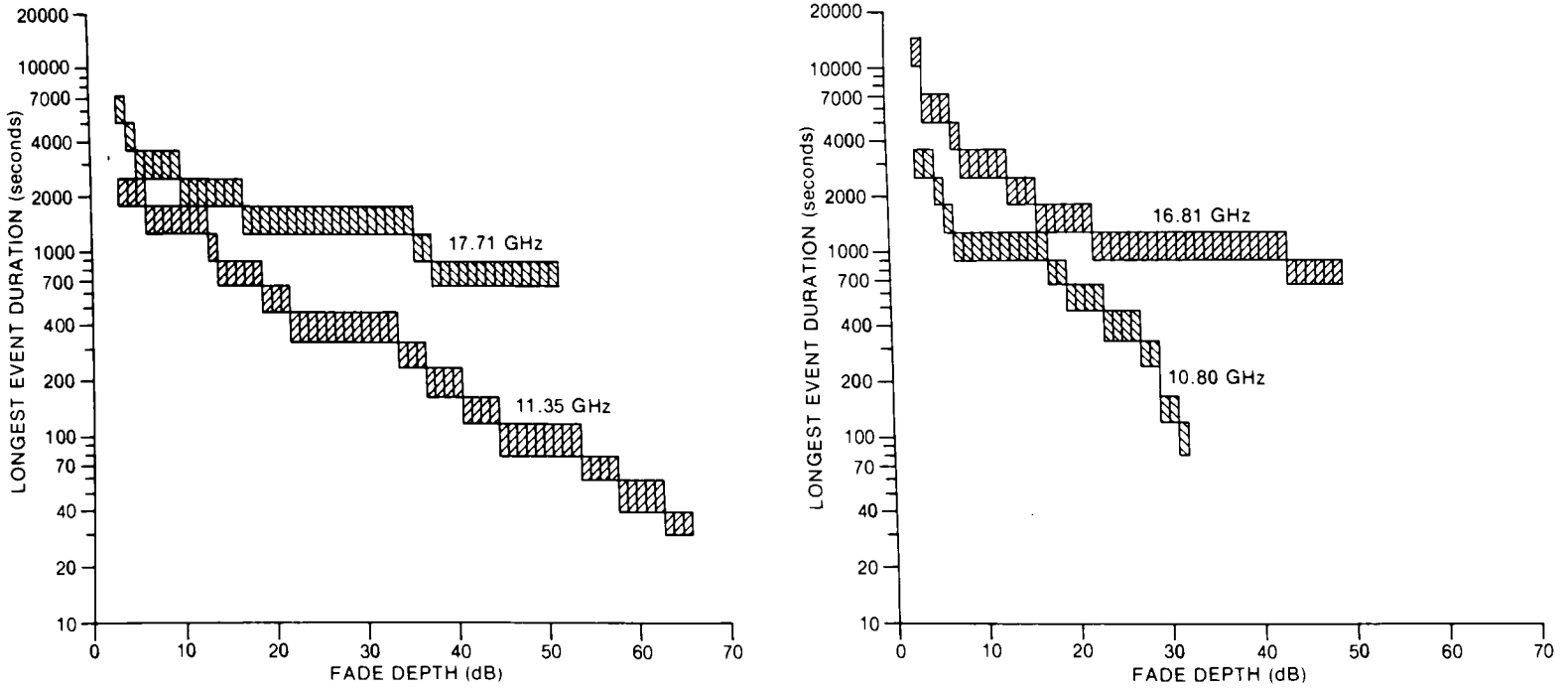

Figure 44. Duration of longest observed rainfall fades. Left: Kingsmere path; Right: Corkery path.

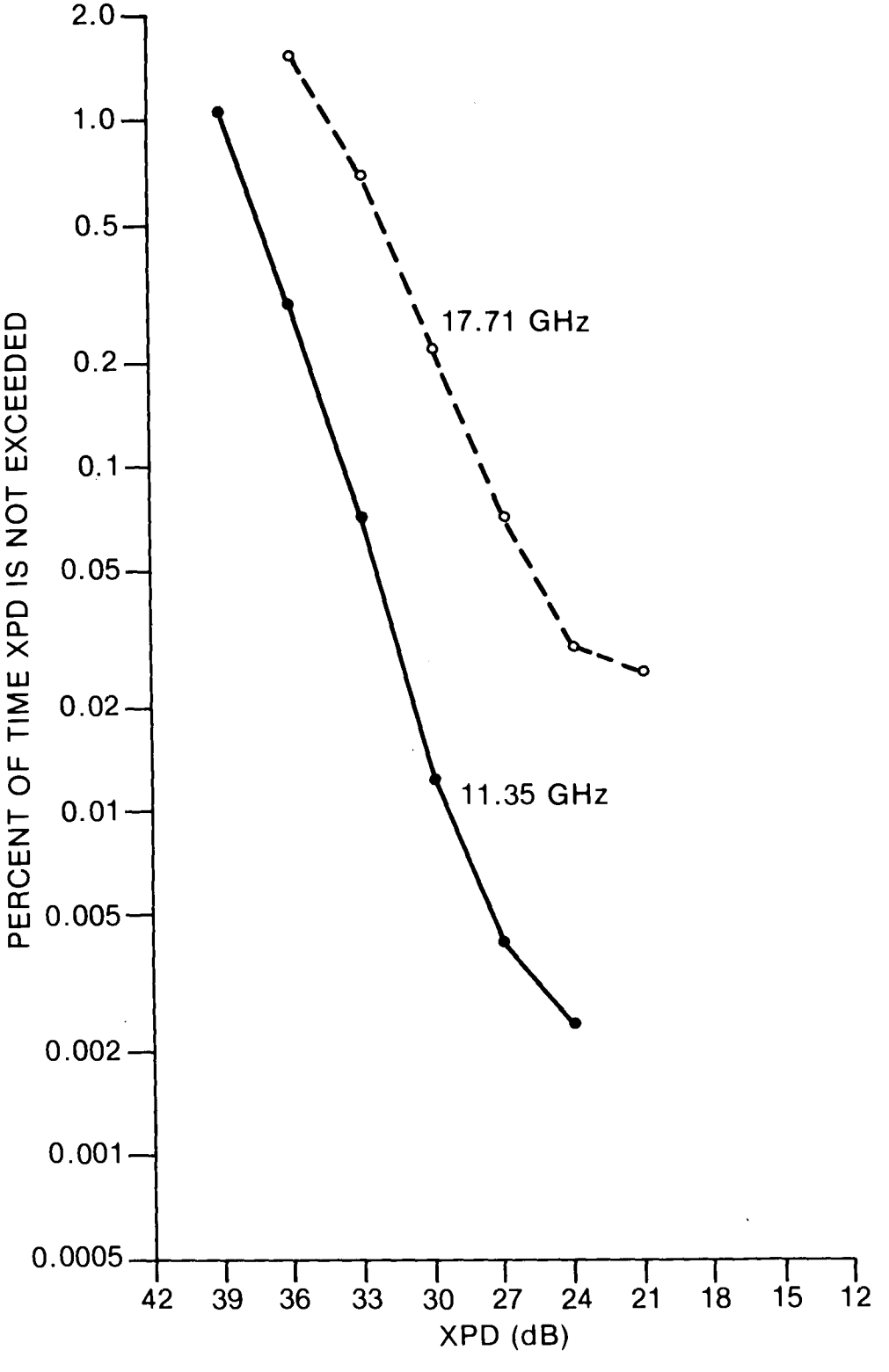

Figure 45. Cumulative distributions of cross-polarization discrimination during rainfall; Kingsmere path.

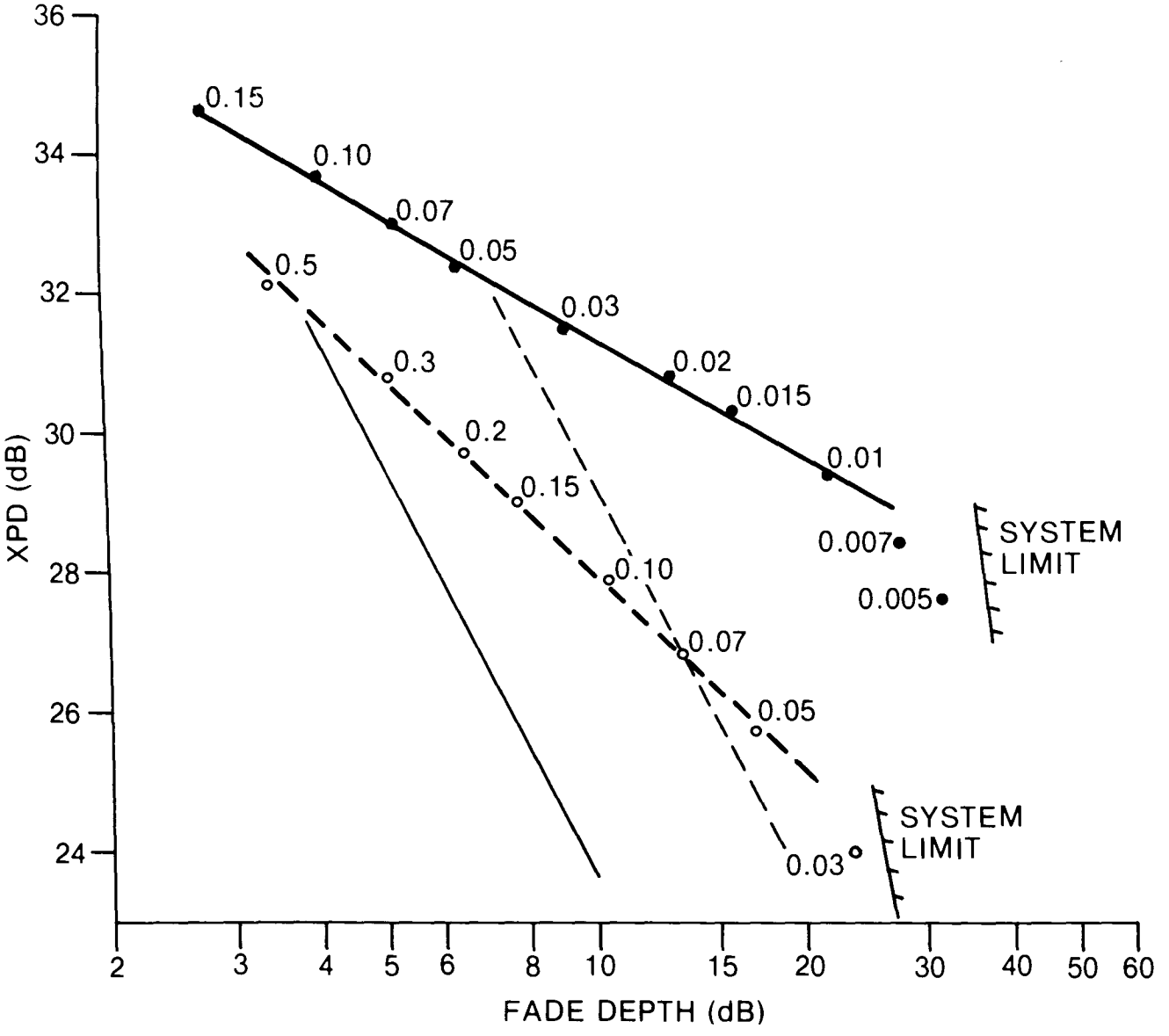

Figure 46. Equiprobable fade depth and cross-polarization discrimination during rainfall; Kingsmere path. Solid lines and dots: 11.35 GHz; dashed lines and circles: 17.71 GHz. Points are labelled with percentages of time jointly observed. Ordinate is logarithmic.

the results are linear in this form of presentation. However, when compared to the simple semi-empirical expression given by Olsen (1982b) and adopted by the CCIR (1982c):

$$XPD\ (p\%) = 12 + 30 \log f - 20 \log CPA(p\%)$$

it is found that the observed slopes are -5.8 at 11.35 GHz and -8.8 at 17.71 GHz rather than -20, while the observed frequency dependence appears to be in the opposite sense, with larger XPD at the smaller frequency for constant CPA, as illustrated in Figure 46.

The expression above assumes that the effective angle of tilt with respect to the horizontal of the equatorial plane of the raindrops along the path has a fixed value of 7.3°. For other values of this effective canting angle the value of the constant in the expression would change, moving the semi-empirical lines parallel to those in Figure 46. Thus it appears that the discrepancy might result from the use of a fixed value of the canting angle when, in fact, this parameter is dependent on the rainfall rate and so on the co-polar attenuation. If it is assumed that the basic theory of rainfall depolarization is a correct physical description at any instant - not just statistically - this theory can then be applied to the individual measurements of XPD and CPA in order to calculate momentary effective raindrop canting angles. If the assumption is correct then there should be agreement of the calculations at different frequencies for the same instant of time and the statistics of the canting angle distribution should predict the form of the equiprobability results in Figure 46.

Begin with equation (5) of Olsen and Nowland (1978) which relates XPD to CPA,

$$XPD = U - 20 \log CPA - 20\ (d-b) \log R \qquad (1)$$

where R is point rainfall rate, and d and b are the exponents in the power law relationships of differential attenuation and phase-shift and of co-polar attenuation, respectively, to rainfall rate. The expression for U simplifies in the terrestrial case (elevation angle = 0°) and for horizontal linear polarization, to

$$U = - 20 \log (m \sin 2\ |\phi|) - 20 \log \frac{c}{2a} \qquad (2)$$

where ϕ is the effective canting angle, m is a canting angle distribution factor, and c and a are constants in the power law relationships of which d and b, above, are the exponents. This can be rewritten as

$$U = 0.0053\ \sigma^2 - 20 \log \sin 2\ |\phi| + 30 \log f \qquad (3)$$

where σ is the effective standard deviation of the (assumed Gaussian) canting angle distribution. The frequency term is a convenient approximation to the term in c/2a, which is adequate in the frequency range 10 GHz < f < 35 GHz (Olsen 1982b).

With a single linear polarization one cannot disentangle the mixture of σ and ϕ terms which contribute to the depolarization. However, on the

assumption of $\sigma = 0$, we can define the equivalent mean canting angle ϕ_o. Since the σ term is linear and the ϕ term logarithmic, this means that the true ϕ value is related to ϕ_o by a multiplying factor. Typical ranges of the relevant terms in the expression for U as listed in Table 3.2.

TABLE 3.2

Depolarization Factors Dependent on Canting Angle

σ (Deg)	0.0053 σ^2 (dB)	ϕ (Deg)	-20 log sin 2$\lvert\phi\rvert$ (dB)
10	0.53	0.6	33.58
20	2.12	1.0	29.14
25	3.31	2	23.13
30	4.77	3	19.62
35	6.49	4	17.13
40	8.48	6	13.64
45	10.73	8	11.19

We now estimate the effect of the rainfall dependent term in equation (1). From Olsen and Nowland (1978) the factor (d-b) is seen to be small over the frequency range of interest to us, and the effect of this term is consequently minor. In particular at 11.35 GHz, d-b = -0.015, so that 20 $(d-b)_{11}$ = -0.3; at 17.71 GHz, d-b = 0.10 so that 20 $(d-b)_{17}$ = 2.0. The dependence of CPA on rainfall rate is taken from Olsen, Rogers and Hodge (1978) to be, at 11.35 GHz

$$CPA_{11} = 0.0167\ R^{1.16}\ l \qquad (4)$$

where l is path length in km and the numerical values correspond to the Laws and Parsons LP_H rainfall model at 0°C. A realistic median value for rain cell sizes in the Ottawa area is l = 6 km (Strickland 1974), so we define a mean 6 km rainfall rate at 11.35 GHz

$$R_6 = \left(\frac{CPA_{11}}{0.0167 \times 6}\right)^{0.861} \qquad (5)$$

This produces the results for the rainfall-dependent correction factors in Table 3.3

TABLE 3.3

Rainfall-dependent Correction Factors

CPA_{11} (dB)	R_6 (mm/hr)	Log R_6	20 (d-b) Log R_6	
			11 GHz	17 GHz
2	13	1.12	-0.33	2.2
4	24	1.38	-0.41	2.8
10	53	1.72	-0.52	3.4
25	116	2.07	-0.62	4.1
40	174	2.24	-0.67	4.5

Note that a factor of two change in path length, i.e., to 3 or 12 km, will produce a change of 0.26 in log R_6 and so a change of 0.08 in the correction term at 11 GHz and 0.5 at 17 GHz. Thus over the range of interest a fixed value of -0.5 at 11 GHz and +3.0 at 17 GHz will be adequate. Note that the CPA values at 17 GHz corresponding to those tabulated at 11 GHz are about three times larger at the same rainfall rate.

We now combine equations (3) and (1), rearrange and insert the numerical correction estimate to obtain, at 11 GHz

$$- \log \sin 2\left|\phi_o\right| = \frac{XPD_{11} - 0.5}{20} + \log CPA_{11} - f^{1.5} \qquad (6)$$

and at 17 GHz

$$- \log \sin 2\left|\phi_o\right| = \frac{XPD_{17} + 3.0}{20} + \log CPA_{17} - f^{1.5} \qquad (7)$$

Because of the finite cross-polarization discrimination of the microwave antennas, the measured levels of XPD cannot be used directly in these expressions. Unfortunately, we do not know the phase relationship between the cross-polarized vector field produced by the scattering mechanism and the cross-polarized vector arising from antenna imperfections, etc. However, we can define lower and upper limits by assuming that the vectors are in-phase or out-of-phase, and comparing the signal amplitudes. For any measured XPD, then, there are two possible corrected values corresponding to these limits, and two values defining the possible range of ϕ_o at each frequency. This argument is illustrated by Figure 47, which is a scatter plot of XPD versus CPA for a single rainfall event. Each plotted point represents a 5-second average measurement of XPD and CPA. The slightly curved line at the right is the limit at which accuracy of measurement begins to decrease rapidly as receiver noise levels are approached. For a mean equivalent canting angle of 2° an observed point would lie within the three-cusped envelope shown. The lowest curve indicates the limit at which the scattered and clear-air fields are in-phase, and the other two curves show the out-of-phase limits, all for an angle of 2°. Note that the in-phase and out-of-phase limits approach each other for large values of CPA. For other canting angles these curves move along the asymptotic horizontal line at the clear-air cross-

polarization isolation value with no change in shape, smaller angles to the right and larger angles to the left. Thus one can find limits on the value of ϕ_o for each observed point. If the original assumptions are correct, then moment by moment the XPD/CPA relationship should be satisfied at all frequencies. In practice, then, it is a strong test of the assumptions that the limits on ϕ_o from the various independent frequency measurements shall always be consistent and shall overlap.

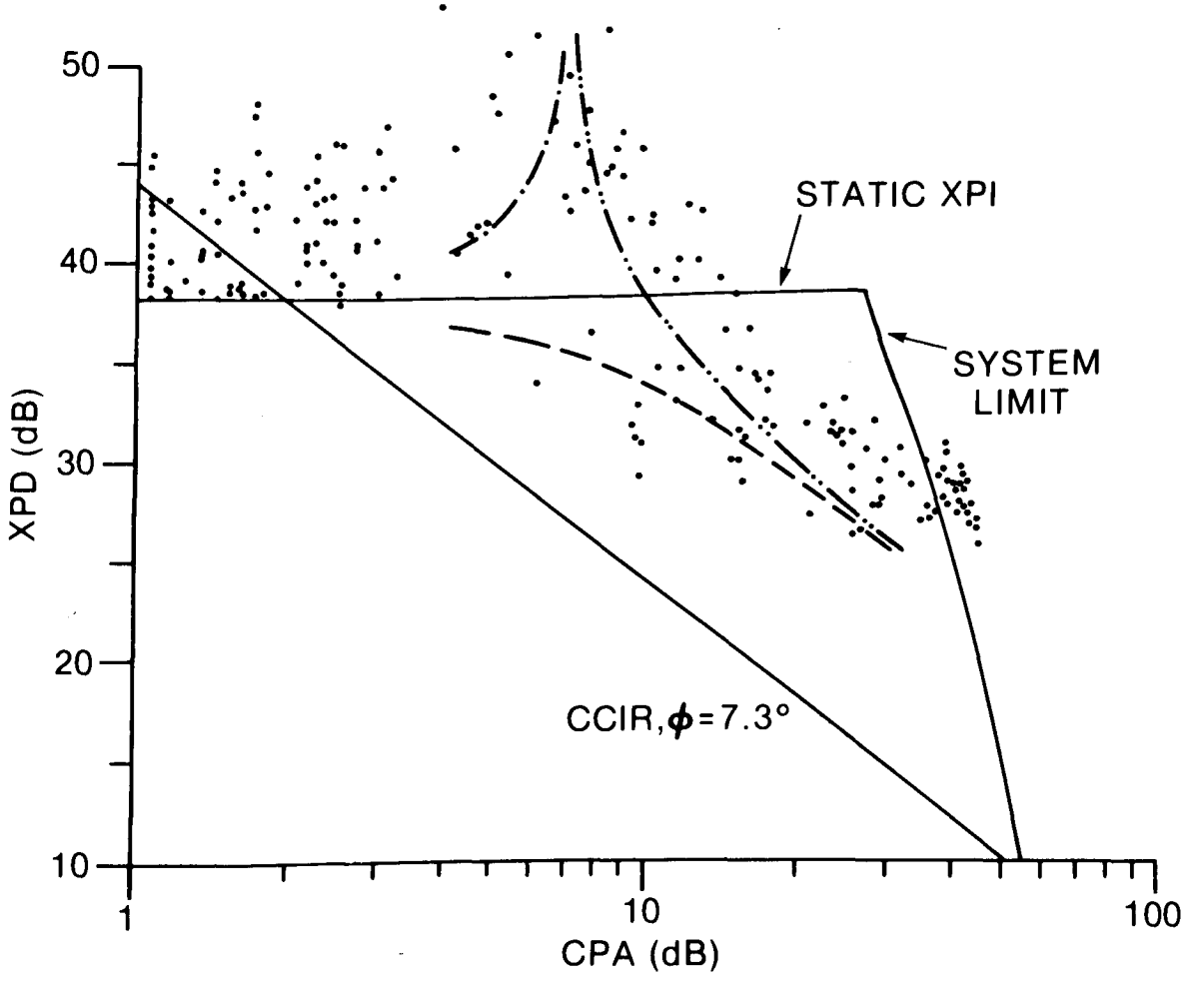

Figure 47. Scatter plot of cross-polarization discrimination and fade depth (CPA) during a typical rain event; 11.35 GHz. The dashed and dashed-dotted lines correspond to $\phi = 2°$, as explained in the text.

In Figure 48 are shown the results of a typical set of computations. The heavy continuous line shows the received signal at 11.08 GHz during a moderate rain event which produced about 30 dB of fading at maximum. The upper and lower limits on ϕ_o, computed every five seconds, are shown by a dotted line and a dashed line, respectively. It is immediately clear that a strong correlation exists between the canting angle and the fade depth, with smaller canting angles corresponding to deeper fades. This is precisely the sense of variation needed to explain the flat slope of the equiprobability curves of Figure 46, which is perhaps not surprising since the same data have been manipulated through the same theoretical apparatus. What is slightly surprising is the consistency of the calculated canting angles; that is, the variation of canting angle during the developing rain event is well-behaved, not violently oscillating. This apparently indicates that over time scales of minutes the collective behaviour of the rainfall and the associated wind shear is slowly varying and consistent when integrated along path lengths of a few kilometres. The values of ϕ_o calculated at all frequencies for this event do agree, confirming the assumptions discussed above. Finally, the upper and lower limits on the equivalent canting angle do approach one another most closely at the times of greatest attenuation, which is fortunate since our knowledge is most accurate where it is most important. This behaviour is seen consistently in all the rainfall events studied.

In Figure 49 are shown the median values of the upper and lower limits on the canting angle calculated at the 11 GHz frequencies on both paths. It appears that there is a monotonic decrease of the canting angle as co-polar attenuation increases to about 10 dB, and then a levelling-off, so that an approximately constant value of about 2.5° is reached on the Corkery path, and about 1.2° on the Kingsmere path. It also appears that the statistics at the different frequencies on the Corkery path are in agreement, as anticipated above. The linearity of the curves at smaller co-polar attenuations in this presentation is in agreement with the logarithmic dependence on canting angle expected from equation (3). Unfortunately, quantitative prediction of the results of Figure 46 is not possible from Figure 49, because the two sets of data are not the same. However, as an example, at 11.35 GHz use of the median upper limit on the canting angle predicts XPDs about 2 to 3 dB greater than those of the observed equiprobability data.

In Figure 50 the median values at the 11.08 GHz upper limit and the 11.35 GHz upper limit are presented again, together with the limiting curves for the first and ninth deciles of the distributions. These latter exhibit the same behaviour as the medians. The narrowness of the distribution at 11.35 GHz on the Kingsmere path is particularly striking, especially as the percentage width remains relatively constant down to the smallest angles for which the statistics are reliable. For the Corkery path at 11.08 GHz the distribution broadens significantly at larger values of the co-polar attenuation. In fact, the original data show that the distribution becomes bimodal in this region, and this is confirmed by the lower limit results and by those at 10.80 GHz. In part, the higher median values on the Corkery path are the result of this split of the distribution, one portion of which approximates that on the Kingsmere path and the other of which tends to a limiting value near 4°.

The differences in behaviour of the mean equivalent canting angle on the two paths find a ready explanation in the effect of height above ground

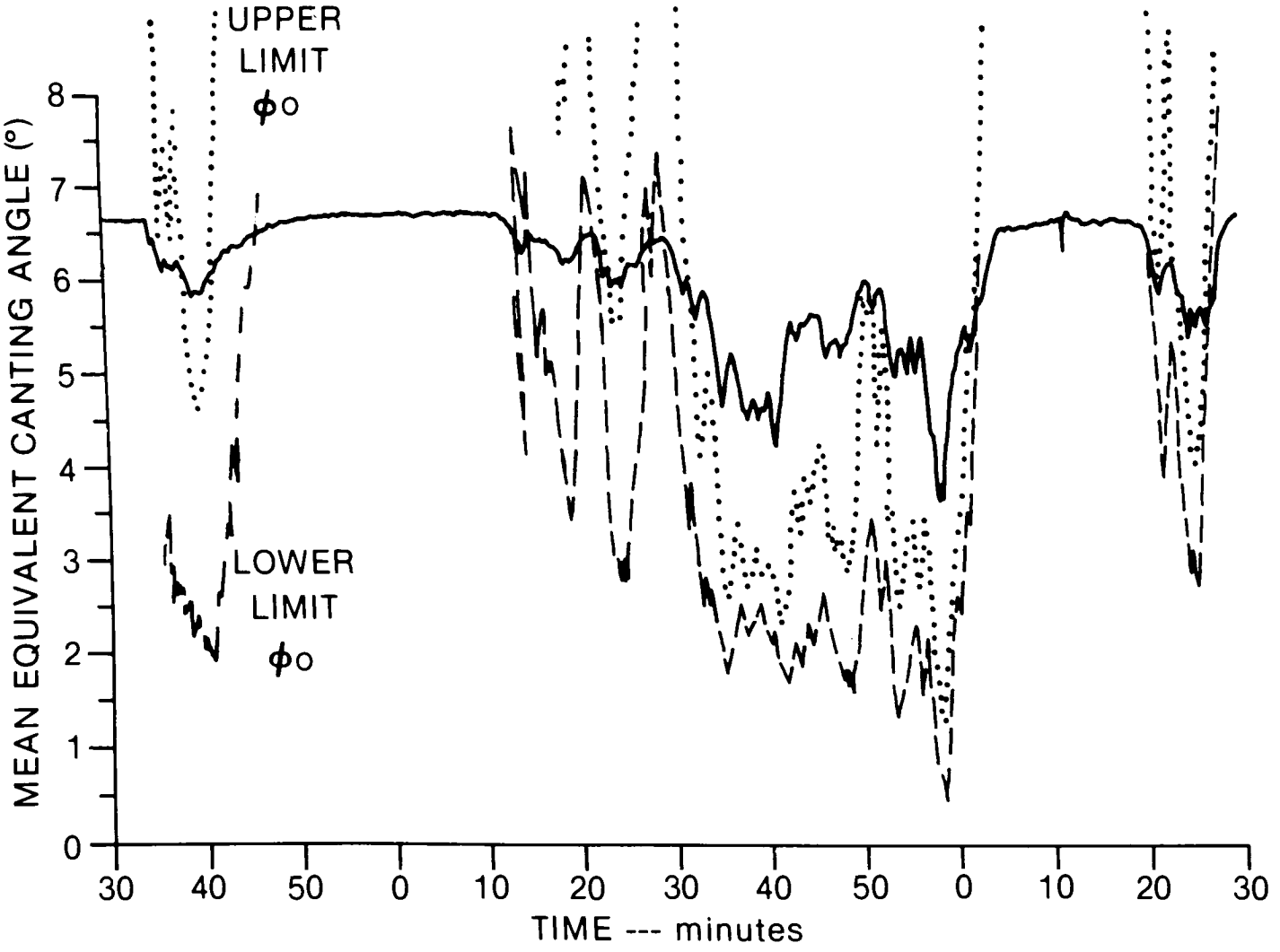

Figure 48. Variation of mean equivalent canting angle limits during a typical rain event; 11.08 GHz. Solid curve: observed signal level, abscissa scale 10 dB per major division; dotted curve: canting angle upper limit; dashed curve: canting angle lower limit.

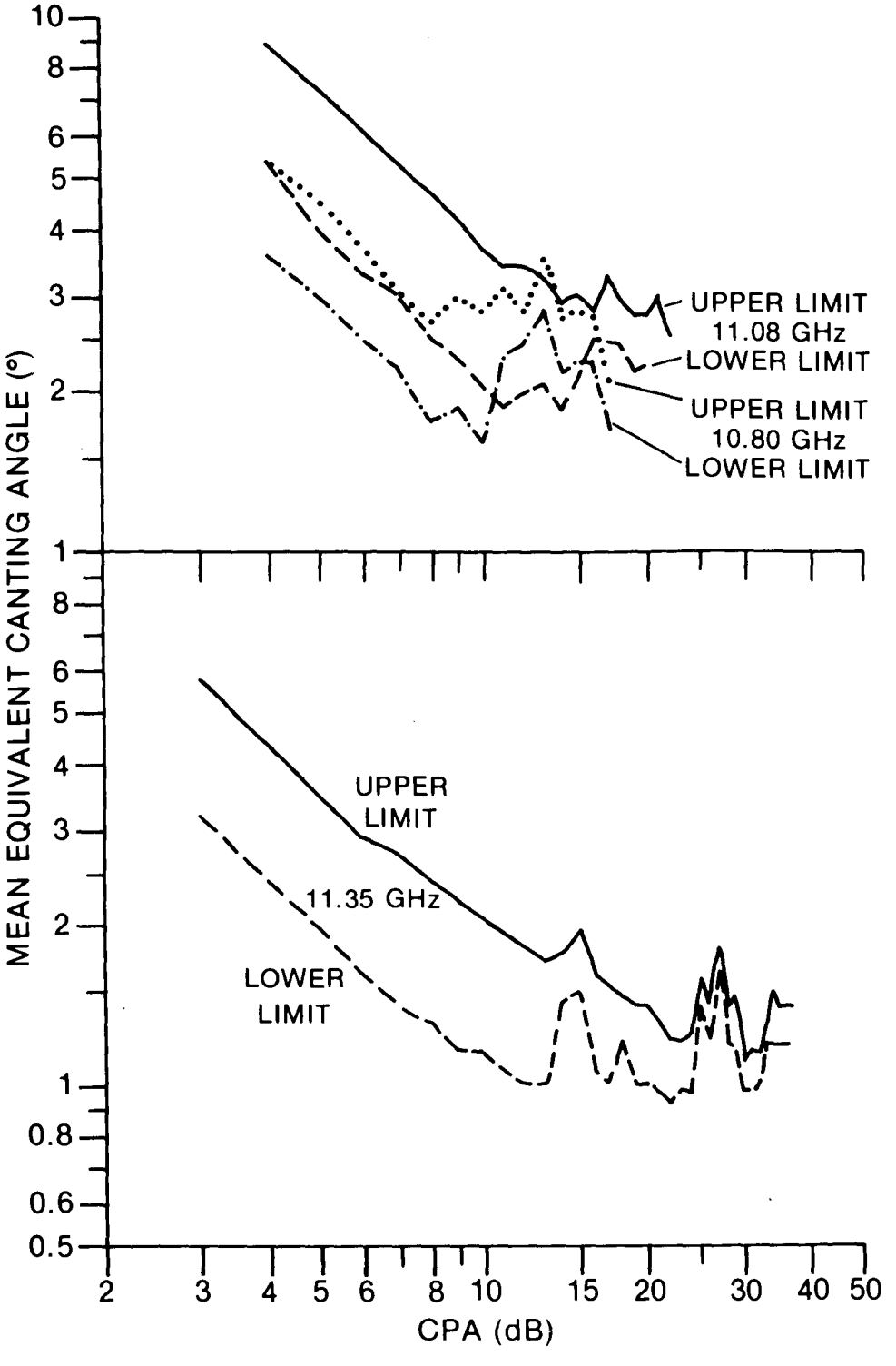

Figure 49. Median values of mean equivalent canting angle limits. Upper: Corkery path; Lower: Kingsmere path.

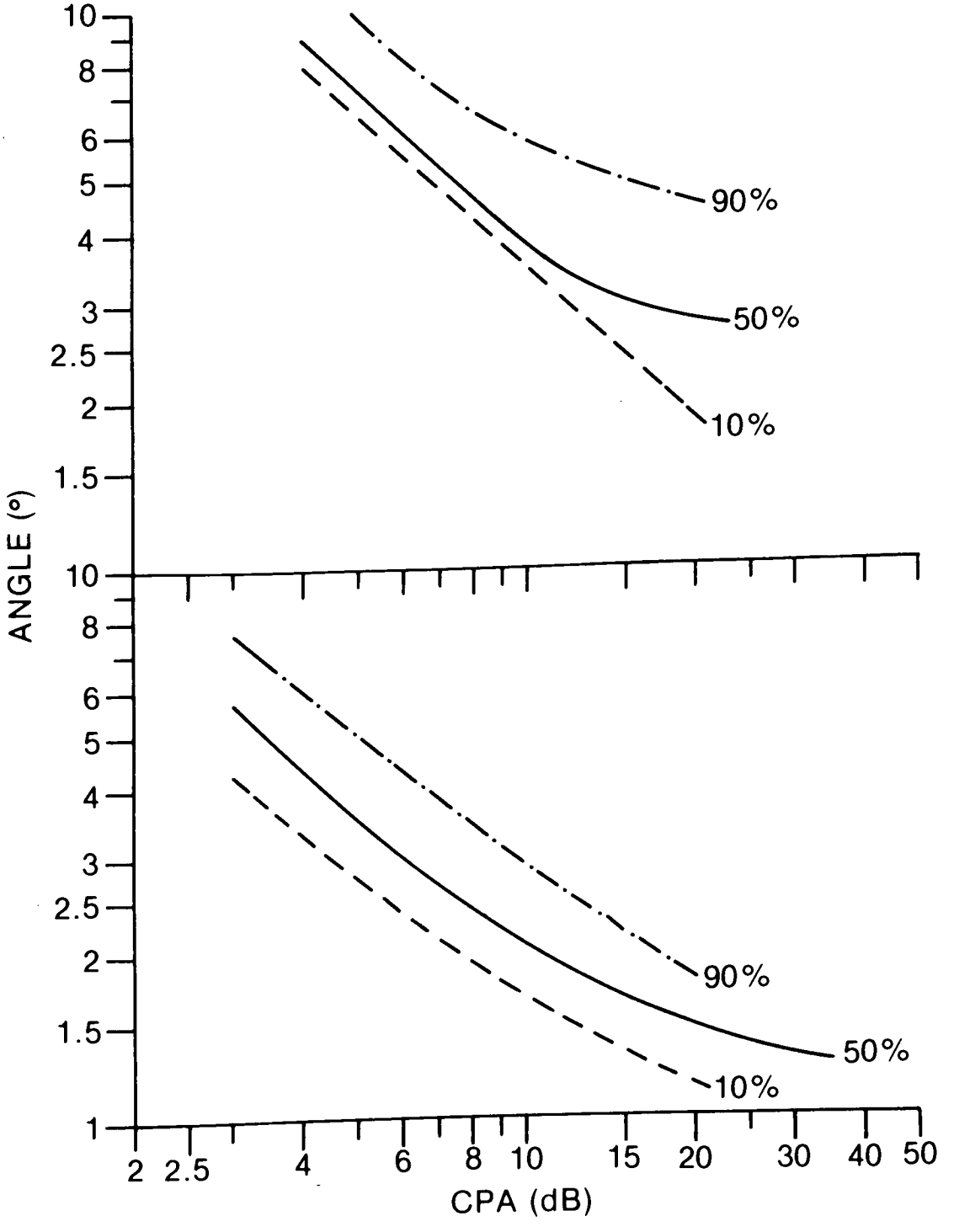

Figure 50. 10%, 50%, and 90% values of mean equivalent canting angle upper limits. Upper: 11.08 GHz, Corkery path; Lower: 11.35 GHz, Kingsmere path.

on wind gradient, as discussed by Brussaard (1976). The reason why the mean canting angle is not zero in general, is that the raindrops tend to fall with their minor axes aligned with the direction of the local relative wind, and this direction is not vertical because of the wind gradient which exists in the lower few hundred meters of the atmosphere. Now, as shown in Figures 3 and 51, the Kingsmere path has everywhere a clearance exceeding 40 m, and averaging about 80 m over the river valley which exerts some orographic influence on storm movement. The Corkery path, in contrast and as shown in Figures 2 and 51, nowhere has a clearance exceeding 40 m, and the average value is about 30 m. This is just the sense of variation, and roughly the magnitude, to produce the observed canting angle effect, although quantitative comparison is impossible because wind data are lacking. In addition, over the range 3 to 8 km from the receiving end at CRC, the Corkery path has its effective clearance reduced by a wooded area from the nominal value of about 25 m above ground to perhaps only 10 to 15 m: over the rest of the path the ground clearance is 30 to 35 m above farmland. Thus the Corkery path has indeed two distinct sections differing by a factor of two or three in mean path clearance, so that each portion of the bimodal distribution can be associated with one of these, in excellent qualitative agreement with expectations from Brussaard's work.

4. CONCLUSION

All the results of the present experiment have been presented and discussed in the preceding section. In summary, we have obtained cumulative distributions of fading and depolarization statistics at 11 and 17 GHz on two adjacent 16 km paths, as well as information on fade durations and rates of change. Throughout, comparison has been made with the most recent documentation of the CCIR, although in some areas the present results go beyond the information on which that documentation was based. Perhaps the most striking difference from currently adopted practice is the suggestion that raindrop canting angles depend on rainfall rate. If confirmed by experiments designed for the purpose, this should lead to significant changes in predictions of rainfall depolarization, which now appear to be overly pessimistic.

Intercomparison of the data presented lead to the conclusion that at 17 GHz rainfall fading dominates clear-air fading, but that at 11 GHz they are roughly comparable in importance. Also, at the 11 GHz frequencies clear-air depolarization may be an even more severe limitation on dual-polarized systems than clear-air fading. Rainfall depolarization does not appear to be a limitation at any frequency.

As with any simple experiment of limited duration, the present experiment suggests questions that remain to be answered. Of these, the outstanding one concerns the mechanism of clear-air depolarization, fundamental understanding of which is still elusive. The continued investigation of this subject appears well justified because of the limitations it may impose on dual-polarized systems. The present experiment therefore justifies itself by its own results and also by the suggestions for further work arising from it, all directed to improving the predictability of microwave radio propagation.

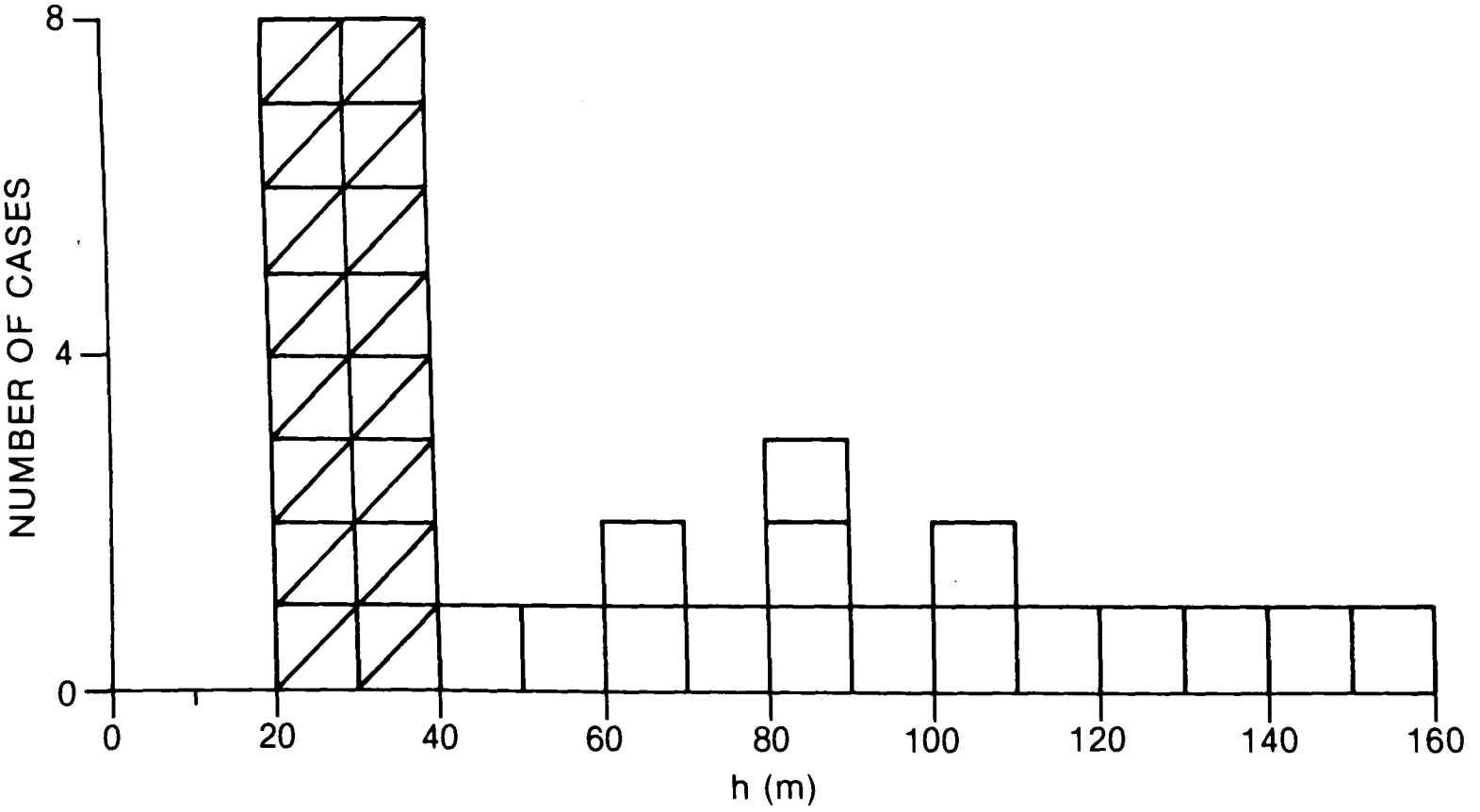

Figure 51. Histogram of mean clearance in 1 km horizontal intervals for experimental paths. Cross-latched values for Corkery path; other values for Kingsmere path.

5. ACKNOWLEDGEMENTS

The original impetus for this experiment came from the late Dr. A.W. Adey, who directed its initial development. The major part of system construction, and later of operational maintenance, was the responsibility of Mr. W.E. Mather: his dedication and persistence, and those of Mr. W.G. Phillips who succeeded him, were invaluable. The digital recording system was developed by Mr. J.J. Schlesak. To these, and to Mr. W. Rolfe for his technical supervision, I wish to record my thanks.

I am especially grateful to Dr. R.L. Olsen for his continual encouragement and for innumerable discussions of every aspect of microwave propagation phenomena. Without his expert knowledge freely shared, this report would have been a meagre skeleton of its present form.

6. REFERENCES

Brussaard, G., *A Meteorological Model for Rain-induced Cross-polarization*, IEEE Trans. Antennas Propagat., AP-24, 5-11, 1976.

CCIR, *Propagation Data Required for Line-of-sight Radio-relay Systems*, XVth Plenary Assembly, Report 338-3, International Telecommunications Union, Geneva, 1982a.

CCIR, *Attenuation by Precipitation and Other Atmospheric Particles*, XVth Plenary Assembly, Report 721, International Telecommunications Union, Geneva, 1982b.

CCIR, *Cross-polarization Due to the Atmosphere*, XVth Plenary Assembly, Report 722, International Telecommunications Union, Geneva, 1982c.

Drufuca, G., *Rain Attenuation Studies*, Stormy Weather Group Report MW-77, McGill University, Montreal, 1973.

Lin, S.H., *Statistical Behaviour of a Fading Signal*, Bell Syst. Tech. J., 50, 3211-3270, December 1971.

Lin, S.H., *Impact of Microwave Depolarization During Multipath Fading on Digital Radio Performance*, Bell Syst. Tech. J., 56, 645-674, May 1977.

Martin, L., *La réutilisation des fréquences en polarisations croisées avec diversité d'espace sur 50 km a 7 GHz*, Ann. Télécommunic., 32, 552-559, 1977.

Mottl, T.O., *Dual-polarized Channel Outages During Multipath Fading*, Bell Syst. Tech. J., 56, 675-701, May 1977.

Nowland, W.L., R.L. Olsen and I.P. Shkarofsky, *Theoretical Relationship Between Rain Attenuation and Depolarization*, Electron. Lett., 13, 676-678, 1977.

Olsen, R.L., *Cross-polarization During Clear-air Conditions on Terrestrial Links: A Review*, Radio Sci., 16, 631-647, Sept-Oct, 1981a.

Olsen, R.L., *Cross-polarization During Precipitation on Terrestrial Links: A Review*, Radio Sci., 16, 761-779, Sept-Oct, 1981b.

Olsen, R.L. and W.L. Nowland, *Semi-empirical Relations for the Prediction of Rain Depolarization Statistics: Their Theoretical and Experimental Basis*, in Proceedings of the International Symposium on Antennas and Propagation, Sendai, Japan, 477-480, Institute of Electronics and Communications Engineers of Japan, Tokyo, 1978.

Olsen, R.L., D.V. Rogers and D.B. Hodge, *The aR^b Relation in the Calculation of Rain Attenuation*, IEEE Trans. Antennas Propagat., AP-26, 318-329, 1978.

Ruthroff, C.L., *Multiple Path Fading on Line-of-sight Microwave Radio Systems as a Function of Path Length and Frequency*, Bell Syst. Tech. J., 2375-2398, Sept. 1971.

Segal, B., *High-intensity Rainfall Statistics for Canada*, CRC Report 1329-E, Communications Research Centre, Ottawa, 1979.

Segal, B., *Rain Attenuation Statistics for Terrestrial Microwave Links*, CRC Report 1351-E, Communications Research Centre, Ottawa, 1982.

Strickland, J.I., *Radar Measurements of Site-diversity Improvement During Precipitation*, J. Recherches Atmos., 8, 451-464, Jan-June, 1974.

Webster, A.R. and W.I. Lam, *Microwave Angle-of-arrival Measurements Under Anomalous Tropospheric Propagation Conditions*, in Pre-prints of the URSI Commission F Open Symposium on "Effects of the Lower Atmosphere on Radio Propagation at Frequencies above 1 GHz", Lennoxville, Canada, 3.2.1-3.2.5, Communications Research Centre, Ottawa, 1980.

CRC DOCUMENT CONTROL DATA

1. **ORIGINATOR:** Department of Communications/Communications Research Centre

2. **DOCUMENT NO:** CRC Report No. 1358

3. **DOCUMENT DATE:** September 1982

4. **DOCUMENT TITLE:** Measurements at 11 and 17 GHz of Terrestrial Microwave Fading and Depolarization

5. **AUTHOR(s):** R.S. Butler

6. **KEYWORDS:** (1) Microwave
(2) Fading
(3) Depolarization

7. **SUBJECT CATEGORY (FIELD & GROUP: COSATI)**

20 Physics

20 14 Wave Propagation

8. **ABSTRACT:**

This report presents the results of a microwave propagation experiment which was conducted in the 11 GHz and 17 GHz frequency ranges on two adjacent 16 km paths near Ottawa, Canada. Direct and cross-polarized signal levels were measured for six months in mid-1979, and significant attenuation and depolarization were observed during periods of rainfall as well as at certain times when the atmosphere was clear.

The probabilities of occurrence of attenuation and depolarization, and the relations between them, comprise a major part of the report. Statistics of the durations and of the rates-of-change of attenuation are also presented. There is also a discussion of the relation of depolarization during rainfall to the canting angles of raindrops, and a procedure is developed by which the statistics of the canting angles are obtained.

Throughout the report, reference is made to relevant CCIR documents to test the appropriateness to Canadian conditions of presently recommended predictions of various propagation phenomena. Finally, the magnitudes of attenuation during rainfall and attenuation in clear air, and of depolarization in both circumstances, are compared and assessed for their effects on microwave communication system design.

9. **CITATION:**

DATE DUE
DATE DE RETOUR

AUG AOUT 1 9 1988			

LOWE-MARTIN No. 1137

Government of Canada Gouvernement du Canada